

พอลิเมอร์ยึดติดเยื่อเมือกชนิดซิลโฟนามีด-โคโทซานสำหรับระบบนำส่งยา



นางสาวพฤศจิกา สุวรรณศรี

จุฬาลงกรณ์มหาวิทยาลัย

CHULALONGKORN UNIVERSITY

บทคัดย่อและแฟ้มข้อมูลฉบับเต็มของวิทยานิพนธ์ตั้งแต่ปีการศึกษา 2554 ที่ให้บริการในคลังปัญญาจุฬาฯ (CUIR)  
เป็นแฟ้มข้อมูลของนิสิตเจ้าของวิทยานิพนธ์ ที่ส่งผ่านทางบัณฑิตวิทยาลัย

The abstract and full text of theses from the academic year 2011 in Chulalongkorn University Intellectual Repository (CUIR)  
are the thesis authors' files submitted through the University Graduate School.

วิทยานิพนธ์นี้เป็นส่วนหนึ่งของการศึกษาตามหลักสูตรปริญญาวิทยาศาสตรดุษฎีบัณฑิต

สาขาวิชาปิโตรเคมี

คณะวิทยาศาสตร์ จุฬาลงกรณ์มหาวิทยาลัย

ปีการศึกษา 2557

ลิขสิทธิ์ของจุฬาลงกรณ์มหาวิทยาลัย

SULFONAMIDE-CHITOSAN MUCOADHESIVE POLYMERS FOR DRUG DELIVERY SYSTEM

Miss Phruetchika Suvannasara



A Dissertation Submitted in Partial Fulfillment of the Requirements  
for the Degree of Doctor of Philosophy Program in Petrochemistry

Faculty of Science

Chulalongkorn University

Academic Year 2014

Copyright of Chulalongkorn University

Thesis Title	SULFONAMIDE-CHITOSAN	MUCOADHESIVE
	POLYMERS FOR DRUG DELIVERY SYSTEM	
By	Miss Phruetchika Suvannasara	
Field of Study	Petrochemistry	
Thesis Advisor	Associate Professor Nongnuj Muangsin, Ph.D.	
Thesis Co-Advisor	Assistant Professor Nalena Praphairaksit, Ph.D.	

---

Accepted by the Faculty of Science, Chulalongkorn University in Partial Fulfillment of the Requirements for the Doctoral Degree

..... Dean of the Faculty of Science  
(Professor Supot Hannongbua, Dr.rer.nat.)

THESIS COMMITTEE

..... Chairman  
(Professor Pattarapan Prasassarakich, Ph.D.)

..... Thesis Advisor  
(Associate Professor Nongnuj Muangsin, Ph.D.)

..... Thesis Co-Advisor  
(Assistant Professor Nalena Praphairaksit, Ph.D.)

..... Examiner  
(Associate Professor Nuanphun Chantarasiri, Ph.D.)

..... Examiner  
(Associate Professor Wimonrat Trakarnpruk, Ph.D.)

..... External Examiner  
(Assistant Professor Nitinat Suppakarn, Ph.D.)

พฤศจิกายน สุวรรณศร : พอลิเมอร์ยึดติดเยื่อเมือกชนิดซัลโฟนามิด-ไคโทซานสำหรับระบบนำส่งยา (SULFONAMIDE-CHITOSAN MUCOADHESIVE POLYMERS FOR DRUG DELIVERY SYSTEM) อ.ที่ปรึกษาวิทยานิพนธ์หลัก: รศ. ดร.นงนุช เหมือนสิน, อ.ที่ปรึกษาวิทยานิพนธ์ร่วม: ผศ. สพญ. ดร.นลินา ประไพรัชสิทธิ์, 108 หน้า.

วัตถุประสงค์ของงานวิจัยนี้คือเพิ่มคุณสมบัติการยึดติดเยื่อเมือกของไคโทซานโดยการดัดแปรและนำมาใช้เป็นพอลิเมอร์สำหรับระบบนำส่งยา ไคโทซานที่ถูกดัดแปรทั้งสองชนิดคือ ซัลฟานิลาไมด์-ไคโทซานและสเตียริก-4-คาร์บอกซีเบนซิลซัลโฟนามิด-ไคโทซานถูกสังเคราะห์ขึ้นโดยการนำอนุพันธ์ของซัลโฟนามิดมาต่อติดกับไคโทซานและเอ็น-ไตรเมทิลไคโทซานคลอไรด์ด้วยพันธะโคเวเลนต์ตามลำดับ ไคโทซานที่ถูกดัดแปรแล้วจึงถูกเตรียมทั้งในรูปแบบของไฮโดรเจลและ self-assembly สำหรับซัลฟานิลาไมด์-ไคโทซานซึ่งเป็นพอลิเมอร์ชนิดยึดติดเยื่อเมือกถูกเตรียมในรูปแบบของโครงข่ายไฮโดรเจลที่มีการเชื่อมต่อกันทางกายภาพเพื่อช่วยลดปัญหาของการลื่นหลุดจากเยื่อเมือกเนื่องจากภาวะน้ำเกิน โดยเฉพาะในสภาวะเลียนแบบกระเพาะอาหาร (SGF, pH 1.2) สำหรับเส้นใยระดับนาโนเมตรของสเตียริก-4-คาร์บอกซีเบนซิลซัลโฟนามิด-ไคโทซานที่ถูกเตรียมขึ้นด้วยเทคนิค self-assembly เนื่องจากเป็นวิธีที่ง่ายและมีความคงตัวโดยนำพอลิเมอร์ที่ถูกสังเคราะห์มากระจายตัวอีกครั้งในน้ำกลั่นที่ระดับความเข้มข้น 3.33 มิลลิกรัมต่อมิลลิลิตร พบว่าเส้นใยระดับนาโนเมตรที่ถูกเตรียมได้มีการกระจายตัวทางความกว้างที่ค่อนข้างต่ำและมีขนาดเส้นผ่านศูนย์กลาง  $112.23 \pm 11.96$  นาโนเมตร นอกจากนี้เส้นใยระดับนาโนเมตรที่มีการจัดเรียงตัวทางโมเลกุลอย่างเป็นระเบียบนั้นทำให้มีความเสถียรต่อความร้อนสูงและยังช่วยเพิ่มคุณสมบัติการยึดติดเยื่อเมือกเมื่อเทียบกับไคโทซานดั้งเดิม ดังนั้นซัลฟานิลาไมด์-ไคโทซานไฮโดรเจลและเส้นใยระดับนาโนเมตรของสเตียริก-4-คาร์บอกซีเบนซิลซัลโฟนามิด-ไคโทซานจึงมีความเหมาะสมที่จะนำไปใช้ในระบบนำส่งยาในสภาวะเลียนแบบกระเพาะอาหาร

สาขาวิชา ปีโตรเคมี

ปีการศึกษา 2557

ลายมือชื่อนิสิต .....

ลายมือชื่อ อ.ที่ปรึกษาหลัก .....

ลายมือชื่อ อ.ที่ปรึกษาร่วม .....

# # 5273918823 : MAJOR PETROCHEMISTRY

KEYWORDS: MUCOADHESION / HYDROGEL / SELF-ASSEMBLY / NANOFIBERS / DRUG CARRIER

PHRUETCHIKA SUVANNASARA: SULFONAMIDE-CHITOSAN MUCOADHESIVE POLYMERS FOR DRUG DELIVERY SYSTEM. ADVISOR: ASSOC. PROF. NONGNUJ MUANGSIN, Ph.D., CO-ADVISOR: ASST. PROF. NALENA PRAPHAIRAKSIT, Ph.D., 108 pp.

The objective of this research was to increase mucoadhesive properties of chitosan and then evaluate for using as mucoadhesive drug carrier. Two mucoadhesive modified chitosan, sulfanilamide-chitosan (SM-chitosan) and stearic-4-carboxybenzenesulfonamide-*N*-trimethylchitosan (SA-4-CBS), were synthesized by covalent attachment of sulfonamide derivatives to chitosan and *N*-trimethyl chitosan chloride (TMC) in the form of hydrogel and self-assembly, respectively. Mucoadesive SM-chitosan was prepared in the form of physically crosslinked hydrogel to overcome the problem of slippery mucilage due to overhydration, especially in gastric environment (SGF, pH 1.2). An easy and stable one step was presented to fabricate self-assembled well-ordered SA-4-CBS-TMC nanofiber. Nanofiber was designed by only re-dispersing the compound in distilled water at a concentration of 3.33 mg/mL. The self-assembled nanofibers had a diameter of  $112.23 \pm 11.96$  nm with a narrow width distribution. Furthermore, the ordered molecular organization of nanofibers led to high thermal stability and enhanced mucoadhesive properties compared to native chitosan. Therefore, both SM-chitosan and SA-4-CBS-TMC could be suitable to use in gastrointestinal tract.

Field of Study: Petrochemistry

Academic Year: 2014

Student's Signature .....

Advisor's Signature .....

Co-Advisor's Signature .....

## ACKNOWLEDGEMENTS

This study was performed at Program in Petrochemistry, Faculty of Science, Chulalongkorn University, Thailand and was financially supported by the 90th Anniversary of Chulalongkorn University Fund and Ratchadaphiseksomphot Endowment Fund of Chulalongkorn University (CU-56-639-HR).

I would like to express my sincere gratitude to my thesis advisor, Associate Professor Nongnuj Muangsin and my thesis co-advisor, Assistant Professor Nalena Praphairaksit for their active valuable guidance, helpful suggestions and kindly support. All of achievements during my study would not be possible without their creative mind and their enthusiastic guidance.

I also would like to express my appreciation to my chairman and my examiners, Professor Pattarapan Prasassarakich, Associate Professor Nuanphun Chantarasiri, Associate Professor Wimonrat Trakarnpruk and Assistant Professor Nitinat Suppakarn for all appreciate comments and suggestions and their assistance to complete my thesis.

I would like to thank all of my lab mates for helping me and sharing happy time.

Finally, I would like to express my heartfelt appreciation to my parents, Patpong Suvannasara and Raweewun Suvannasara and my lovely sister, Kochakorn Suvannasara for thoughtful attention and continuous encouragements.

## CONTENTS

	Page
THAI ABSTRACT .....	iv
ENGLISH ABSTRACT .....	v
ACKNOWLEDGEMENTS .....	vi
CONTENTS .....	vii
LIST OF TABLES .....	xii
LIST OF FIGURES .....	xiii
LIST OF SCHEMES .....	xvi
LIST OF ABBREVIATIONS .....	xvii
CHAPTER I INTRODUCTION.....	1
1.1 Introduction.....	1
1.2 The objective of this research.....	6
1.3 The scope of this research.....	6
CHAPTER II THEORY AND LITERATURE REVIEWS .....	10
2.1 Introduction.....	10
2.2 Self-assembly.....	11
2.3 Hydrogel.....	12
2.4 Bioadhesion/Mucoadhesion.....	13
2.4.1 Mucous membrane .....	13
2.4.2 Mucoadhesive interactions .....	14
2.4.2.1 Chemical bonding .....	14
2.4.2.2 Theories of mucoadhesion.....	15
2.4.2.3 Mucoadhesion.....	17

	Page
2.4.3 Mucoadhesive polymers .....	19
2.4.4 Advantage of mucoadhesive drug delivery system.....	20
2.5 Chitosan.....	20
2.5.1 Structure of chitosan.....	20
2.5.2 Physico-chemical properties of chitosan .....	21
2.5.3 Pharmaceutical applications.....	22
2.5.4 Mucoadhesive chitosan .....	22
2.6 Carbodiimide .....	23
2.6.1 Reaction of EDAC carbodiimide crosslinker.....	24
2.6.2 Application of EDAC crosslinking .....	25
CHAPTER 3 ACIDIC RESISTANCE OF MUCOADHESIVE SULFANILAMIDE-CHITOSAN BASED ON HYDROGEL .....	27
3.1 Introduction.....	27
3.2 Experimental Section .....	29
3.2.1 Materials.....	29
3.2.1.1 Polymers.....	29
3.2.2 Instruments .....	30
3.2.3 Synthesis of SM-chitosan using <i>N</i> -carboxymethyl ester as an intermediate .....	31
3.2.3.1 Synthesis of <i>N</i> -carboxymethyl ester.....	31
3.2.3.2 Synthesis of SM-chitosan .....	31
3.2.4 Characterization .....	32
3.2.4.1 <sup>1</sup> H Nuclear magnetic resonance spectroscopy ( <sup>1</sup> H NMR) .....	32
3.2.4.2 Fourier transformed infrared spectroscopy (FT-IR).....	33



	Page
3.2.4.3 Thermogravimetric analysis (TGA).....	33
3.2.5 Determination of the degree of CO <sub>2</sub> Me+CO <sub>2</sub> H substitution (% $DS_{[CO_2Me+CO_2H]}$ ) and the degree of SM substitution (% $DS_{[SM]}$ ) on the chitosan by <sup>1</sup> H NMR .....	33
3.2.6 In vitro bioadhesion of mucin to chitosan, <i>N</i> -carboxymethyl ester and SM-chitosan .....	34
3.2.6.1 Mucus glycoprotein.....	34
3.2.6.2 Adsorption of mucin on chitosan, <i>N</i> -carboxymethyl ester and SM-chitosan .....	34
3.2.7 Statistical analysis .....	35
3.3 Results and discussion .....	35
3.3.1 Synthesis and structural analysis of <i>N</i> -carboxymethyl ester and SM- chitosan .....	35
3.3.2 Characterization of <i>N</i> -carboxymethyl ester and SM-chitosan .....	36
3.3.2.1 <sup>1</sup> H Nuclear magnetic resonance spectroscopy ( <sup>1</sup> H NMR) .....	36
3.3.2.2 Fourier transformed infrared spectroscopy (FT-IR).....	38
3.3.2.3 Thermogravimetric analysis (TGA).....	39
3.3.4 Determination of the degree of CO <sub>2</sub> Me±CO <sub>2</sub> H substitution (% $DS_{[CO_2Me+CO_2H]}$ ) and the degree of SM substitution (% $DS_{[SM]}$ ) on the chitosan .....	41
3.3.5 In vitro bioadhesion of mucin to chitosan, <i>N</i> -carboxymethyl ester and SM-chitosan .....	42
3.4 Conclusion .....	45
CHAPTER IV SELF-ASSEMBLY MUCCOADHESIVE NANOFIBERS .....	46
4.1 Introduction.....	46

	Page
4.2 Experimental section.....	48
4.2.1 Materials.....	48
4.2.1.1 Polymers.....	48
4.2.1.2 Chemicals.....	48
4.2.1.3 Dialysis membrane .....	49
4.2.2 Instruments .....	49
4.2.3 Synthesis of <i>N</i> -trimethyl chitosan chloride (TMC).....	50
4.2.4 Synthesis of 4-carboxybenzenesulfonamide- <i>N</i> -trimethyl chitosan (4-CBS-TMC).....	51
4.2.5 Synthesis and self-assembly of SA-4-CBS-TMC Nanofiber.....	51
4.2.6 Determination of the degree of quaternization (%DQ) and degree of 4-CBS substitution (%DS <sub>4-CBS</sub> ).....	52
4.2.7 Characterization .....	53
4.2.7.1 <sup>1</sup> H Nuclear magnetic resonance spectroscopy ( <sup>1</sup> H NMR) .....	53
4.2.7.2 Fourier transformed infrared spectroscopy (FT-IR).....	53
4.2.7.3 X-ray diffraction (XRD).....	53
4.2.7.4 Elemental analysis (EA) .....	53
4.2.7.5 Thermogravimetric analysis (TGA).....	54
4.2.7.6 Scanning electron microscopy (SEM) .....	54
4.2.8 Swelling properties .....	54
4.2.9 Determination of the mucoadhesiveness.....	55
4.2.10 Statistical analysis.....	55
4.3 Results and discussion .....	56
4.3.1 Synthesis and structural analysis of SA-4-CBS-TMC.....	56

	Page
4.3.2 Characterization of TMC, 4-CBS-TMC and SA-4-CBS-TMC .....	56
4.3.2.1 <sup>1</sup> H Nuclear magnetic resonance spectroscopy ( <sup>1</sup> H NMR) .....	56
4.3.2.2 Fourier Transformed Infrared spectroscopy (FT-IR) .....	57
4.3.2.3 X-ray diffraction (XRD).....	58
4.3.2.4 Thermogravimetric analysis (TGA).....	59
4.3.3 The degree of quaternization and the degree of 4-CBS substitution .....	60
4.3.4 Effect of the concentration on self-assembly of SA-4-CBS-TMC .....	61
4.3.4.1 Spherical shapes and short fibrous bundles .....	65
4.3.4.2 Tree-like morphology or hyperbranched structure .....	67
4.3.4.3 Nanofiber formations .....	68
4.3.4.4 Thin films.....	71
4.3.5 Swelling behaviour .....	71
4.3.6 Mucoadhesive properties .....	73
4.4 Conclusions .....	75
CHAPTER V CONCLUSION AND SUGGESTION .....	76
5.1 Conclusion .....	76
5.2 Suggestions for the future work .....	76
REFERENCES .....	77
APPENDIX A Standard curve of mucin (type II) and free and adsorbed mucin on polymers (Chapter III).....	91
Standard curve of mucin glycoprotein (type II).....	92
Free and adsorbed mucin glycoprotein (type II) on polymers.....	94
APPENDIX B Swelling behavior (Chapter IV) .....	97

	Page
APPENDIX C Mucoadhesive properties (Chapter IV) .....	104
APPENDIX D Preparation of stock solution.....	106
VITA.....	108

### LIST OF TABLES

	Page
<b>Table 3.1</b> The instruments in this study.....	31
<b>Table 3.2</b> Degree of CO <sub>2</sub> Me+CO <sub>2</sub> H substitution and SM substitution onto chitosan and the solubility test in various solvent.....	42
<b>Table 4.1</b> The instruments in this study.....	50
<b>Table A1</b> Absorbance of various concentrations of mucin glycoprotein (type II) in SGF (pH 1.2), SDF (pH 4.0), PB (pH 5.5) and SIF (pH 6.4) which was determined by UV-Vis spectrophotometer.....	92
<b>Table A2</b> Absorption of free and adsorbed mucin glycoprotein (type II) on chitosan, <i>N</i> -carboxymethyl ester and SM-chitosan in SGF (pH 1.2) determined by UV-Vis spectrophotometer.....	94
<b>Table A3</b> Absorption of free and adsorbed mucin glycoprotein (type II) on chitosan, <i>N</i> -carboxymethyl ester and SM-chitosan in SDF (pH 4.0) determined by UV-Vis spectrophotometer.....	95
<b>Table A4</b> Absorption of free and adsorbed mucin glycoprotein (type II) on chitosan, <i>N</i> -carboxymethyl ester and SM-chitosan in PB (pH 5.5) determined by UV-Vis spectrophotometer.....	95
<b>Table A5</b> Absorption of free and adsorbed mucin glycoprotein (type II) on chitosan, <i>N</i> -carboxymethyl ester and SM-chitosan in SIF (pH 6.4) determined by UV-Vis spectrophotometer.....	96
<b>Table B1</b> Swelling behaviors of chitosan, TMC and 4-CBS-TMC in SGF (pH 1.2).....	98

<b>Table B2</b> Swelling behaviors of chitosan, TMC and 4-CBS-TMC in SDF (pH 4.0).....	99
<b>Table B3</b> Swelling behaviors of chitosan, TMC and 4-CBS-TMC in PB (pH 5.5). .....	100
<b>Table B4</b> Swelling behaviors of chitosan, TMC and 4-CBS-TMC in SGF (pH 6.4). .....	101
<b>Table B5</b> Swelling behaviors of chitosan, TMC and 4-CBS-TMC in SJF (pH 7.4).....	102
<b>Table B6</b> Swelling behaviors of chitosan, TMC and 4-CBS-TMC in water.....	103
<b>Table C1</b> The component of bioadhesion in SGF (pH 1.2) and PB (pH 5.5). .....	105

## LIST OF FIGURES

	Page
<b>Figure 1.1</b> Structures of mucoadhesive thiolated chitosan (a) chitosan- iminothiolane (b) chitosan-glutathione (c) chitosan-thioglycolic acid and (d) chitosan-thioethylamidine. ....	2
<b>Figure 1.2</b> The chemical structure of mucoadhesive 4-CBS-chitosan.....	3
<b>Figure 1.3</b> Structure of hybrid synthetic-natural PMMA grafting on CTS-g-GMA. ....	4
<b>Figure 1.4</b> Structure of TMC derived from partial quaternization of chitosan. ....	5
<b>Figure 1.5</b> Mucoadhesive SM-chitosan based on hydrogel and physically crosslinked interaction. ....	7
<b>Figure 1.6</b> Design of self-assembled mucoadhesive SA-4-CBS-TMC nanofiber and their morphology in distilled water.....	8
<b>Figure 2.1</b> (a) Mucous membrane structure and (b) Histological section from the gastric antrum, showing the mucous of stomach. ....	14
<b>Figure 2.2</b> (a) Schematic representation of the diffusion theory of bioadhesion. Blue polymer layer and red mucus layer before contact; (b) Upon contact; (c) The interface becomes diffuse after contact for a period of time. ....	17

<b>Figure 2.3</b> Some scenarios where mucoadhesion can occur: (a) Dry or partially hydrated dosage forms contacting surfaces with substantial mucus layers (e.g. aerosolized particles deposited in the nasal cavity) (b) Fully hydrated dosage forms contacting surfaces with substantial mucus layers (e.g. particle suspensions in the gastrointestinal tract) (c) Dry or partially hydrated dosage forms contacting surfaces with thin/discontinuous mucus layers (e.g. a tablet placed onto the oral mucosa) and (d) Fully hydrated dosage forms contacting surfaces with thin/discontinuous mucus layer (e.g. aqueous microparticles administered into the vagina).....	18
<b>Figure 2.4</b> Chemical structure of chitosan.....	21
<b>Figure 2.5</b> Diagram depicting aggregation/disaggregation of pig gastric mucin in the presence of mucin [6].....	23
<b>Figure 2.6</b> Chemical structures of EDAC and DCC.....	24
<b>Figure 2.7</b> Carboxyl-to-amine crosslinking with the popular carbodiimide, EDAC. ....	24
<b>Figure 2.8</b> Carboxyl-to-amine-crosslinking using the carbodiimide EDAC and sulfo-NHS.....	25
<b>Figure 3.1</b> Physical appearance of SM-chitosan in distilled water and physical crosslinked interaction of SM-chitosan hydrogel.....	36
<b>Figure 3.2</b> <sup>1</sup> H NMR spectra of the (a) chitosan, (b) SM and (c) <i>N</i> -carboxymethyl ester and (d) SM-chitosan.....	37
<b>Figure 3.3</b> FT-IR spectra of the (a) chitosan, (b) SM and (c) <i>N</i> -carboxymethyl ester and (d) SM-chitosan.....	39
<b>Figure 3.4</b> TGA thermograms of the (a) chitosan, (b) SM and (c) <i>N</i> -carboxymethyl ester and (d) SM-chitosan.....	40
<b>Figure 3.5</b> Adsorption of mucin on chitosan, <i>N</i> -carboxymethyl ester and SM-chitosan at SGF (pH 1.2), SDF (pH 4.0), PB (pH 5.5) and SIF (pH 6.4). Data	

are shown as the mean $\pm$ SD and are derived from three independent repeats. Means with a different lower case letter are significantly different ( $P < 0.01$ ). .....	44
<b>Figure 4.1</b> $^1\text{H}$ NMR spectra of the (a) chitosan, (b) TMC and (c) 4-CBS-TMC. ....	57
<b>Figure 4.2</b> FT-IR spectra of the (a) chitosan, (b) TMC, (c) 4-CBS-TMC and (d) SA-4-CBS-TMC. ....	58
<b>Figure 4.3</b> XRD patterns of (a) chitosan, (b) 4-CBS-TMC and (c) SA-4-CBS-TMC. ....	59
<b>Figure 4.4</b> TGA thermogram of (a) chitosan, (b) TMC, (c) 4-CBS-TMC and (d) SA-4-CBS-TMC. ....	60
<b>Figure 4.5</b> (a) The molecular structure of SA-4-CBS-TMC and (b) The molecular design of SA-4-CBS-TMC nanofibers. ....	63
<b>Figure 4.6</b> (a) A schematic phase diagram of SA-4-CBS-TMC assemblies, which are dependent on concentration in distilled water, ranging from 0.33 to 13.33 mg/mL. (b) The formation stages of SA-4-CBS-TMC particles dependent on re-dispersion in distilled water. ....	64
<b>Figure 4.7</b> The morphologies of SA-4-CBS-TMC at low concentration (0.33 mg/mL): (a) spherical shapes, (b) fibrous bundles, (c) fibrous bundle merge and (d) the proposed self-assembly of fibrous bundles. ....	66
<b>Figure 4.8</b> The morphologies of SA-4-CBS-TMC at high concentration (0.67 mg/mL): the (a) initial nucleus, (b) central nucleus, (c) short helical nanofibers of $\sim 100$ nm and (d) proposed self-assembly of hyperbranched structures. ....	68
<b>Figure 4.9</b> Morphologies of SA-4-CBS-TMC at high concentration (3.33 mg/mL). (a) Elongated nanofibers, (b) a cross-section of nanofibers (c) connected horizontal nanofibers are depicted, and (d) the histogram of SA-4-CBS-TMC nanofiber widths measured from SEM images. ....	69

<b>Figure 4.10</b> The morphology of SA-4-CBS-TMC at the high concentration (13.33 mg/mL).....	71
<b>Figure 4.11</b> Swelling behaviors of the chitosan, TMC and 4-CBS-TMC in simulated gastric fluid (SGF, pH 1.2), 0.1 N simulated duodenum buffer (SDF, pH 4.0), 0.1 N phosphate buffer (PB, pH 5.5), simulated jejunum fluid (SJF, pH 6.4), simulated ileum fluid (SIF, pH 7.4) and water. ....	72
<b>Figure 4.12</b> The component of mucoadhesion (cps) of chitosan, TMC, 4-CBS-TMC and SA-4-CBS-TMC in SGF, pH 1.2 and PB, pH 5.5. Data are shown as the mean $\pm$ 1 SD and are derived from three independent repeats. ....	74
<b>Figure A1</b> Standard curve of mucin glycoprotein (type II) in SGF (pH 1.2), SDF (pH 4.0), PB (pH 5.5) and SIF (pH 6.4). ....	93

### LIST OF SCHEMES

	Page
<b>Scheme 3.1</b> Reaction scheme of the covalent attachment of SM to chitosan using methyl acrylate as an intermediate. ....	32
<b>Scheme 4.1</b> Reaction scheme for the covalent attachment of SA and 4-CBS to TMC. ....	52



## LIST OF ABBREVIATIONS

%	Percentage
$\lambda$	Wavelength (lambda)
$\mu\text{g}$	Microgram
$\mu\text{L}$	Microliter
$\mu\text{mol}$	Micromole
$\text{\AA}$	Angstrom
Aq	Aqueous
$^{\circ}\text{C}$	Degree Celsius
cm	Centimeter
$\text{cm}^{-1}$	Wavenumber (unit)
4-CBS	4-Carboxybenzenesulfonamide
%DD	Degree of deacetylation
%DS <sub>4-CBS</sub>	Degree of 4-carboxybenzenesulfonamide substitution
%DS <sub>SM</sub>	Degree of sulfanilamide substitution
EA	Elemental analysis
Eq	Equation
FT-IR	Fourier transformed infrared spectroscopy
$^1\text{H}$ NMR	$^1\text{H}$ Nuclear magnetic resonance spectroscopy
Hz	Hertz
kDa	Kilodalton

kV	Kilovolt
mbar	Millibar
mg	Milligram
M	Molarity
MW	Molecular weight
N	Normality
Nm	Nanometer
PAS	Periodic-Schiff
PB	Phosphate buffer
pH	A measure of the acidity or basicity of an aqueous solution
pK <sub>a</sub>	Acid dissociation constant
ppm	One part per million
rpm	Revolutions per minute
SEM	Scanning electron microscope
SD	Standard deviation
SDF	Simulated duodenum buffer
SGF	Simulated gastric fluid
SIF	Simulated intestinal fluid
SM	Sulfanilamide
TGA	Thermogravimetric analysis
TMC	<i>N</i> -Trimethyl chitosan chloride (Quaternized chitosan)
UV-Vis	Ultraviolet-visible spectroscopy

v/v	Volume/volume
w/v	Weight/volume
w/w	Weight/weight
XRD	X-ray diffraction



# CHAPTER I

## INTRODUCTION

### 1.1 Introduction

Nowadays, mucoadhesive polymers have been one of the most attractive areas in the field of pharmaceutical and medical application such as tissue engineering and drug delivery system. In the development of mucoadhesive drug delivery system, it prolongs residence time at the site of the intended drug molecule which is important for selective and effective drug absorption [1].

Chitosan is a cationic mucoadhesive polyaminosaccharide, derived by the deacetylation of chitin, with many significant biological properties such as biodegradability, biocompatibility and bioactivity [2]. Due to the presence of reactive groups such as amino groups ( $-NH_2$ ) and hydroxyl groups ( $-OH$ ) in its structure providing hydrogen bonding, the linear molecule expressing sufficient chain flexibility and the cationic polyelectrolyte nature of chitosan providing a strong electrostatic interaction with a negative charged mucosal membrane, chitosan can be mucoadhesive polymer [3].

He et al. studied in vitro evaluation of the interaction between mucin and chitosan in aqueous solution by turbidimetric measurements, adsorption isotherms of mucus glycoprotein to chitosan microspheres [2].

Dhawan et al. prepared chitosan microspheres and evaluated mucoadhesive properties by different methods such as thermal crosslinking, chemical crosslinking using glutaraldehyde and physical crosslinking using tripolyphosphate and emulsification and ionotropic gelation. Chitosan microspheres prepared by emulsification and ionotropic gelation exhibited more mucoadhesive as compared with other methods [4].

Nagarwal et al. prepared chitosan nanoparticles from the ionotropic gelation method to load 5-fluorouracil for ophthalmic delivery. The nanoparticles were smooth

and spherical shape in the size range of 114-197 nm. The interaction between nanoparticles and mucin was studied by measuring viscosity change [5].

Sogias et al. studied the role of primary amino groups, electrostatic interaction, hydrogen bonding and hydrophobic effects on aggregation of gastric mucin in the presence of chitosan [6].

Chitosan with thiol groups, or the so-called thiomers, as a new generation of mucoadhesive polymers provides much higher adhesive properties than native chitosan generally considered to be mucoadhesive polymer due to the formation of covalent bonds between the chitosan and the mucus layer which are stronger than non-covalent bonds [7, 8]. There are a number of thiolated chitosan (Figure 1.1) including chitosan-iminothiolane [9], chitosan-glutathione [10], chitosan-thioglycolic acid [8] and chitosan-thioethylamidine [11].

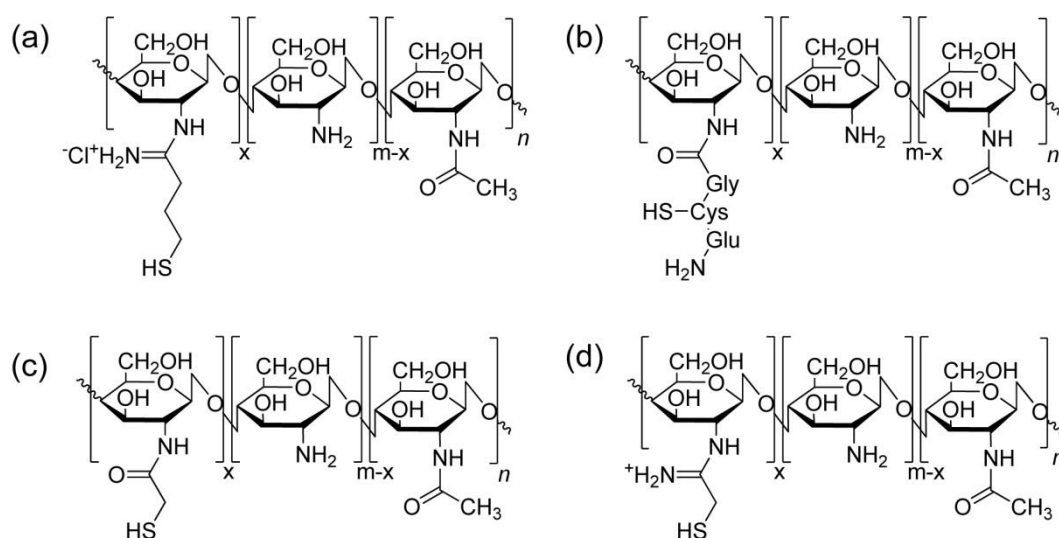


**Figure 1.1** Structures of mucoadhesive thiolated chitosan (a) chitosan-iminothiolane (b) chitosan-glutathione (c) chitosan-thioglycolic acid and (d) chitosan-thioethylamidine.

However, thiol groups are less stable at pH above 5 due to their oxidizing to be disulfide bonds during the coupling reaction [12]. Besides, at pH of less than 5.0 the

level of thiolated anions, which is the functional group responsible for thiol/disulfide interactions with the mucus membrane, is decreased [13].

To overcome the stability of thiol, 4-carboxybenzenesulfonamide (4-CBS) as sulfonamide derivative was used to modify chitosan to be mucoadhesive 4-carboxybenzenesulfonamide-chitosan (4-CBS-chitosan) (Figure 1.2). It exhibited 20-fold stronger mucoadhesion to mucin type II than native chitosan [14].

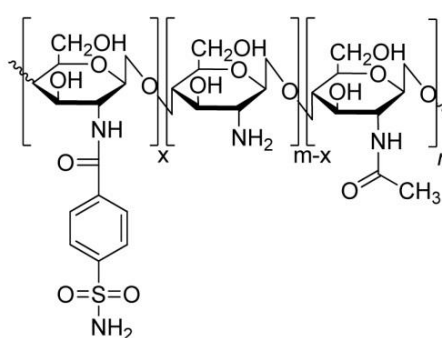


**Figure 1.2** The chemical structure of mucoadhesive 4-CBS-chitosan.

Suvannasara et al. prepared electrospayed mucoadhesive 4-CBS-chitosan microspheres for acetazolamide (ACZ) delivery. 4-CBS-chitosan microspheres had 90% encapsulation efficiency for ACZ and gave a sustained release ~100% over 3 h in simulated gastric fluid (0.1 N HCl; pH 1.2) which are a possible drug carrier in acidic conditions, such as at the gastric mucosal wall [15].

Sulfonamide derivative, sulfanilamide-chitosan (SM-chitosan), was prepared in the form of hydrogel. Hydrogels, water swollen and cross-linked polymeric structures, have gained increasing interest to improve mucoadhesive systems for controlling the release of drug [16]. Hydrogel can respond to surrounding conditions such as pH, ionic strength, temperature and electric current [17]. Chitosan was formed hydrogel in a presence of chemically crosslinked and physically crosslinked hydrogel [18, 19].

Moura et al. prepared in situ forming chitosan hydrogel via ionic/covalent co-crosslinking (glycerol-phosphate disodium salt complex/genipin). The resulting

hydrogels maintained the thermosensitive character, improved mechanical properties and chemical stability [20].

Pena et al. produced a novel hybrid synthetic-natural chitosan-g-glycidyl methacrylate (CTS-g-GMA) with methyl methacrylate (PMMA) (Figure 1.3). The strong intermolecular interactions between CTS-g-GMA and PMMA was occurred by covalent bonding. Highly functional performance of CTS-g-GMA-g-PMMA showed simple route with thermal stability [21].

Sajeesh et al. prepared mucoadhesive hydrogel microparticles based on poly(methacrylic acid-vinyl pyrrolidone)-chitosan by ionic-gelation method for oral drug delivery. Mucoadhesive hydrogel was improved the release of insulin at acidic pH [22].

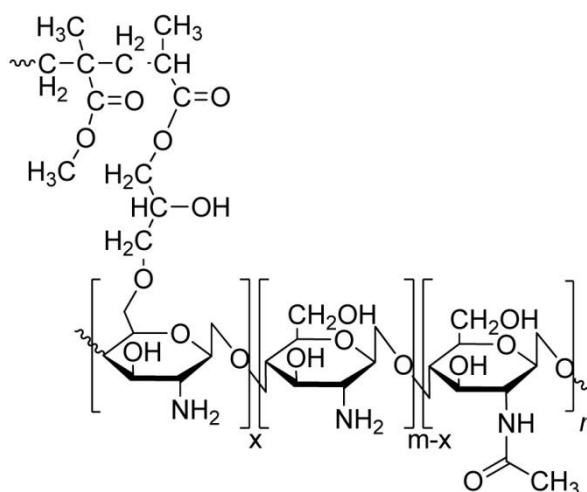


**Figure 1.3** Structure of hybrid synthetic-natural PMMA grafting on CTS-g-GMA.

Although chitosan hydrogel by chemical crosslinking on the surface with crosslinking agents improve the mechanical properties and chemical stability, the chemical crosslinkers may induce toxicity before administration [23]. To construct a mucoadhesive hydrogel, we synthesized SM-chitosan hydrogel as physically crosslinked hydrogel using methyl acrylate as an intermedia to reduce the problem of adhesion failure due to overhydration.

Another method to improve the mucoadhesive properties of sulfonamide derivative based on chitosan, chitosan was quaternized to be *N,N,N*-trimethyl chitosan chloride (TMC) (Figure 1.4) to increase the solubility in a much broader pH [24]. The quaternization degree has an effect on the solubility and high quaternization provides consequently more effective in mucoadhesive properties [25].

Thanou et al. studied the effect of degree of quaternization of *N*-trimethyl chitosan chloride for enhanced transport of hydrophilic compounds across intestinal Caco-2 cell monolayer. *N*-trimethyl chitosan chloride is able to open the tight junctions of intestinal epithelia at physiological pH values to improve the paracellular permeability of intestinal epithelia [26].

Snyman et al. evaluated mucoadhesive properties of TMC in a neutral and basic environment. The results show that the degree of quaternization of TMC had a pronounced effect on the mucoadhesive properties of this polymer. Although the mucoadhesive profiles for the TMC polymers were lower than the original chitosan, they still retained sufficient mucoadhesive properties for successful inclusion into mucoadhesive dosage forms [1].

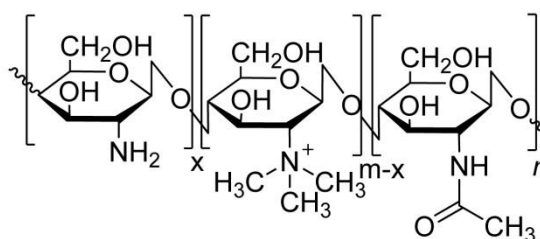


**Figure 1.4** Structure of TMC derived from partial quaternization of chitosan.

The design of self-assembly into nanotubes, nanospheres, nanofibrils and other ordered structures at the nano-scale is a key issue in nanotechnology for controlled release, cell culture and tissue engineering [27, 28]. A typical self-assembly molecule contains two regions: a hydrophobic aliphatic tail such as palmitic acid, phospholipids and stearic acid, and hydrophilic sequence attached to that tail. The role of electrostatic interaction, hydrophobic interaction and hydrogen bonding has an important role on the morphology of self-assembly.



Hu et al. synthesized an amphiphilic stearic acid grafted copolymer based on chitosan oligosaccharide for gene delivery. The self-aggregation of micelles in aqueous solution was prepared with a narrow distribution and a volume average hydrodynamic diameter 70.6 nm. It could be used as an effective DNA condensation carrier for gene delivery system [29].

Taubert et al. prepared of reactive amphiphilic block copolymers as mimetics for biological membrane. Synthetic block copolymers cannot only be biocompatible, but also because there are virtually no limits to combinations of monomers, biological and synthetic blocks, ligands, receptors, and other proteins. Polymer hybrid materials show a great promise for applications in biomedicine and biotechnology [30].

Therefore, to overcome the drawback of chitosan related with physical and chemical properties, and improved mucoadhesion, the self-assembled stearic acid-4-carboxybenzenesulfonamide-*N*-trimethylchitosan (SA-4-CBS-TMC) was prepared.

## **1.2 The objective of this research**

- To overcome the problem of slippery mucilage due to overhydration, instability of thiolated hydrogel as the candidate of mucoadhesive polymers in acidic conditions and reduce preparation step, mucoadhesive SM-chitosan was prepared in form of physically crosslinked hydrogel.

- To present an easy and stable one step to fabricate and design SA-4-CBS-TMC mucoadhesive nanofiber based on the effect of re-dispersed concentration of polymer for using as drug carrier in acidic environment.

## **1.3 The scope of this research**

The scope and the methodology of this research were summarized into 3 topics as follows:

- 1.) Acidic resistance of mucoadhesive SM-chitosan based on hydrogel.

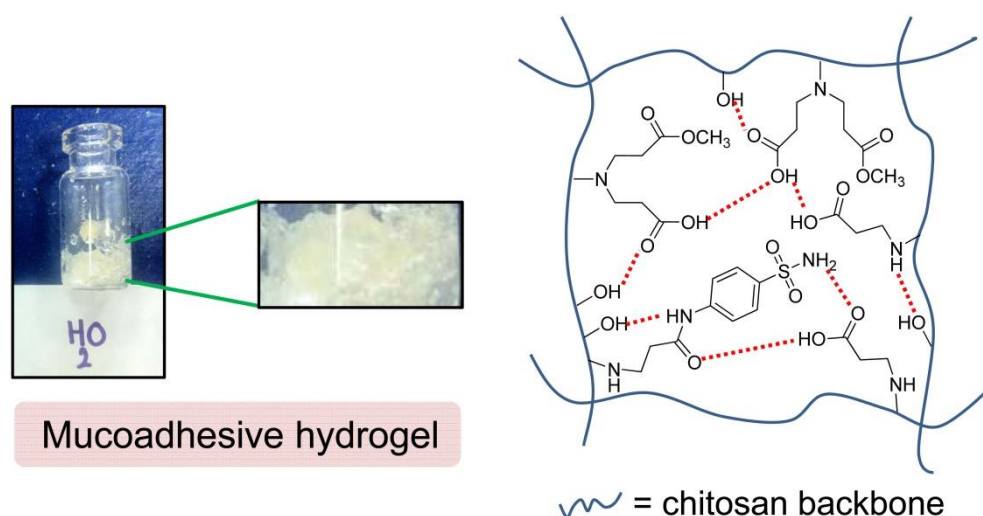


**Figure 1.5** Mucoadhesive SM-chitosan based on hydrogel and physically crosslinked interaction.

- Review literatures for related research work such as the advantage of mucoadhesive polymers, hydrogel preparation and acidic resistance polymers.
- Synthesize SM-chitosan using *N*-carboxymethyl ester as an intermedia via micheal reaction.
- Characterize and analyze the chemical structure and physico-thermal properties of *N*-carboxymethyl ester and SM-chitosan by using  $^1\text{H}$  NMR, FTIR and TGA.
- Determine the degree of  $\text{CO}_2\text{Me}+\text{CO}_2\text{H}$  substitution ( $\% \text{DS}_{[\text{CO}_2\text{Me}+\text{CO}_2\text{H}]}$ ) and the degree of SM substitution ( $\% \text{DS}_{[\text{SM}]}$ ) on the chitosan by using  $^1\text{H}$  NMR.
- Determine mucoadhesive properties of chitosan, *N*-carboxymethyl ester and SM-chitosan in simulated gastric fluid (SGF, pH 1.2), 0.1 N simulated duodenum buffer (SDF, pH 4.0), 0.1 N phosphate buffer (PB, pH 5.5) and simulated jejunum fluid (SJF, pH 6.4) by the Periodic Acid Schiff (PAS) method.
- Prepare and compare the gelation properties of *N*-carboxymethyl ester and SM-chitosan in distilled water, DMSO, 1% (v/v) acetic acid and SGF, pH 1.2.

- Summarize and discuss the results.

2.) Self-assembly mucoadhesive nanofibers.

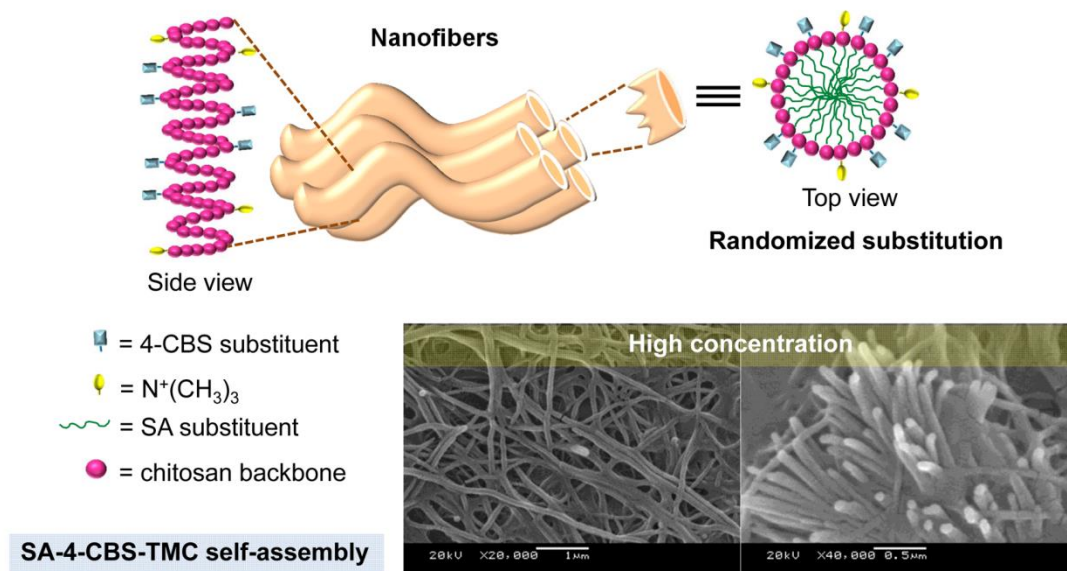


**Figure 1.6** Design of self-assembled mucoadhesive SA-4-CBS-TMC nanofiber and their morphology in distilled water.

- Review literatures for related research work such as preparation techniques of nanofiber for drug delivery system, the balance of energies to various morphologies, the role of hydrogen bonding, cation-dipole interaction and amphiphilic packing, and the advantage of mucoadhesive polymers.

- Synthesize *N*-trimethyl chitosan chloride (TMC), 4-carboxybenzenesulfonamide-*N*-trimethyl chitosan (4-CBS-TMC) and SA-4-CBS-TMC using carbodiimide (EDAC) as a coupling agent.

- Characterize and analyze the chemical structure and physico-thermal properties of TMC, 4-CBS-TMC and SA-4-CBS-TMC by using  $^1\text{H}$  NMR, FTIR, XRD, elemental analysis (EA) and TGA.

- Determine the degree of quaternization (%DQ) and degree of 4-CBS substitution (%DS<sub>4-CBS</sub>) by using  $^1\text{H}$  NMR.

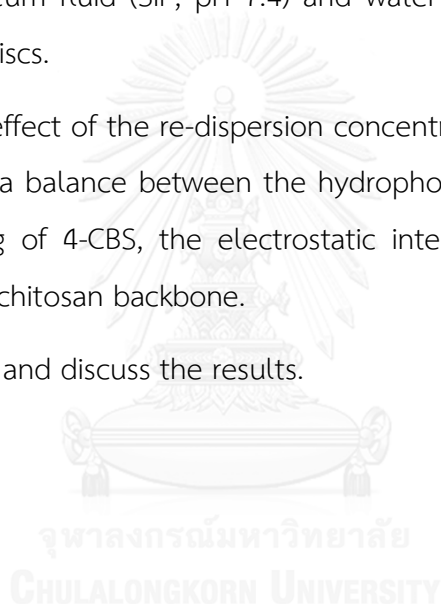
- Fabricate self-assembled SA-4-CBS-TMC by re-dispersing the compound in distilled water with various concentration (0.33, 0.67, 3.33 and 13.33 mg/mL) and studies the morphology and surface appearance of different concentration on self-assembly of SA-4-CBS-TMC particles by using SEM.

- Determine mucoadhesive properties of chitosan, TMC, 4-CBS-TMC and SA-4-CBS-TMC in simulated gastric fluid (SGF, pH 1.2) and 0.1 N phosphate buffer (PB, pH 5.5) by a Brookfield viscometer.

- Determine swelling behaviors of chitosan, TMC and 4-CBS-TMC in SGF, SDF, PB, SJF, simulated ileum fluid (SIF, pH 7.4) and water by measuring the change of diameter of the flat discs.

- Study the effect of the re-dispersion concentration on self-assembly of SA-4-CBS-TMC relied on a balance between the hydrophobic effect of stearic acid (SA), the aromatic stacking of 4-CBS, the electrostatic interaction of  $-N^+(CH_3)_3$  and the hydrogen bonding of chitosan backbone.

- Summarize and discuss the results.



## CHAPTER II

### THEORY AND LITERATURE REVIEWS

#### 2.1 Introduction

The cultural and economic pressures from humans seeking high quality of life and long lifespan have promoted the development of new strategies for the practice of medicine. This has coincided with, and likely promoted, the emergence of bionanotechnology. The current question is not whether bionanotechnology will have an impact on our quality of life but rather how to best harness this technique for a wide range of medical applications and when the resulting products will be brought to the clinic. Over the past decade, the focus of nanoscience has shifted from the development of novel nanostructures and the investigation of their formation mechanisms to the exploration of their applications. A broad range of nanostructures, from carbon nanotubes, buckyballs, inorganic nanoparticles, and dendrimers to self-assembled micelles and nano-objects of natural or synthetic molecules has been evaluated in disease diagnostics, drug delivery, tissue engineering and regenerative medicine.

The rapidly growing needs for new medical therapies continue to challenge the field of nanotechnology and nanoscience. The earliest examples of nanomedicines are essentially reformulations of existing drugs using nanostructured materials; however, the development of future medicines that could be more predictive, preemptive, personalized, and re-generative demands customized fabrication of nanostructures with properties specifically tailored for the desired medical propose. The consequently requires a better structural and functional control of materials and drugs at the molecular level. This is where self-assembly can make a major contribution, allowing for the necessary control of bioactive architectures with adjustable sizes, shapes, and more importantly, surface chemistries, that can emulate three-dimensional structures of biological proteins.

## 2.2 Self-assembly

Self-assembly is a type of process in which a disordered system of pre-existing components forms an organized structure or pattern as a consequence of specific, local interactions among the components themselves, without external direction. When the constitutive components are molecules, the process is termed molecular self-assembly.

Self-assembly can be classified as either static or dynamic. In static self-assembly, the ordered state forms as a system approaches equilibrium, reducing its free energy. However in dynamic self-assembly, patterns of pre-existing components organized by specific local interactions are not commonly described as self-assembled by scientists in the associated disciplines. These structures are better described as self-organized.

Macromolecular self-assembly presents a very attractive strategy to construct nanoscale materials due to its simplicity in application [31]. They were generated predominantly from DNA, peptides, proteins, lipids, copolymer and dendrimers. They play a far more crucial role in governing the structures and functions of the entire body than any individual molecules [32].

Peptides may be the best candidate for self-assembly in medical application since they are major components in biological systems, their inherent biocompatibility and easy to synthesize using conventional technology. In particular,  $\beta$ -sheet-forming peptides demonstrate the extraordinary ability to assemble into one-dimensional nanostructures through intermolecular hydrogen bonding [33]. Interactions among one-dimensional peptide-based nanostructures can lead to the formation of three-dimensional networks. The chemical design versatility of peptide, in combination with their ability to adopt specific secondary structures, provides a unique platform for the design of materials with controllable structural features at the nanoscales. Additionally, the biodegradability, further tunable by incorporation of specific amino acid sequences or control over their self-assembled structures, allows for the construction of bioactive hydrogels that can mimic the structure and function of native extracellular matrix. The oligopeptides could serve as an effective, low-cost alternative for functional mimicry

of large proteins. The relationship of function and structure in natural proteins is pervasive, with the spatial organization provided by specific folding and residue interactions directly contributing to the functional activity. Through self-assembly, we hope to precisely combine functional peptide sequences with the versatile structure of self-assembling synthetic molecules to produce customized nanoscale engineered biomaterials for various medical applications.

### 2.3 Hydrogel

Hydrogel is a network of polymer chains that are large number of hydrophilic formed by crosslinking polymer chains through physical, ionic or covalent interactions. It is well known as a colloidal gel is capable of absorbing and retaining considerable amounts of water without dissolving. Hydrogels are highly absorbent (they can contain over 90% water) natural or synthetic polymeric networks. Hydrogels also possess a degree of flexibility very similar to natural tissue, due to their significant water content. In most cases, they are homogeneous materials, and their bulk properties are characterized and considered with regard to applications [34].

CH hydrogels can be classified in chemically and physically crosslinked networks. Chemical hydrogels are formed by irreversible covalent links, whereas physical hydrogels are formed by various reversible non-covalent links. Chemical CH hydrogels can be obtained by: (i) crosslinking with CH itself; (ii) crosslinking with CH itself in the presence of a non-reactive polymer; and (iii) a crosslinking reaction between CH chains and the reactive chains of another type of polymer. In these hydrogels, networks are mainly formed by covalent bonds derived by the reaction between the amino groups of CH and the reactive functional groups (at least two) of a suitable crosslinking agent such as dialdehydes, oxalic acid or genipin; eventually other secondary interactions can be found in the hydrogel network. Physical CH hydrogels can be simply formed by polymer dissolution in acidic aqueous media containing monoprotic acids (i.e., hydrochloric and acetic), over concentrations suitable to guarantee the formation of intermolecular interactions and thus a three-dimensional network (entangled hydrogels). Moreover, ionic interactions with negatively charged multifunctional entities (small inorganic and organic ions or ionic polymers) can induce the formation

of ionically crosslinked hydrogels. Finally, physical hydrogels can be obtained through secondary interactions of CH chains with polymers such as poly(vinyl alcohol), poly(vinyl pyrrolidone) and poly(ethylene glycol), or through the use of CH derivatives with pendant chains capable of mutual interactions (graft-type hydrogels).

## **2.4 Bioadhesion/Mucoadhesion**

Bioadhesion defined any adhesive interaction formed between two biological surfaces such as platelet aggregation and wound healing or a bond between a biological and a synthetic surface such as cell adhesion to culture dishes and adhesion of synthetic hydrogels to soft tissues, which are held together for extended periods of time by interfacial forces [35, 36].

Mucoadhesion is the ability of macromolecules such as proteins and peptides to adhere at mucosal membranes which are the moist surfaces lining the walls of various body cavities.

### **2.4.1 Mucous membrane**

Mucous membranes (mucosae) are the moist surfaces lining the walls of various body cavities such as the gastrointestinal and respiratory tracts. They are viscosity gel layer that protects tissues and composed primarily of crosslinked and entangled mucin fibers secreted by goblet cells and submucosal gland [37, 38]. Mucous membrane consist of a connective tissue layer (the lamina propria) above which is an epithelial layer, the surface of which is made moist usually by the presence of a mucus layer. The epithelia may be either single layered (e.g. the stomach, small and large intestine and bronchi) or multilayered/stratified (e.g. in the oesophagus, vagina and cornea). The former contain goblet cells which secrete mucus directly onto the epithelial surfaces, the latter contain, or are adjacent to tissues containing, specialized glands such as salivary glands that secrete mucus onto the epithelial surface. Mucus is present as either a gel layer adherent to the mucosal surface or as a luminal soluble or suspended form. The major components of all mucus gels are mucin glycoproteins, lipids, inorganic salts and water, the latter accounting for more than 95% of its weight, making it a highly hydrated system. The mucin glycoproteins are the most important structure-forming component of the mucus gel, resulting in its characteristic gel-like, cohesive



and adhesive properties. The thickness of this mucus layer varies on different mucosal surfaces, from 50 to 450 Am in the stomach [39, 40], to less than 1 Am in the oral cavity [41]. The major functions of mucus are that of protection and lubrication (they could be said to act as anti-adherents).

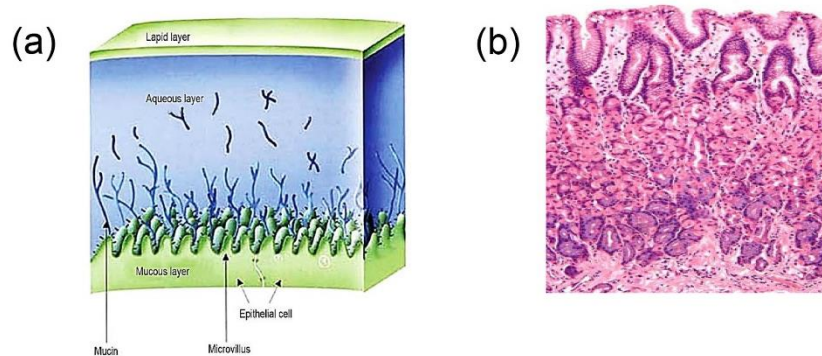


**Figure 2.1** (a) Mucous membrane structure and (b) Histological section from the gastric antrum, showing the mucous of stomach.

## 2.4.2 Mucoadhesive interactions

### 2.4.2.1 Chemical bonding

Mucoadhesion involves different kinds of interaction forces between mucoadhesive materials and the mucus surface; these include ionic bonds, covalent bonds, electrostatic attraction, hydrogen bonding, Van der Waals forces and hydrophobic bonds [42].

1.) Ionic bonds: where two oppositely charged ions attract each other via electrostatic interactions to form a strong bond.

2.) Covalent bonds: where electrons are shared, in pair, between the bonded atom in order to 'fill' the orbitals in both. These are also strong bond.

3.) Hydrogen bonds: here a hydrogen atom, when covalently bonded to electronegative atoms such as oxygen, fluorine or nitrogen, carries a slight positively charge and is therefore is attracted to other electronegative atoms. The hydrogen can

therefore be thought of as being shared, and the bond formed is generally weaker than ionic or covalent bonds.

4.) Van der Waals bonds: these are some of the weakest forms of interaction that arise from dipole–dipole and dipole-induced dipole attractions in polar molecules, and dispersion forces with non-polar substances.

5.) Hydrophobic bonds: more accurately described as the hydrophobic effect, these are indirect bonds (such groups only appear to be attracted to each other) that occur when non-polar groups are present in an aqueous solution. Water molecules adjacent to non-polar groups form hydrogen bonded structures, which lowers the system entropy. There is therefore an increase in the tendency of non-polar groups to associate with each other to minimise this effect.

#### 2.4.2.2 Theories of mucoadhesion

Six general theories of adhesion which have been adapted for the explanation of the experimental observations made during the bioadhesion process [43]. However, each theoretical model can only explain a limited number of the diverse range of interactions which constitute the bioadhesive bond [44].

1.) The electronic theory: electron transfer occurs upon contact of the adhesive interface and adhering surfaces due to differences in their electronic structure. This is proposed to result in the formation of an electrical double layer at the interface, with subsequent adhesion due to attractive forces.

2.) The wetting theory: the oldest established theory of adhesion applies to liquid or low-viscosity bioadhesive systems and considers surface and interfacial energies. It involves the ability of a liquid to spread spontaneously onto a surface as a prerequisite for the development of adhesion. The affinity of a liquid for a surface can be found using techniques such as contact angle goniometry to measure the contact angle of the liquid on the surface, with the general rule being that the lower the contact angle, the greater the affinity of the liquid to the solid. The spreading coefficient ( $S_{AB}$ ) can be calculated from the surface energies of the solid and liquids using the equation:

$$S_{AB} = \gamma_B - \gamma_A - \gamma_{AB} \dots \dots \dots (2.1)$$

where  $\gamma_A$  is the surface tension (energy) of the liquid A,  $\gamma_B$  is the surface energy of the solid B and  $\gamma_{AB}$  is the interfacial energy between the solid and liquid.  $S_{AB}$  should be positive for the liquid to spread spontaneously over the solid.

The work of adhesion  $W_A$  represents the energy required to separate the two phases, and is given by:

$$W_A = \gamma_A + \gamma_B - \gamma_{AB} \dots \dots \dots (2.2)$$

The greater the individual surface energies of the solid and liquid relative to the interfacial energy, the greater the work of adhesion.

3.) The adsorption theory: the initial attachment of adhesives between two surfaces based on the basis of hydrogen bonding, van der Waals forces and hydrophobic bonding [45]. It has been proposed that these forces are the main contributors to the adhesive interaction. A subsection of this, the chemisorption theory, assumes an interaction across the interface occurs as a result of strong covalent bonding.

4.) The diffusion theory: interdiffusion of polymers chains is formed the bioadhesive interpenetrate into glycoprotein mucin chains across an adhesive interface [46]. This process is driven by concentration gradients and is affected by the available molecular chain lengths and their mobilities. The depth of interpenetration depends on the diffusion coefficient and the time of contact. Sufficient depth of penetration creates a semi-permanent adhesive bond (Figure 2.2).

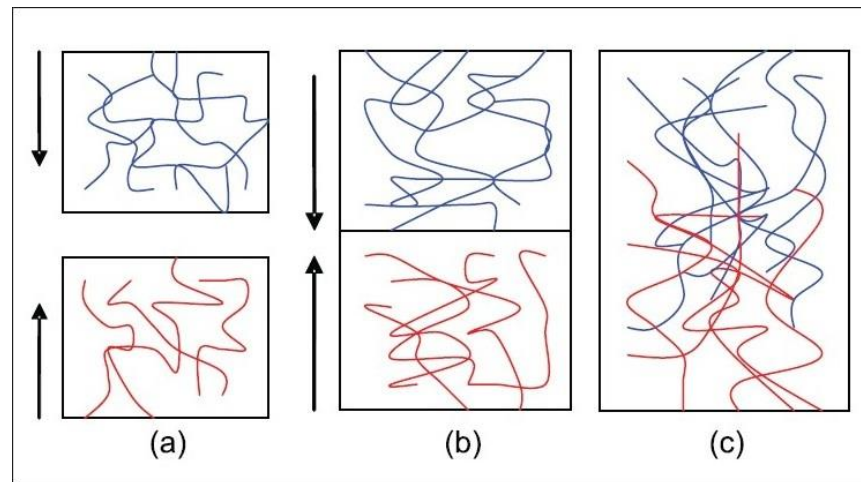


**Figure 2.2** (a) Schematic representation of the diffusion theory of bioadhesion. Blue polymer layer and red mucus layer before contact; (b) Upon contact; (c) The interface becomes diffuse after contact for a period of time.

5.) The mechanical theory: adhesion arises from an interlocking of a liquid adhesive into irregularities on a rough surface. However, rough surfaces also provide an increased surface area available for interaction along with an enhanced viscoelastic and plastic dissipation of energy during joint failure, which are thought to be more important in the adhesion process than a mechanical effect [47].

6.) The fracture theory: differs a little from the other five in that it relates the adhesive strength to the forces required for the detachment of the two involved surfaces after adhesion. This assumes that the failure of the adhesive bond occurs at the interface. However, failure normally occurs at the weakest component, which is typically a cohesive failure within one of the adhering surfaces.

#### 2.4.2.3 Mucoadhesion

Due its relative complexity, it is likely that the process of mucoadhesion cannot be described by just one of these theories. In considering the mechanism of mucoadhesion, a whole range scenarios for in-vivo mucoadhesive bond formation are possible (Figure 2.3). These include:

1.) Dry or partially hydrated dosage forms contacting surfaces with substantial mucus layers (typically particulates administered into the nasal cavity).

2.) Fully hydrated dosage forms contacting surfaces with substantial mucus layers (typically particulates of many First Generation mucoadhesives that have hydrated in the luminal contents on delivery to the lower gastrointestinal tract).

3.) Dry or partially hydrated dosage forms contacting surfaces with thin/discontinuous mucus layers (typically tablets or patches in the oral cavity or vagina).

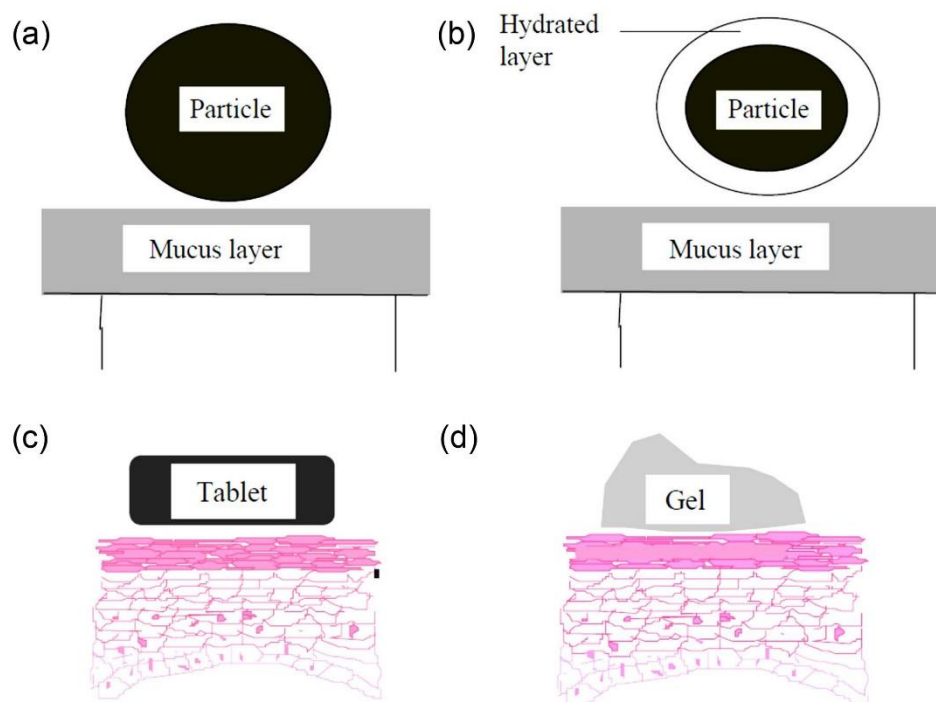


**Figure 2.3** Some scenarios where mucoadhesion can occur: (a) Dry or partially hydrated dosage forms contacting surfaces with substantial mucus layers (e.g. aerosolized particles deposited in the nasal cavity) (b) Fully hydrated dosage forms contacting surfaces with substantial mucus layers (e.g. particle suspensions in the gastrointestinal tract) (c) Dry or partially hydrated dosage forms contacting surfaces with thin/discontinuous mucus layers (e.g. a tablet placed onto the oral mucosa) and (d) Fully hydrated dosage forms contacting surfaces with thin/discontinuous mucus layer (e.g. aqueous microparticles administered into the vagina).

4.) Fully hydrated dosage forms contacting surfaces with thin/discontinuous mucus layers (typically aqueous semisolids or liquids administered into the oesophagus or eye).

### 2.4.3 Mucoadhesive polymers

Mucoadhesive polymers have numerous hydrophilic groups, such as hydroxyl, carboxyl, amide, and sulfate to adhere on mucosal tissue. These groups attach to mucus or the cell membrane by various interactions such as hydrogen bonding and hydrophobic or electrostatic interactions. These hydrophilic groups also cause polymers to swell in water and, thus, expose the maximum number of adhesive sites. An ideal polymer for a bioadhesive drug delivery system should have the following characteristics [48]:

- 1.) The polymer and its degradation products should be nontoxic and nonabsorbable.
- 2.) It should be nonirritant.
- 3.) It should preferably form a strong noncovalent bond with the mucus or epithelial cell surface.
- 4.) It should adhere quickly to moist tissue and possess some site specificity.
- 5.) It should allow easy incorporation of the drug and offer no hindrance to its release.
- 6.) The polymer must not decompose on storage or during the shelf life of the dosage form.
- 7.) The cost of the polymer should not be high so that the prepared dosage form remains competitive.

Mucoadhesive polymers include synthetic polymers, for instance, poly(acrylic acid) [49], hydroxypropyl methylcellulose [50], poly(methylacrylate) derivatives [51] and thiolated polymers [7], as well as naturally occurring polymers such as hyaluronic acid [52] and chitosan [53]. Among these various possible bioadhesive polymeric hydrogels, poly(acrylic acid) has been considered as a good mucoadhesive. However,

due to a high transition temperature and higher interfacial free energy, poly(acrylic acid) does not wet the mucosal surface to the optimal level, causing loose interdiffusion of the polymer. Therefore, poly(acrylic acid) is copolymerized with polyethylene glycol (PEG) or poly(vinyl pyrrolidone) to improve these properties. It is important to realize that balanced adhesive and cohesive properties for a polymer is essential for its application in a transmucosal drug delivery systems, especially for the removable devices.

#### 2.4.4 Advantage of mucoadhesive drug delivery system

Mucoadhesive drug delivery systems, designed to adhere to mucosal surface, become interesting nowadays for transmucosal routes such as pulmonary, nasal, and oral routes due to their several advantages such as:

- 1.) Prolong residence time of the dosage form on mucosal tissue for increasing drug absorption and bioavailability of drug.
- 2.) High concentration gradient drug at the site of adhesion-absorption membrane which will create a driving force for the paracellular passive uptake.
- 3.) Immediate absorption from the bioadhesive drug delivery system without previous dilution and possible degradation in luminal fluids of body.
- 4.) Enhancement of topical action of certain drugs such as antibiotic against certain bacteria that colonize the stomach.

### 2.5 Chitosan

Chitosan was discovered by Rouget in 1859 after boiling chitin in concentrated potassium hydroxide and was given a formally name by Hoppe-Seyler in 1894. It was a form of fiber chemically biopolysaccharide processed from outer skeletons of arthropods, the epidermis of crustacean shells such as shrimp and crabs shells, prawns, lobsters and cell walls of some fungi such as *aspergillus* and *mucor*.

#### 2.5.1 Structure of chitosan

Chitosan ( $C_6H_{11}O_4N)_n$  is a linear polycationic biopolyaminosaccharide with high molecular weight composed of randomly distributed  $\beta$ -(1-4)-linked 2-acetamido-2-

deoxy-*D*-glucopyranose and 2-amino-2-deoxy-*D*-glucopyranose (Figure 2.4). It was obtained on commercially industrial scales by thermo-alkaline *N*-deacetylation of chitin which can be controlled by time, temperature and concentration of alkaline treatment [54]. Therefore, the degree of deacetylation has significant effect on the solubility, rheological properties and biological properties of chitosan [55]. NMR spectroscopy was used to determine deacetylation of chitosan and showed in the range of 60-100% for commercial scale. The chemical structure of a fraction of the repeating units of chitosan backbone contains hydroxyl groups (–OH) and amine pendent groups (–NH<sub>2</sub>) while the rest contains acetamide group (–NHCO) in its place. Both hydroxyl groups and reactive primary amine groups can be used to chemically alter its properties under mild reaction conditions [56].

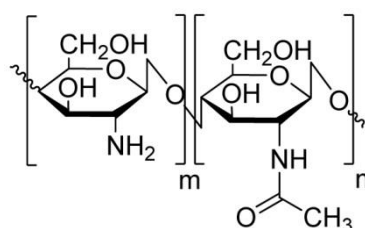


**Figure 2.4** Chemical structure of chitosan.

### 2.5.2 Physico-chemical properties of chitosan

Chitosan is firmly established as a biodegradable, biocompatible, low toxic and mucoadhesive polymer [57]. It is a cationic polysaccharide that can be degraded by several enzymes such as chitinases which are secreted by intestinal microorganisms, lysozyme which is highly concentrated in mucosal surfaces and by human chitotriosidase [58]. Chitosan exhibits the capacity to promote the absorption of poorly absorbed macromolecules across epithelial barriers by transient widening of cell tight junctions casing high mucoadhesive properties for drug delivery system [59]. Moreover, it is also a known antimicrobial agent against various bacteria such as *Escherichia coli* [60-62]. Chitosan is a weak base with  $pK_a$  of the *D*-glucosamine residue about 6.2-7.0, therefore; it is insoluble at neutral and alkaline pH values. However, chitosan provided



salt with inorganic and organic acids by dissolving in acetic acid, hydrochloric acid, glutamic acid and lactic acid to improve the solubility. The solubility of chitosan depends on degree of deacetylation and pH of solution providing the protonated positive charge of amino group.

### 2.5.3 Pharmaceutical applications

Recently, chitosan has been a variety of promising pharmaceutical uses and is presently considered as a novel carrier material in drug delivery systems [63]. Chitosan was evaluated in the form of beads [64], microsphere [65], microcapsules [66], tablets [67] and also used as a matrix for sustained release [68], a component of gels [69] and membranes [70].

Due to its low-toxicity, biocompatibility with human body tissue, chitosan has displayed their effectiveness for all forms of dressings-artificial skin, corneal bandages and suture thread in surgery-as well as for implants in bone repair or dental surgery [71]. Lastly, chitosan is an excellent medium for carrying and slow release of medicinal active principles in plants, animals and man. If degree of deacetylation and molecular weight can be controlled, it would be good advantage for developing size of chitosan for drug delivery system [72].

### 2.5.4 Mucoadhesive chitosan

Chitosan exhibited strong mucosal adhesion based on electronic interactions of cationic chitosan with negatively charged mucin [73]. Interactions with mucin appear to be both electrostatic, via  $\text{NH}_3^+$  groups on the chitosan with either  $\text{COO}^-$  or  $\text{SO}_3^-$  groups on the mucin carbohydrate side chains and/or hydrophobic, via  $-\text{CH}_3$  groups on acetylated chitosan residues with  $-\text{CH}_3$  groups on mucin side chains (depending on the degree of acetylation of the chitosan, local solvent conditions, for example, pH, ionic strength, and the degree of sulphonation and sialic acid content of the mucin). Moreover, these dramatic changes in solution turbidity are related to the aggregation of mucin particles in the presence of small portions of chitosan and subsequent disaggregation caused by excess of the cationic polymer in the solution (Figure 2.5).

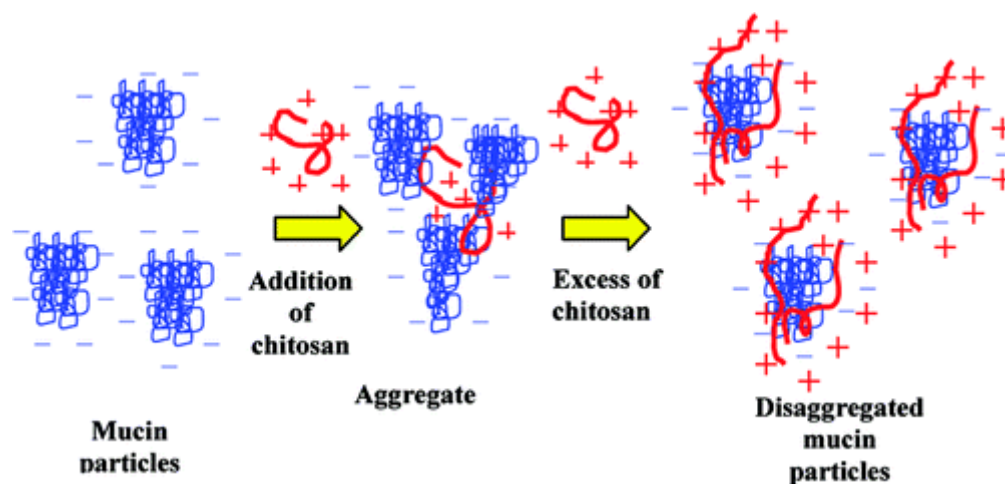


**Figure 2.5** Diagram depicting aggregation/disaggregation of pig gastric mucin in the presence of mucin [6].

## 2.6 Carbodiimide

A carbodiimide or methanediimine is a carboxyl-reactive chemical group consisting of the formula  $RN=C=NR$ . It hydrolyzes to form ureas or thioureas making them rarely found in nature. Carbodiimide provides the most popular and versatile method and was often used to activate carboxylic acids in order to produce the amide or ester functional group such as occur in proteins crosslinking, peptide synthesis to nucleic acid, preparation of immunoconjugates and many other biomolecules. Additives, such as *N*-hydroxybenzotriazole or *N*-hydroxysuccinimide, are often added to increase yields and decrease side reactions.

The water soluble 1-ethyl-3-(3-dimethylaminopropyl) carbodiimide hydrochloride (EDAC) and the water insoluble *N,N'*-dicyclohexyl carbodiimide (DCC) were the most readily available and commonly used carbodiimides for using as aqueous and non-aqueous organic synthesis, respectively (Figure 2.6).

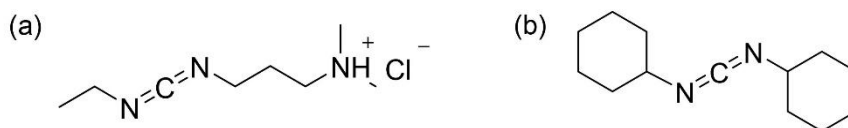


Figure 2.6 Chemical structures of EDAC and DCC.

### 2.6.1 Reaction of EDAC carbodiimide crosslinker

EDAC (also EDC or EDCI) is a water soluble carbodiimide which is typically efficient in acidic (pH 4.5) condition. It is generally used to react with carboxylic groups to form an active *O*-acylisourea intermediate which is easily displaced by nucleophilic attack from primary amino groups in the reaction mixture (Figure 2.7). The formation of an amide bond using EDAC is straightforward, but with several side effect complicating the subject. The primary amine forms an amide bond with the original carboxyl group and a soluble isourea derivative as EDAC by product is released. Because the *O*-acylisourea intermediate is unstable in aqueous solution, it fails to react with an amine resulting in hydrolysis of the intermediate. The use of solvents with low-dielectric constants such as dichloromethane or chloroform can minimize this side reaction.

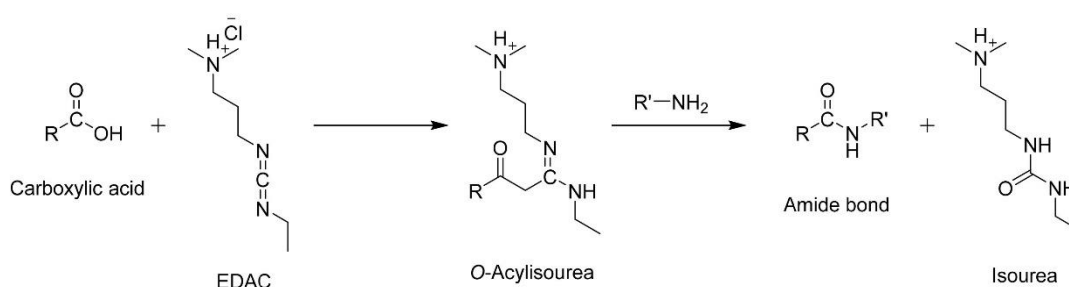
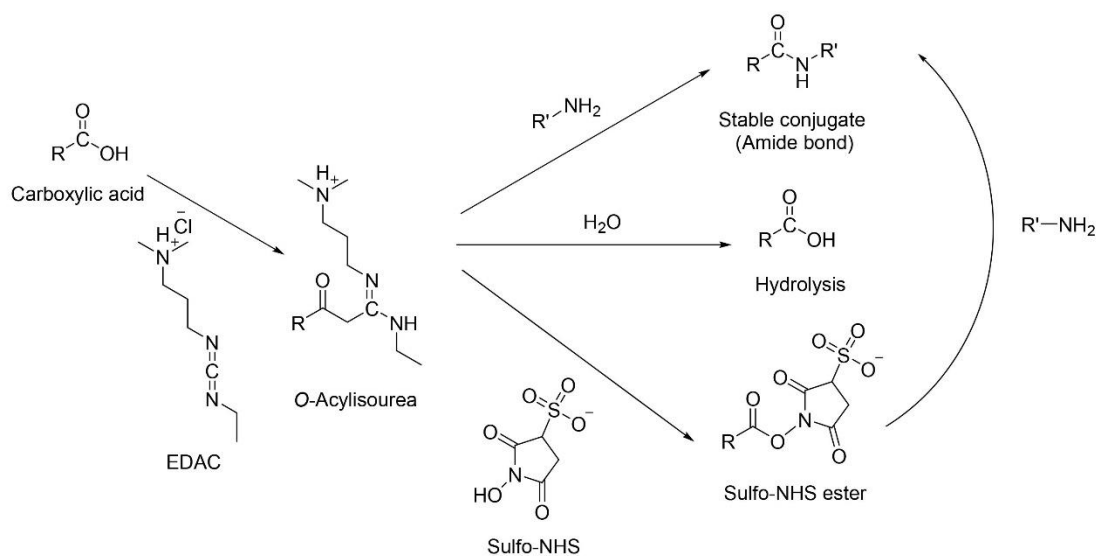


Figure 2.7 Carboxyl-to-amine crosslinking with the popular carbodiimide, EDAC.

Additionally, EDAC is often used in combination with *N*-hydroxysuccinimide (NHS) or its water soluble sulfo-NHS to increase coupling efficiency or create a stable amine-reactive intermediates (Figure 2.8). EDAC couples NHS to carboxyls, forming an NHS ester that is considerably more stable than the *O*-acylisourea intermediate while

allowing for efficient conjugation to primary amines at physiologic pH. EDAC can also be used to activate phosphate groups in the presence of imidazole for conjugation to primary amine. The method is sometimes used to modify, label, crosslink or immobilize oligonucleotides through their 5' phosphate groups.



**Figure 2.8** Carboxyl-to-amine-crosslinking using the carbodiimide EDAC and sulfo-NHS.

### 2.6.2 Application of EDAC crosslinking

EDAC is a powerful and versatile tool for crosslinking of primary amines to carboxylic acid groups. Peptides and proteins contain both primary amines and carboxylic acids (N- and C-termini, respectively, as well as in the side-chain of certain amino acids). Therefore, EDAC enables peptides and proteins to be easily conjugated to one another or to any compounds or solid surfaces that bear either carboxyl or amino groups and can use in the applications as follows.

- Peptide conjugation to carrier proteins
- Label carboxyl groups with amine compounds
- Immobilize peptides for affinity purification

- Attach peptides to surface materials



## CHAPTER 3

### ACIDIC RESISTANCE OF MUCOADHESIVE SULFANILAMIDE-CHITOSAN BASED ON HYDROGEL

#### 3.1 Introduction

Hydrogel, water swollen network of crosslinked polymer, which exhibited a large number of hydrophilic sites and was capable of absorbing and retaining considerable amounts of water without dissolving and demonstrate extraordinary capacity (>20%) for imbibe water into their network structure. These hydrogel were essential function for adhering on mucus membrane to consider in the field of the controlled drug release system due to the adequately strong interchain bridges between the polymer and the biological medium via a combination of surface and diffusional phenomena [47].

Chitosan, the one of the important marine polysaccharide, has been a candidate interested polymer for using as drug carrier due to its appealing properties such as biocompatibility, biodegradability, nontoxicity, biological properties such as immunological activity or healing properties, low production cost to human health and mucoadhesive properties [74-76]. It is a weak base obtained by deacetylation of chitin and is soluble in acidic condition ( $\text{pH} < 6.5$ ) [19]. Chitosan hydrogel has been interested and proven to be potential carrier for delivery of different drug molecules. Chitosan forms a hydrogel in the presence of small anionic molecules like citrates, sulfates and phosphates [77, 78] and anionic of metals such as Pt (II), Pd (II) and Mo (VI) [79, 80]. The properties of hydrogel depend on charge density, the size of charge anionic agent including the degree of deacetylation and the concentration of chitosan [81]. However, chitosan hydrogel showed low mechanical strength, limited ability to control release of encapsulated compound and to use in tissue engineering and poor acidic resistance [23].

Modification of chitosan by readily reacted at amino and/or hydroxyl groups can improve the properties of hydrogel. Variation of the functional groups onto chitosan to provide higher mucoadhesive ability, for example, thiolated chitosan as a new generation of mucoadhesive chitosan having free thiol group in polymeric backbone can form disulfide bonds with the cysteine-rich sub-domains present in mucin. There are a number of thiolated chitosan including chitosan-iminothiolane [9], chitosan-glutathione [10], chitosan-thioglycolic acid [82], and chitosan-thioethylamidine [11]. However, thiol group are less stable at pH above 5 due to their oxidizing to be disulfide bonds [13].

Previously, 4-carboxybenzenesulfonamide-chitosan (4-CBS-chitosan) revealed a 20-fold stronger mucoadhesion to mucin type II than native chitosan in the simulated gastric fluid (SGF; pH 1.2) [14]. Therefore, in this study, sulfanilamide as sulfonamide derivative was interested to provide higher mucoadhesion in acid condition. Nevertheless, the problem of these polymers was not swell enough to strongly adhere on mucus membrane. In order to prepare strongly mucoadhesion, modified chitosan was prepared in the form of hydrogel. These hydrogels were essential function for adhering on mucus membrane to consider in the field of the controlled drug release system via transmucosal delivery routes, such as pulmonary, nasal and oral routes due to the adequately strong interchain bridges between the polymer and the biological medium via a combination of surface and diffusional phenomena.

Mucoadhesive modified chitosans based on hydrogel were developed in order to prolong the residence time of the dosage at the site of application or absorption and intensified contact with the mucosa increasing the drug concentration gradient, and thus contribute to the therapeutic advantage of the system [83]. They displayed mucoadhesive properties at different hydration, but maximum adhesion will exist at an optimum hydration level. Modified chitosan was formed hydrogel in a presence of (1) chemically crosslinked hydrogel via covalent crosslinkers such as glutaraldehyde, oxalic acid, formaldehyde, glyoxal, and genipine (2) physically crosslinked hydrogel via ionic crosslinkers such as sodium tripolyphosphate and dextran or hydrogen bond of grafting with acrylic acid, poly(ethylene glycol) and polyaniline [18, 19]. Attempts have

been made to improve the acidic stability of modified chitosan hydrogel by chemical crosslinking on the surface with crosslinking agents [23]. However, most of the chemical crosslinkers may induce toxicity before administration and the preparation was not easy.

The present work is exclusively concerned with physically crosslinked hydrogel. These hydrogels have the sufficient ability to complete opening of the interpolymeric pores within the polymer matrix for the mobilization of the polymer chains, resulting in high mucoadhesion. Nevertheless, high content of physical crosslinking in chains with high swelling degree causes the formation of slippery mucilage due to overhydration [42].

To construct a mucoadhesive hydrogel, we synthesized sulfanilamide-chitosan (SM-chitosan) hydrogel using methyl acrylate as an intermediate. To reduce the problem of adhesion failure, overhydration of modified chitosan hydrogel was reduced by introducing of methyl ester group instead of some part of carboxylic acid group of acrylic acid and introducing of an aromatic part of SM. An aromatic part of SM quite limited of hydrogen bond providing high crosslinked content of hydrogel to reduce over swelling. Herein this research studied the interaction of an aromatic group as hydrophobic moiety, electrostatic force and hydrogen bonding of SM via methyl acrylate on chitosan affected on the formation of hydrogel, their acidic resistance and their interaction with mucus membrane.

## **3.2 Experimental Section**

### **3.2.1 Materials**

The following materials were obtained from commercial suppliers.

#### **3.2.1.1 Polymers**

Chitosan with a weight average molecular weight of 500 kDa and 81% degree of deacetylation was provided by Seafresh Chitosan (Lab.) Co., Ltd. in Thailand.



### 3.2.1.2 Chemicals

- Acetic acid, AR grade (Union chemicals)
- Acetone, commercial grade (Merck, Germany)
- Basic fuchsin (pararosaniline), analytical grade (Sigma-Aldrich, USA)
- Ethanol 95 %, commercial grade (Merck, Germany)
- Hydrochloric acid fuming 37%, AR grade (Merck, Germany)
- Methyl acrylate, analytical grade (Sigma-Aldrich, USA)
- Mucin from porcine stomach (type 2), analytical grade (Sigma-Aldrich, USA)
- Periodic acid, analytical grade (Sigma-Aldrich, USA)
- Potassium dihydrogen phosphate, AR grade (Merck, Germany)
- Potassium bromide, AR grade (Merck, Germany)
- Sodium chloride, AR grade (Merck, Germany)
- Sodium hydrogen phosphate, AR grade (Merck, Germany)
- Sodium hydroxide, AR grade (Merck, Germany)
- Sodium tripolyphosphate, AR grade (Sigma-Aldrich, USA)
- Sulfanilamide, AR grade (Sigma-Aldrich, USA)

### 3.2.1.3 Dialysis membrane

Dialysis membrane with molecular weight cut-off at 12,000-14,000 Da (Membrane Filtration Product, Inc.) was used to purify all modified chitosan.

### 3.2.2 Instruments

The instruments used in this study are listed in Table 3.1.

**Table 3.1** The instruments in this study.

Instrument	Manufacture	Model
Analytical balance	Mettler	AT 200
Diaphragm vacuum pump	Becthai	ME 2
Digital camera	Sony	T 70
Freeze dryer	Labconco	Freeze 6
FT-IR spectrometer	PerkinElmer	Spectrum RX I
Micropipette	Mettler Toledo	Volumate
NMR spectrometer	Agilent Technologies	Varian 400 MHz
PH-meter	Metrohm	744
TGA	PerkinElmer	Pyris Diamond TG/DTA
UV-VIS spectrometer	PerkinElmer	Lambda 800

### 3.2.3 Synthesis of SM-chitosan using *N*-carboxymethyl ester as an intermediate

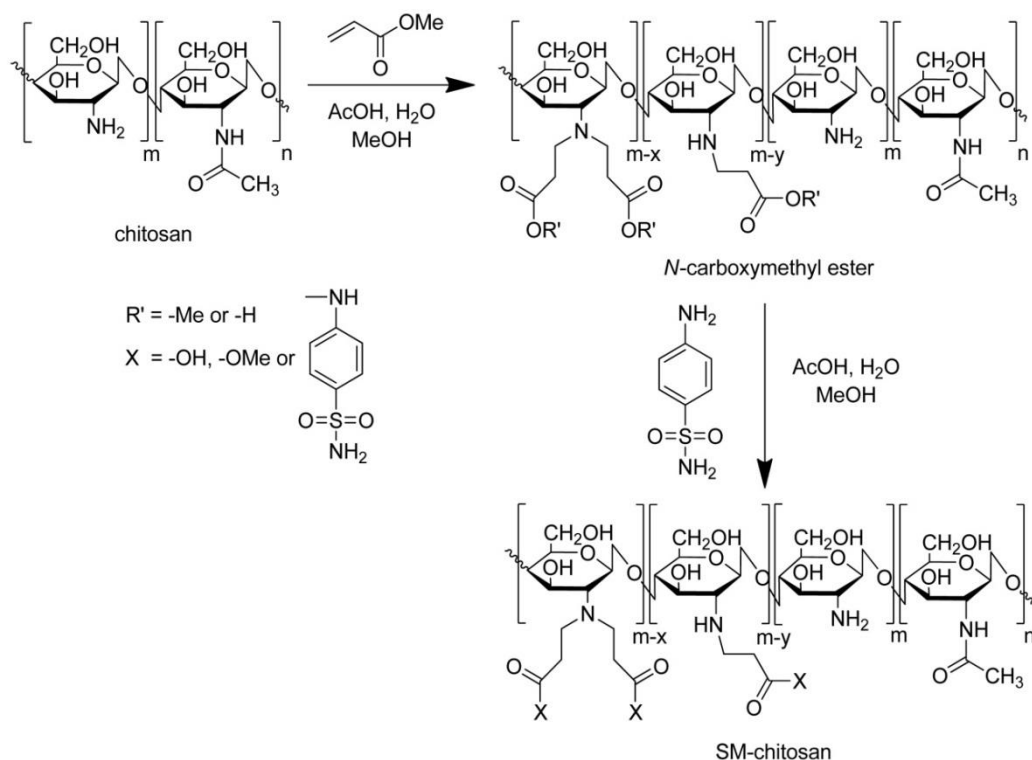
#### 3.2.3.1 Synthesis of *N*-carboxymethyl ester

Chitosan (1.00 g) was dissolved in 100 mL of 1% (v/v) acetic acid at room temperature overnight and then diluted with methanol (30 mL). Methyl acrylate was added into the solution and stirred at 65 °C for 3 days (Scheme 3.1). The reaction mixture was concentrated under reduced pressure to remove excess methyl acrylate and methanol. The remaining mixture was dialyzed for 1 day and lyophilized at -44 °C and 0.01 mbar to obtain *N*-carboxymethyl ester.

#### 3.2.3.2 Synthesis of SM-chitosan

*N*-carboxymethyl ester solution (0.25 g) in 15 mL of 1% (v/v) lactic acid and 15 mL of ethanol was added SM (0.05 g) and Zn/NH<sub>4</sub>Cl and then stirred for 3 days at 65 °C (Scheme 3.1). The reaction mixture was precipitated by excess acetone and

dialyzed for 1 day. The product was lyophilized at  $-44\text{ }^{\circ}\text{C}$  and 0.01 mbar to obtain SM-chitosan.



**Scheme 3.1** Reaction scheme of the covalent attachment of SM to chitosan using methyl acrylate as an intermediate.

### 3.2.4 Characterization

#### 3.2.4.1 $^1\text{H}$ Nuclear magnetic resonance spectroscopy ( $^1\text{H}$ NMR)

The  $^1\text{H}$  NMR spectra was performed on a Mercury Varian NMR spectrometer operated at 400 MHz (Agilent Technologies, CA, USA), using pulse accumulating of 64 scans. It was the most sensitive technique to determine the degree of substitution and characterized chitosan,  $N$ -carboxymethyl ester and SM-chitosan structure. The 30 mg of each compound were dissolved in 2% (v/v) trifluoroacetic acid ( $\text{CF}_3\text{COOH}$ ) in deuterium oxide ( $\text{D}_2\text{O}$ ).

### 3.2.4.2 Fourier transformed infrared spectroscopy (FT-IR)

FTIR measurement was carried on a Perkin Elmer Spectrum RX-1 with scanning from 600 to 4000  $\text{cm}^{-1}$ . The chitosan, *N*-carboxymethyl ester and SM-chitosan were dried, mixed with KBr at 1:100 (w/w), ground into a fine powder and pressed as pellets.

### 3.2.4.3 Thermogravimetric analysis (TGA)

Thermogravimetric (TG) analysis was carried out with METTLER STAR SW 9.01 TGA under a nitrogen atmosphere. All analyses were performed with 3-6 mg and placed onto aluminium pan in the balance system. TG was continuously recorded as a function of temperature at a temperature range of 30-600 $^{\circ}\text{C}$  and a heating rate of 25  $^{\circ}\text{C}/\text{min}$ .

### 3.2.5 Determination of the degree of $\text{CO}_2\text{Me}+\text{CO}_2\text{H}$ substitution ( $\% DS_{[\text{CO}_2\text{Me}+\text{CO}_2\text{H}]}$ ) and the degree of SM substitution ( $\% DS_{[\text{SM}]}$ ) on the chitosan by $^1\text{H}$ NMR

The degree of  $\text{CO}_2\text{Me}+\text{CO}_2\text{H}$  ( $\% DS_{[\text{CO}_2\text{Me}+\text{CO}_2\text{H}]}$ ) was the proportion of methyl ester and carboxylic group in the chitosan backbone. SM substitution ( $\% DS_{[\text{SM}]}$ ) on an intermedia of *N*-carboxymethyl ester was interest as it was related to the mucoadhesive property. Degree of substitution (DS) of  $\text{CO}_2\text{Me}$ ,  $\text{CO}_2\text{H}$  and SM were determined by  $^1\text{H}$  NMR spectra as previously reported [84] using Eqs. (3.1) and (3.2).

$$\% DS_{[\text{CO}_2\text{Me}+\text{CO}_2\text{H}]} = \left[ \frac{[H_b]}{[H3-H6]} \times \frac{5}{2} \right] \times 100 \dots \dots \dots (3.1)$$

$$\% DS_{[\text{SM}]} = \left[ \frac{[\text{SM}]}{[H3-H6]} \times \frac{5}{2} \right] \times 100 \dots \dots \dots (3.2)$$

where  $[H_b]$  is the integral of the singlet protons at 2.65 ppm,  $[\text{SM}]$  is the integral of the benzene ring of SM protons at 7.97-8.00 ppm and  $[H3-H6]$  is the integral of the H3-H6 protons of chitosan at 3.44-3.63 ppm.

### 3.2.6 In vitro bioadhesion of mucin to chitosan, *N*-carboxymethyl ester and SM-chitosan

#### 3.2.6.1 Mucus glycoprotein

The Periodic Acid Schiff (PAS) method is widely used for both the quantitative and qualitative analysis of mucins, glycoproteins, glycogen and other polysaccharides in tissues and cells. The PAS colorimetric assay for the detection of glycoproteins was used to determine the free mucin concentration, so as to evaluate the amount of mucin adsorbed onto the chitosan, *N*-carboxymethyl ester and SM-chitosan. Schiff reagent contained 100 mL of 1% (w/v) basic fuchsin (pararosaniline) in an aqueous solution and 20 mL of 1 M HCl. To this was added sodium metabisulphite (1.67% (w/v) final) just before use, and the resultant solution was incubated at 37 °C until it became colorless or pale yellow. The PAS reagent was freshly prepared by adding 10  $\mu$ L of 50% (v/v) periodic acid solution to 7 mL of 7% (v/v) acetic acid solution.

#### 3.2.6.2 Adsorption of mucin on chitosan, *N*-carboxymethyl ester and SM-chitosan

A 0.5% (w/v) mucin solution in each of four broadly solutions that differ in pH, namely simulated gastric fluid (SGF, pH 1.2), 0.1 N simulated duodenum buffer (SDF, pH 4.0), 0.1 N phosphate buffer (PB, pH 5.5) and simulated intestinal fluid (SIF, pH 6.4) media, were prepared. Chitosan, *N*-carboxymethyl ester and SM-chitosan were dispersed (at 20 mg/1.5 mL final) in the above mucin solutions and shaken at 37 °C for 2 hours. Then the dispersions were centrifuged at 12,000 rpm for 2 mins to pellet the polymer-mucin and the supernatant was harvested and used for the measurement of the free mucin content. The mucin concentration was calculated by reference to the calibration curve, and the amount of mucin adsorbed to the polymers was calculated as the difference between the total amount of mucin added and the free mucin content in the supernatant. Standard calibration curves were prepared from the eight mucin standard solutions (0.05, 0.1, 0.2, 0.3, 0.4, 0.5, 0.6 and 1 mg/mL). After adding 0.1 mL of periodic acid reagent, the solutions were incubated at 37 °C for 2 h before 0.1 mL of Schiff reagent was added and incubated at room temperature for 30 mins.

Next, 0.1 mL aliquots of the solution were transferred in triplicate into a 96-well microtiter plate and the absorbance at 555 nm was recorded. The mucin contents were then calculated by reference to the standard calibration curve.

### 3.2.7 Statistical analysis

All measurements were performed in triplicate in each experiment with the results presented as the mean  $\pm$  1 SD. Statistical analysis was performed by one-way ANOVA using Microsoft Excel (Microsoft Corporation) with  $P < 0.05$  considered to indicate statistical significance.

## 3.3 Results and discussion

### 3.3.1 Synthesis and structural analysis of *N*-carboxymethyl ester and SM-chitosan

To well understand the synthesis of SM-chitosan, michael reaction of chitosan with methyl acrylate has been successfully prepared. The covalent attachment of SM to *N*-carboxymethyl ester as an intermediate was achieved via coupling the carboxylic acid (-COOH) or ester group (-CO<sub>2</sub>R) of *N*-carboxymethyl ester to the primary amine group (-NH<sub>2</sub>) of SM. The obtained SM-chitosan showed the appearance as an odorless, white fibrous polymer and was easily dissolved in 1% (v/v) acetic acid solution to form a high viscosity pale yellow gel. It could not be dissolved in distilled water DMSO and SGF; nevertheless, it became swollen gel in distilled water and SGF (Figure 3.1). The phenomena occurred due to the formation of hydrogen bonds between the oxygen of the hydroxyl group and the carboxylic acid group of the methacrylate side chain or the nitrogen of sulfonamide unit. This interaction allowed the absorption liquids and swelling which transformed the system into a hydrogel. Moreover, the aromatic stacking of SM was used to control the swelling degree of hydrogel to against high content of crosslink in chains and the structure of SM-chitosan hydrogel formed by physically crosslinked interaction. The obtained SM-chitosan was characterized by <sup>1</sup>H NMR, FT-IR and TGA analysis.



**Figure 3.1** Physical appearance of SM-chitosan in distilled water and physical crosslinked interaction of SM-chitosan hydrogel.

### 3.3.2 Characterization of *N*-carboxymethyl ester and SM-chitosan

#### 3.3.2.1 $^1\text{H}$ Nuclear magnetic resonance spectroscopy ( $^1\text{H}$ NMR)

The chemical structures of chitosan, *N*-carboxymethyl ester and SM-chitosan were characterized by  $^1\text{H}$  NMR as showed in Figure 3.2. Data for SM-chitosan was as follows:  $^1\text{H}$  NMR ( $\text{D}_2\text{O}/\text{CF}_3\text{COOH}$ ):  $\delta$  (ppm) 7.99 (d, 2H,  $J = 8.0$  Hz, Ph), 7.80 (d, 2H,  $J = 8.0$  Hz, Ph), 4.63 (s, 1H, H1), 4.36 (s, 1H, H1'), 3.67-3.48 (m, 4H, H3, H4, H5 and H6), 2.94 (s, 1H, H2), 2.65 (s,  $\text{H}_b$ ) and 1.85 (s, 3H,  $\text{NHCOCH}_3$ ).

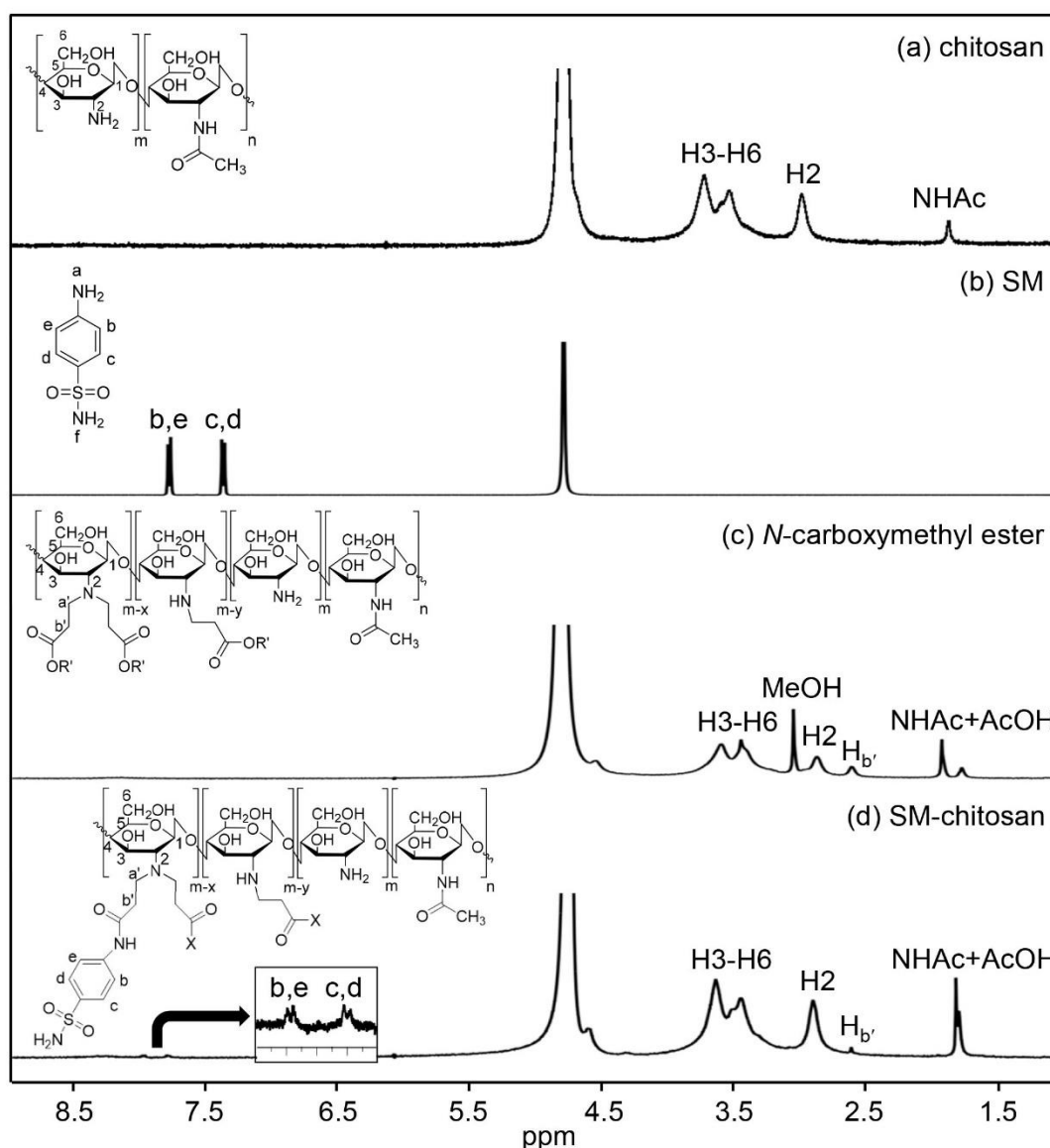


**Figure 3.2**  $^1\text{H}$  NMR spectra of the (a) chitosan, (b) SM and (c) *N*-carboxymethyl ester and (d) SM-chitosan.

The  $^1\text{H}$  NMR spectrum of chitosan (Figure 3.2a) showed a signal at 1.78 ppm (s, 3H) due to the acetyl protons of the GluNAc units, a singlet at 2.89 ppm (s, 2H) attributed to the H at the C2 position of the GluN units, whilst the signals due to the hydrogen atoms (H3-H6) in the chitosan ring were observed at around 3.63-3.44 ppm.

The  $^1\text{H}$  NMR spectrum of SM (Figure 3.2b) showed the signals at 7.80 ppm (d, 2H,  $J = 7.6$  Hz) and 7.39 (d, 2H,  $J = 7.6$  Hz), which were assigned to the aromatic protons of the sulfonamide ring, respectively.



The  $^1\text{H}$  NMR spectra of the *N*-carboxymethyl ester (Figure 3.2c) showed the characteristic peaks of both chitosan and methyl acrylate segments. Both the GluNAc and GluN groups overlapped with  $\text{H}_a$  position contributed to the multiple peak regions of numeric carbons (H3-H6) from 3.56 to 3.41 ppm, a singlet peak at 2.83 ppm from the C2-H position of GluN and a singlet peak at 2.57 ppm from the  $\text{H}_b$  position. The chemical shift at 1.88 ppm (s, 3H) was assigned to the acetyl proton of GluNAc.

The  $^1\text{H}$  NMR spectra of the SM-chitosan (Figure 3.2d) showed the characteristic peaks of chitosan, methyl ester and SM segments. The aromatic proton position of SM showed at 7.99 ppm (d, 2H,  $J = 8.0$  Hz) and 7.80 ppm (d, 2H,  $J = 8.0$  Hz). The intensity of a singlet peak of  $\text{H}_b$  position at 2.65 ppm was reduced because methyl ester or carboxylic group was substituted by SM. These results support that the SM-chitosan were successfully synthesized.

### 3.3.2.2 Fourier transformed infrared spectroscopy (FT-IR)

FT-IR was a one of the important and widely analytical techniques to determine functional group of compounds based on the vibration of molecule. FT-IR analysis was performed to determine the SM-chitosan formed between *N*-carboxymethyl ester and SM as shown in Figure 3.3. The FT-IR spectrum of the SM-chitosan (Figure 3.3d) revealed the characteristic peaks of both chitosan (Figure 3.3a) and SM (Figure 3.3b). It showed a broad absorption peak at  $3418\text{ cm}^{-1}$  corresponding to O-H and N-H symmetrical stretching vibrations and the typical bands of symmetric C-H stretching vibration showed at  $2920\text{ cm}^{-1}$  and  $2880\text{ cm}^{-1}$  attributed to pyranose ring [85]. The peaks at  $1647\text{ cm}^{-1}$  and  $1597\text{ cm}^{-1}$  were assigned to C=O stretching of amide I overlapped with C=O stretching of methyl ester of methyl acrylate and N-H stretching of amide II overlapped with N-H stretching of sulfonamide unit, respectively. Nevertheless, the absorption at  $1723\text{ cm}^{-1}$  was disappeared when compared with *N*-carboxymethyl ester spectrum (Figure 3.3c) due to the substitution of SM at carboxyl side chain. The absorption band at  $1154\text{ cm}^{-1}$  was assigned to the anti-symmetric stretching of C-O-C bridge, and  $1071$  and  $1028\text{ cm}^{-1}$  were assigned to the skeletal vibrations involving the C-O stretching. An increase in the absorbance of the peak at  $1827\text{-}1504\text{ cm}^{-1}$  was also observed when compared with that at  $1233\text{-}1024\text{ cm}^{-1}$  of the C-O-C cyclic ethers stretching. This is in accordance with that the substitution of the C=C aromatic ring stretching of SM at  $1647\text{ cm}^{-1}$  possibly overlapped the amide I band stretching of chitosan. Moreover, the intensity peak of asymmetric and symmetric S=O stretching at  $1317\text{ cm}^{-1}$  and  $1151\text{ cm}^{-1}$  did not change reflects the fact that the

substitution of SM onto chitosan backbone was not so high related with the  $^1\text{H}$  NMR result.

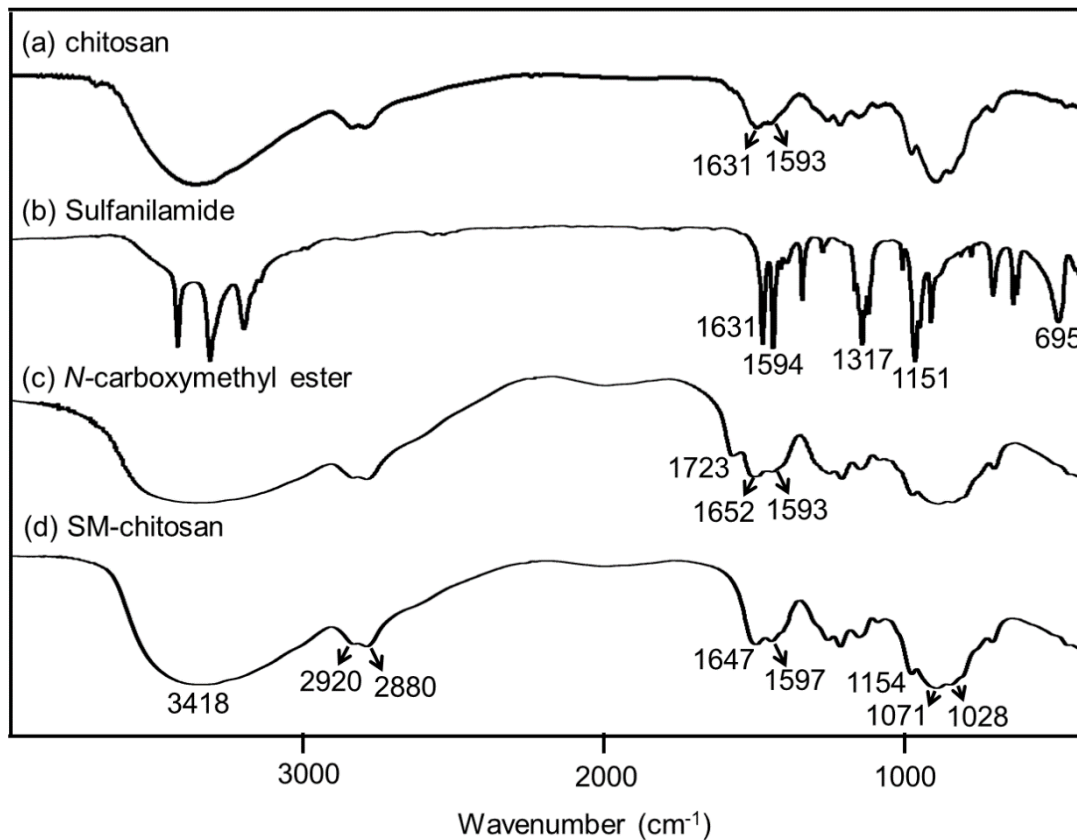


**Figure 3.3** FT-IR spectra of the (a) chitosan, (b) SM and (c) *N*-carboxymethyl ester and (d) SM-chitosan.

### 3.3.2.3 Thermogravimetric analysis (TGA)

The TG thermograms of the chitosan, SM, *N*-carboxymethyl ester and SM-chitosan are summarized in Figure 3.4 to evaluate the thermal stability of polymers and its degradation temperature. Increasing temperature of the samples led to the increase of weight loss degree (slope) which was different according to various samples and reflected the degradation of each component in the materials.

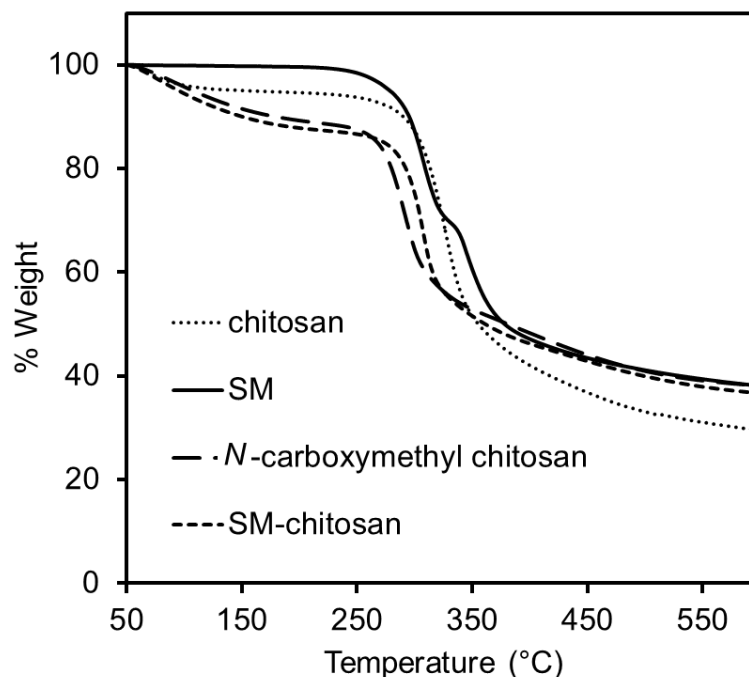


**Figure 3.4** TGA thermograms of the (a) chitosan, (b) SM and (c) *N*-carboxymethyl ester and (d) SM-chitosan.

The TG curve of modified chitosans, *N*-carboxymethyl ester and SM-chitosan, showed a weight loss in two stages and was broadly similar to that for native chitosan. The first stage ranged between 50 °C and 150 °C showed about 10% loss in weight for both samples which are attributed to loss of adsorbed and bound water and residue of acetic acid [86]. While the second stage of *N*-carboxymethyl ester and SM-chitosan began at 270 °C to 315 °C and 295 °C to 333 °C with a 45% and 50% total weight loss, respectively which are likely to be the degradation of modified chitosan backbone. The total weight loss of the SM-chitosan at 600 °C was 63% lower than that of native chitosan at 70%. Therefore, the coupling of SM as aromatic moieties onto the chitosan backbone gave the substituted units higher a thermal stability than that of native chitosan [87] due to hydrophobic interaction, resulting in a lower weight loss than the chitosan. SM-chitosan thermogram showed a higher thermal stability and decomposition temperature than chitosan, and then may be more suitable as a polymer for drug delivery systems.

### 3.3.4 Determination of the degree of $\text{CO}_2\text{Me}\pm\text{CO}_2\text{H}$ substitution ( $\% DS_{[\text{CO}_2\text{Me}+\text{CO}_2\text{H}]}$ ) and the degree of SM substitution ( $\% DS_{[\text{SM}]}$ ) on the chitosan

The determination of the degree of substitution (%DS) played a significant role to evaluate the physical and chemical properties of each sample.  $^1\text{H}$  NMR measurement was an accurate technique to calculate %DS as long as the impurity peaks do not overlap with the sample peaks [88]. The intensity of the signals due to the hydrogen atom of carboxylic acid and carboxylate at C2 position, the hydrogen atoms of C3-C6 of chitosan and the protons of grafted SM via *N*-carboxymethyl ester were used to determine  $\% DS_{[\text{CO}_2\text{Me}+\text{CO}_2\text{H}]}$  and  $\% DS_{[\text{SM}]}$  values (Table 3.2).

From the spectral analysis,  $^1\text{H}$  NMR peak of  $\text{CO}_2\text{Me}$  was overlapped with  $\text{CO}_2\text{H}$  at 2.57 ppm and was determined  $\% DS_{[\text{CO}_2\text{Me}+\text{CO}_2\text{H}]}$  to be 30.56% for 3 days of reaction using Eq. (3.1). However,  $\% DS_{[\text{CO}_2\text{Me}+\text{CO}_2\text{H}]}$  after grafting with SM showed only 11.97% because SM was conjugated at carboxyl position, then  $\% DS_{[\text{CO}_2\text{Me}+\text{CO}_2\text{H}]}$  was decreased. Moreover, the formation of *N*-carboxymethyl ester could not well proceed after 3 days because methyl acrylate was gradually hydrolyzed to be carboxyl groups [89]. In case of  $\% DS_{[\text{SM}]}$  onto chitosan, it was determined to be 6.21% for 3 days using Eq. (3.2).

**Table 3.2** Degree of CO<sub>2</sub>Me+CO<sub>2</sub>H substitution and SM substitution onto chitosan and the solubility test in various solvent.

Condition	DS (%)		Solubility <sup>c</sup>				Gelation <sup>d</sup>		
	CO <sub>2</sub> Me+CO <sub>2</sub> H <sup>a</sup>	SM <sup>b</sup>	H <sub>2</sub> O	DMSO	Aq. AcOH	SGF	H <sub>2</sub> O	DMSO	SGF
Chitosan	-	-	-	-	O	O	-	-	-
<i>N</i> -carboxymethyl ester	30.56	-	X	X	O	X	+++	-	+++
SM-chitosan	11.97	6.21	X	X	O	X	++	-	++

<sup>a</sup>By <sup>1</sup>H NMR absorption spectroscopy from the peak area at δ 2.65 ppm

<sup>b</sup>By <sup>1</sup>H NMR absorption spectroscopy from the peak area at δ 7.75 ppm

<sup>c</sup>O, soluble; X, insoluble; concentration of sample = 1 mg/mL

<sup>d</sup>By immersing in distilled water and dimethylsulfoxide; -, not show swelling properties; ++, medium swelling properties; +++, high swelling properties.

### 3.3.5 In vitro bioadhesion of mucin to chitosan, *N*-carboxymethyl ester and SM-chitosan

Mucoadhesion may be defined as the adhesion across the interface between a polymer and mucus membrane via ionic bonds, covalent bonds, hydrogen bonds, van der Waal bonds or hydrophobic bonds [42]. Generally, mucoadhesion is considered to occur in 3 major stages: wetting, interpenetration, and mechanical interlocking between mucus and polymer [90]. The strength of mucoadhesion due to various factors such as the molecular mass of polymers or contact time has advantages for optimized local drug delivery or optimized systemic delivery such as retaining a dosage form at the site of action or retaining a formulation in intimate contact with absorption site. An increase of molecular mass leads to a higher internal cohesion of molecule provided typically increases the mucoadhesion. Contact time with mucus also induces a higher swelling rate of the polymer and biological membrane to govern a higher mucoadhesion.

Therefore, in this study, the comparison of mucoadhesion of chitosan, *N*-carboxymethyl ester and SM-chitosan was investigated in SGF (pH 1.2), SDF (pH 4), PB (pH 5.5) and SIF (pH 6.4) (Figure 3.6). The result showed that the adsorbed mucin onto *N*-carboxymethyl ester and SM-chitosan in all pH was higher than native chitosan, especially in SGF (pH 1.2). *N*-carboxymethyl ester and SM-chitosan revealed 2.50- and 2.61-folds significantly higher mucoadhesive component than that of native chitosan. The amount of the adsorbed mucin onto polymer depended on  $pK_a$  of polymer and sialic acid of mucus membrane. Chitosan is a cationic polyelectrolyte with  $pK_a$  about 6.5-6.8, whilst the  $pK_a$  and PI values of sialic acid and mucin were 2.6 and ~3-5, respectively [42, 91]. Therefore, the amount of adsorbed mucin onto chitosan decreased at lower pH values in an acidic environment, being maximal (0.77) at PB (pH 5.5) and minimal (0.36) at SGF (pH 1.2) because the amount of ionized sialic acid and protonated amine unit of chitosan were decreased [2]. Therefore, the ionic interaction between amine unit of chitosan protonated to  $NH_3^+$ , and ionized sialic acid,  $COO^-$  or  $SO_3^-$  group, on the mucin glycoprotein side chain was reduced, resulted in the decrease of mucoadhesion of chitosan at SGF (pH 1.2).



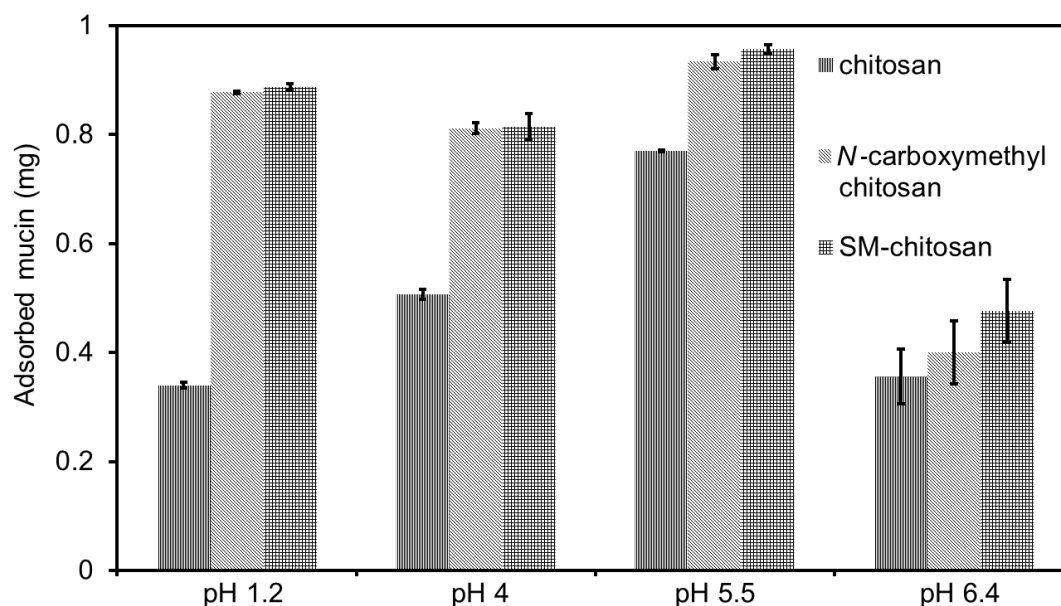


**Figure 3.5** Adsorption of mucin on chitosan, *N*-carboxymethyl ester and SM-chitosan at SGF (pH 1.2), SDF (pH 4.0), PB (pH 5.5) and SIF (pH 6.4). Data are shown as the mean  $\pm$  SD and are derived from three independent repeats. Means with a different lower case letter are significantly different ( $P < 0.01$ ).

For *N*-carboxymethyl ester, not only ionic interaction was formed but also the formation of hydrogen bond amongst the functional group of polymer and mucosal layer also had an influential role on mucoadhesion. The functional groups responsible for hydrogen interaction include hydroxyl, carboxyl and amino group [92]. Then, carboxyl group and hydroxyl group of acrylate side chain provided strong hydrogen bond to govern higher adsorbed mucin than native chitosan. Moreover, the hydrophobic effect, the  $-\text{CH}_2$  moieties of acrylate interacted with the  $-\text{CH}_3$  groups on the mucin side chain was one of the keys to increase mucoadhesion. Nevertheless, in acidic environment (SGF (pH 1.2), SDF (pH 4) and PB (pH 5.5)), adsorbed mucin on *N*-carboxymethyl ester was not showed the significantly different values due to more important role of hydrogen bonding than ionic interaction. It only displayed significantly higher values than that of chitosan for 2.50-, 1.60 and 1.21- folds in SGF (pH 1.2), SDF (pH 4) and PB (pH 5.5), respectively.

In case of SM-chitosan, SM appeared  $pK_a$  value at 10.4. Therefore, SM was deprotonated at low pH. Only ionic interaction of remained amine unit of chitosan, hydrogen bonding of *N*-carboxymethyl ester residue and hydrophobic effect of  $-CH_2$  moieties of acrylate had a crucial role in adsorbed mucin. Furthermore, an aromatic SM side chain was an additionally factor of hydrophobic effect to raise mucoadhesive values of SM-chitosan for 2.61-, 1.61- and 1.24-folds of native chitosan in SGF (pH 1.2), SDF (pH 4) and PB (pH 5.5), respectively. However, it showed only slightly increased values from *N*-carboxymethyl ester.

On the other hand, at SIF (pH 6.4), all polymers were not readily well soluble and were probably presented in a more coiled configuration with less protonated amino groups that can react with mucus membrane resulted in low adsorbed mucin.

### 3.4 Conclusion

In summary, the synthesis and characterization of a novel SM-chitosan hydrogel was reported to improve mucoadhesive properties of native chitosan and acidic resistance especially in SGF (pH 1.2). SM-chitosan showed degree of SM substitution at 6.21%. Moreover, it revealed high mucoadhesive properties in an acidic condition due to hydrogen bonding, ionic interaction and hydrophobic effect. These results suggested that SM-chitosan hydrogel was interesting for the application requiring drug carrier which is suitable for using in gastrointestinal tract (pH < 6).



## CHAPTER IV

### SELF-ASSEMBLY MUCOADHESIVE NANOFIBERS

#### 4.1 Introduction

Over the past few decades, nanofibers have been studied in medical science on the application of wound healing, tissue engineering, artificial organ components and drug delivery due to special properties mainly on their large surface area to volume ratio. Several methods have been developed to fabrication nanofibers, including template synthesis [93, 94], phase separation [95, 96], electrospinning [96] and self-assembly [97, 98]. The template synthesis is an effective route to make nanofibers or nanotubes using a nanoporous membrane as a template. On the other hand, the limitation of this method is it cannot make one-by-one continuous nanofibers and the membrane should be soluble so that it can be removed after synthesis to obtain nanofibers or nanotubes [99]. Although the phase separation requires very minimal in term of equipment, the process takes relatively long period of time to transfer the solid polymer into the nanofibers consisting of dissolution, gelation, extraction using a different solvent, freezing, and drying [99]. Electrospinning has been recognized as an efficient technique to provide nanofibers. However, electrospinning requires a high voltage to create an electrically charged jet of polymer, provides broad range of fiber thickness, low mechanical properties of fiber meshes and does not control over 3D pore structure [100]. Polyethylene oxide was introduced to chitosan to fabricate ultrathin hybrid electrospun nanofibers with diameter ranging from 80-180 nm. However, it swelled rapidly in water and completely lost its fibrous structure within a few days [101]. Bhattarai et al. studied electrospinning to fabricate chitosan based nanofibers that can be a fiber size ~40 nm and the prolonged immersion of membrane in water up to 4 weeks [102]. However, triton X-100<sup>TM</sup> and DMSO were introduced into the solution as a surfactant and cosolvent to reduce bead-like structure that embedded in the fibers and increase fiber yield, respectively. Geng et al. prepared

electrospun homogeneous of nanofibers of pure chitosan dissolved in strongly aqueous acetic acid solution without addition of other solvent [103]. Bead free and more uniform nanofibers were formed by controlling the molecular weight of chitosan at 106,000 g/mol at 7% concentration, dissolved in 90% aqueous acetic acid solution.

The macromolecular self-assembly of nanomaterials into high-order and stable structures has become an attractive strategy with preprogrammed non-covalent bonds [104]. Unlike electrospinning, self-assembly provides the autonomous organization of molecules into patterns or structures without human intervention and produce much thinner nanofibers only several nanometers in diameter [99]. Peptide amphiphiles (PAs), a new class of biomaterials, were designed to understand the self-assembly of amphiphiles and the chemical complexity of peptides. PAs include a class of molecules that form highly hydrophobic chains. These chains can attach to hydrophilic peptides to create amphiphilic hybrid molecules. Niece et al. prepared self-assembly nanofibers by combining two bioactive PA molecules and yielded nanofibers approximately 7 nm in diameter and several micrometers long [105]. Hartgerink et al. prepared PAs of mono-alkyl chains attached via the *N*-terminus without proline residues, representing a highly flexible method for achieving chemical functionality in one-dimensional nanostructures [33]. These PAs can self-assemble into nanofibrous cylindrical micelles with almost equivalent tolerant properties of an amino acid. Paramonov et al. studied the role of hydrogen bonding and amphiphilic packing in the self-assembly of a series of 26 PA derivatives [106]. Due to the ease of synthesis and the chemically tolerant nature of self-assembled PAs, simulating PAs is of great interest. Nevertheless, self-assembled PAs are unstable at physiological pH unless the pH is controlled by the addition of a multivalent cation or by internally cross-linking the PA through covalent bonds [107].

Chitosan, another natural biomaterial, was chosen herein as a molecular model because its polymer chain is biocompatible, stable, non-toxic to human health, mucoadhesive and flexible. Chitosan has been extensively employed in biomedical materials, especially for drug delivery applications [6]. In addition, chitosan is a unique natural alkaline polysaccharide that contains a double helix structure. Chitosan is

easily prepared from chitin and has a reactive amino group that can be chemically modified and can carry a positive charge during reactions. Moreover, chitosan can be prepared into nanofibers without the need to control temperature and pH or to add a co-assembling molecule.

To construct the nanofibers, we designed and synthesized stearic acid-4-carboxybenzenesulfonamide-*N*-trimethylchitosan (SA-4-CBS-TMC) to induce the self-assembly of well-ordered nanofibers in distilled water. The nanofiber assembly relied on a balance between the hydrophobic effect of the stearic acid (SA), the aromatic stacking of 4-carboxybenzenesulfonamide (4-CBS), the electrostatic interactions of  $-N^+(CH_3)_3$  and the hydrogen bonding of the chitosan backbone. The driving force for the hydrophobic packing of the SA chains in an aqueous environment allows the specific presentation of 4-CBS and  $-N^+(CH_3)_3$  hydrophilic signals on the surface of the assembled nanofibers, leading to an enhancement of helical structure. The great improvement derived from utilizing SA-4-CBS-TMC is that the structural features of the final assembly can be finely, easily and readily tuned by modulating only the factors pertaining to the re-dispersed concentration independent of the assembling environment (e.g., pH, co-assembling molecule and temperature) while providing a narrow size distribution.

## 4.2 Experimental section

### 4.2.1 Materials

The following materials were obtained from commercial suppliers.

#### 4.2.1.1 Polymers

Chitosan with a weight average molecular weight of 500 kDa and 81% degree of deacetylation was provided by Seafresh Chitosan (Lab.) Co., Ltd. in Thailand.

#### 4.2.1.2 Chemicals

- Acetic acid, AR grade (Union Chemicals, Thailand)
- Acetone, commercial grade (Merck, Germany)
- 4-Carboxybenzenesulfonamide (4-CBS) 97%, AR grade (Sigma-Aldrich, USA)

- Ethanol 95 %, commercial grade (Merck, Germany)
- 1-ethyl-3-(3-dimethylaminopropyl) carbodiimide hydrochloride (EDAC), (Sigma-Aldrich, USA)
- Hydrochloric acid fuming 37%, AR grade (Merck, Germany)
- *N*-Hydroxysuccinimide (NHS), AR grade (Sigma-Aldrich, USA)
- Methyl iodide (CH<sub>3</sub>I), AR grade (Sigma-Aldrich, USA)
- *N*-Methyl-2-pyrrolidone (NMP), AR grade (Merck, Germany)
- Mucin from porcine stomach (type 2), Analytical grade (Sigma-Aldrich, USA)
- Potassium dihydrogen phosphate, AR grade (Merck, Germany)
- Potassium bromide, AR grade (Merck, Germany)
- Sodium chloride, AR grade (Merck, Germany)
- Sodium hydrogen phosphate, AR grade (Merck, Germany)
- Sodium hydroxide, AR grade (Merck, Germany)
- Sodium tripolyphosphate, AR grade (Sigma-Aldrich, USA)
- Stearic acid, AR grade (Sigma-Aldrich, USA)

#### 4.2.1.3 Dialysis membrane

Dialysis membrane with molecular weight cut-off at 12,000-14,000 Da (Membrane Filtration Product, Inc. was used to purify all modified chitosan.

#### 4.2.2 Instruments

The instruments used in this study are listed in Table 4.1.

**Table 4.1** The instruments in this study.

Instrument	Manufacture	Model
Analytical balance	Mettler	AT 200
Diaphragm vacuum pump	Becthai	ME 2
Digital camera	Sony	T 70
Elemental analysis	Perkin Elmer	PE2400 Series II
Freeze dryer	Labconco	Freeze 6
FT-IR spectrometer	PerkinElmer	Spectrum RX I
Micropipette	Mettler Toledo	Volumate
NMR spectrometer	Agilent Technologies	Varian 400 MHz
pH-meter	Metrohm	744
Scanning electron microscope	Philips and Jeol	XL30CP and JSM-6480LV
TGA	PerkinElmer	Pyris Diamond TG/DTA
UV-VIS spectrometer	PerkinElmer	Lambda 800
Viscometer	Brookfield	Model DV-II
Vortex	Scientific industries	Vortex-genie-2
X-ray diffraction	Rigaku	Dmax 2200 Ultima

#### 4.2.3 Synthesis of *N*-trimethyl chitosan chloride (TMC)

TMC was synthesized according to previously method [108]. Briefly, the mixture of 100 mL of a 1% (w/v) of chitosan in 1% (v/v) acetic acid solution, 5 ml of 15% (w/v) aqueous sodium hydroxide and 30 ml of methyl iodide (CH<sub>3</sub>I) in 30 mL of *N*-methyl pyrrolidone (NMP) was heated at a temperature 60 °C for 45 mins. The product was precipitated with 80 % (v/v) ethanol and isolated by centrifugation (12,000 rpm, 5 mins,

RT). After washing with ethanol, the product was dissolved in 40 mL of (5% w/v) aqueous sodium chloride solution to exchange the iodide ion with a chloride ion. The polymer was precipitated with ethanol and isolated by centrifugation (12,000 rpm, 5 mins, RT). This product was dissolved in 40 mL water, precipitated with ethanol to remove the remaining sodium chloride from material and lyophilized at -44 °C and 0.01 mbar and stored at 4 °C before use. Yield: 92.54%. Elemental analysis (EA) was used to determine which elements are present in the polymers. TMC showed C, 28.02%; H, 5.24% and N, 4.26%.

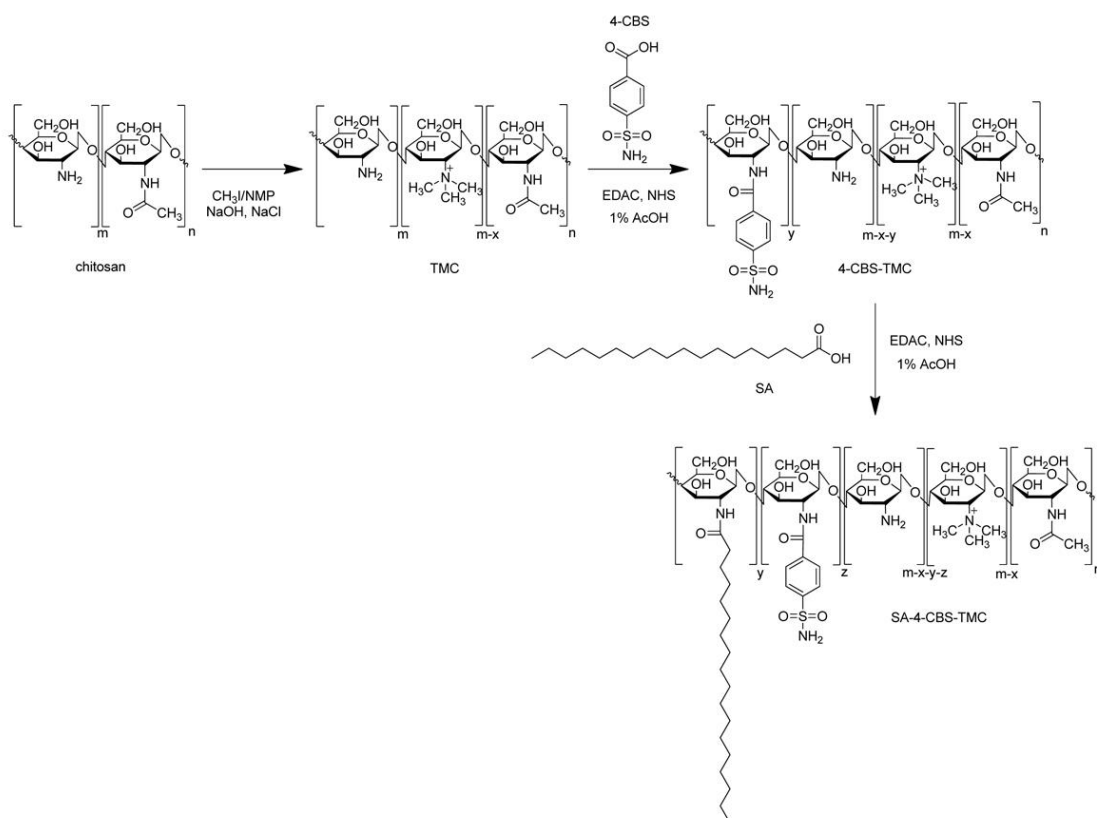
#### **4.2.4 Synthesis of 4-carboxybenzenesulfonamide-*N*-trimethyl chitosan (4-CBS-TMC)**

TMC was fully dissolved (0.01 g/mL) in 1% (v/v) acetic acid at room temperature overnight to provide 100 ml TMC solution, and then 4-CBS (0.2 g, 9.94 mmol), EDAC (0.24 g, 1.25 mmol), and NHS (0.24 g, 1.42 mmol) were added to the mixture as schematically summarized in scheme 4.1. The reaction mixture was refluxed for 12 hours to form the TMC-4-CBS. Excess EDAC and NHS were removed by adding 1 M HCl to remove excess EDAC and NHS and then adding 1 N NaOH to precipitate the mixture. The precipitated mixture was dialyzed in ethanol to remove free acetic acid, HCl, NaOH, *o*-acylurea and unreacted 4-CBS for 1 day. The reaction mixture was then centrifuged, washed with distilled water and freeze dried to being lyophilized at -44 °C and 0.01 mbar. Yield: 89.35%. EA: C, 41.05%; H, 8.06%; N, 6.13%.

#### **4.2.5 Synthesis and self-assembly of SA-4-CBS-TMC Nanofiber**

4-CBS-TMC was fully dissolved (0.01 g/mL) in 1% (v/v) acetic acid at room temperature overnight to provide 20 ml TMC-4-CBS solution. SA (0.1 g, 0.35 mmol), EDAC (0.34 g, 1.76 mmol), and NHS (0.20 g, 1.76 mmol) were dissolved in 7 ml of an ethanol/acetone mixture (ethanol/acetone = 2/5 (v/v)) and then heated at 60 °C for 1 hour. The solution was added into the 4-CBS-TMC solution, followed by stirred and refluxed for another 24 hours as schematically summarized in Scheme 4.1. Finally, the reaction solution was dialyzed against distilled water for 1 day using a dialysis membrane to remove excess EDAC and NHS and lyophilized at -44 °C and 0.01 mbar. Then the lyophilized product was further purified with ethanol to remove byproduct.

The product TMC-4-CBS-SA was redispersed in distilled water and vortexed to form nanofiber. Yield: 85.94%. EA analysis: C, 46.90%; H, 8.04%; N, 5.11%.



**Scheme 4.1** Reaction scheme for the covalent attachment of SA and 4-CBS to TMC.

#### 4.2.6 Determination of the degree of quaternization (%DQ) and degree of 4-CBS substitution (%DS<sub>4-CBS</sub>)

The degree of quaternization and degree of 4-CBS substitution of the TMC were determined by  $^1\text{H}$  NMR spectra using 2% (v/v) trifluoroacetic acid ( $\text{CF}_3\text{COOH}$ ) in  $\text{D}_2\text{O}$  and were calculated using eq (4.1) and (4.2), respectively.

$$\% DQ = \left[ \frac{I_{(CH_3)_3}}{I_{(H3-H6)}} \times \frac{5}{9} \right] \times 100 \dots\dots (4.1)$$

$$\% DQ_{4-CBS} = \left[ \frac{I_{(SO_2NH_2)}}{I_{(H3-H6)}} \times \frac{5}{2} \right] \times 100 \dots\dots (4.2)$$

where  $I_{(CH_3)_3}$  is the integral of the trimethyl amino group (quaternary amino) protons of TMC at 2.64 ppm,  $I_{(SO_2NH_2)}$  is the integral of the benzene ring of 4-CBS-TMC protons at 7.97 ppm and  $I_{(H3-H6)}$  is the integral of the H3-H6 protons of chitosan or 4-CBS-TMC at 3.95-3.20 ppm or 4.10-3.38 ppm, respectively.

#### 4.2.7 Characterization

##### 4.2.7.1 $^1H$ Nuclear magnetic resonance spectroscopy ( $^1H$ NMR)

The  $^1H$  NMR spectra was performed on a Mercury Varian NMR spectrometer operated at 400 MHz (Agilent Technologies, CA, USA), using pulse accumulating of 64 scans. It was the most sensitive technique to determine the degree of substitution and characterized chitosan, TMC and 4-CBS-TMC structure. The 30 mg of each compound were dissolved in 2% (v/v) trifluoroacetic acid ( $CF_3COOH$ ) in deuterium oxide ( $D_2O$ ).

##### 4.2.7.2 Fourier transformed infrared spectroscopy (FT-IR)

FTIR measurement was carried on a Perkin Elmer Spectrum RX-1 with scanning from 600 to 4000  $cm^{-1}$ . The chitosan, TMC and 4-CBS-TMC were dried, mixed with KBr at 1:100 (w/w), ground into fine powders and pressed as pellets.

##### 4.2.7.3 X-ray diffraction (XRD)

XRD was performed on a Rigaku X-ray diffractometer Dmax 2200 Ultima at room temperature with a speed scan of 5°/min using  $CuK\alpha$  radiation ( $\lambda=1.5405 \text{ \AA}$ , 40 kV, 30 mA) to study polymers' aggregation and determined % crystallinity.

##### 4.2.7.4 Elemental analysis (EA)

Carbon, hydrogen and nitrogen of chitosan, TMC, 4-CBS-TMC and SA-4-CBS-TMC were determined by elemental analysis performed on a CHNS/O analyzer (Perkin Elmer, PE2400 Series II).



#### 4.2.7.5 Thermogravimetric analysis (TGA)

Thermogravimetric (TG) analysis was carried out with PerkinElmer Pyris Diamond TG/DTA under a nitrogen atmosphere to study thermal stability. All analyses were performed with 3-6 mg of lyophilized sample and placed onto aluminium pan in the balance system. TG was continuously recorded as a function of temperature at a temperature range of 30-600 °C and a heating rate of 25 °C/min.

#### 4.2.7.6 Scanning electron microscopy (SEM)

The morphology and surface appearance of the SA-4-CBS-TMC with different re-dispersed concentration were examined by SEM (Jeol, JSM-6480LV). The self-assembly of SA-4-CBS-TMC particles was prepared by re-dispersed in distilled water with a concentration of 0.33, 0.67, 3.33 and 13.33 mg/mL and then vortexed for 2 hours. Each sample solution was dropped on stub using double-sided carbon adhesive tape, dried in desiccator overnight and coated with gold-palladium. Coating was achieved at 18 mA for at least 4 min. The scanning was performed under high vacuum at an ambient temperature with a beam voltage of 20 kV.

#### 4.2.8 Swelling properties

The swelling behavior of dried chitosan, TMC and 4-CBS-TMC films were observed the change in the diameter of the films as previously described [14]. Each polymer (1 g) was dissolved in 50 mL of 1% (v/v) acetic acid, and the solution was then poured into a plastic plate (8 cm × 10 cm) and left at ambient conditions until dry. The dried films were cut into 6.0 mm diameter discs using a paper punch. The swelling ratios were measured at particularly predetermined time points after immersion in the respective solutions, distilled water, simulated gastric fluid (SGF, pH 1.2), 0.1 N simulated duodenum buffer (SDF, pH 4.0), 0.1 N phosphate buffer (PB, pH 5.5), simulated jejunum fluid (SJF, pH 6.4) and simulated ileum fluid (SIF, pH 7.4) at room temperature. The swelling ratios were measured at particular predetermined time points after immersion in the respective solutions, and were evaluated by measuring the change in the diameter of the flat discs using a micrometer scale. The swelling ratio ( $S_w$ ) of each film was determined ( $S_w = (D_t - D_0)/D_0 \times 100$ ), where  $D_t$  is the film diameter at time t and  $D_0$  is the initial film diameter.

#### 4.2.9 Determination of the mucoadhesiveness

The mucoadhesive properties of chitosan, TMC, 4-CBS-TMC and SA-4-CBS-TMC were determined based on the viscometric changes of porcine gastric mucin and polymers in both SGF (0.1 N HCl; pH 1.2) and (0.1 N PB; pH 5.5) buffer as previously reported at 37 °C on a Brookfield (Model DV-II) viscometer [14]. Briefly, dried mucin was hydrated with buffer by gentle stirring for 3 hours at 25 °C to yield 20% (w/v) dispersion. 4-CBS-TMC (g) was dissolved in 10% (v/v) acetic acid to yield 4% (w/v) 4-CBS-TMC solutions that was then diluted by a buffer to yield the respectively 1% (w/v) 4-CBS-TMC solution. The 15% (w/v) mucin-1% (w/v) polymer mixtures were mixed with SGF or PB for 24 hours at 37 °C, and then the viscosity was measured. In case of SA-4-CBS-TMC, it was only re-dispersed in buffer. The mucoadhesive properties of the conjugates in SGF were compared with that in the 0.1 N PB (pH 5.5) using same method.

The viscosity coefficient was then determined by Eq. (4.3) as follows:

$$\eta_t = \eta_m + \eta_p + \eta_b \dots\dots(4.3)$$

where  $\eta_t$  is the viscosity coefficient of the system,  $\eta_m$  and  $\eta_p$  are the individual viscosity coefficients of the mucin and polymer, respectively, and  $\eta_b$  is the viscosity component due to the mucoadhesive. All assays were performed in triplicate with the results shown as the mean  $\pm$  one standard deviation (SD).

#### 4.2.10 Statistical analysis

All measurements were performed in triplicate in each experiment with the results presented as the mean  $\pm$  1 SD. Statistical analysis was performed by one-way ANOVA using Microsoft Excel (Microsoft Corporation) with  $P < 0.05$  considered to indicate statistical significance.

## 4.3 Results and discussion

### 4.3.1 Synthesis and structural analysis of SA-4-CBS-TMC

To well understand the synthesis of SA-4-CBS-TMC, the covalent attachment of 4-CBS and SA to TMC was achieved via coupling the carboxylic acid group ( $-\text{COOH}$ ) of 4-CBS and SA to the primary amine groups ( $-\text{NH}_2$ ) of TMC using EDAC (Scheme 4.1). The lyophilized product, SA-4-CBS-TMC, appeared as a white, odorless fibrous polymer. Lyophilized fibrous polymers were characterized using  $^1\text{H}$  NMR (Figure 4.1) and FT-IR (Figure 4.2).

### 4.3.2 Characterization of TMC, 4-CBS-TMC and SA-4-CBS-TMC

#### 4.3.2.1 $^1\text{H}$ Nuclear magnetic resonance spectroscopy ( $^1\text{H}$ NMR)

The chemical structures of TMC and 4-CBS-TMC were characterized by  $^1\text{H}$  NMR and were shown in Figure 4.1. To well understand the chemical structure of TMC, the peaks at chemical shifts 3.95-3.20 (m, 5H), 2.77 (s, 1H), and 1.65 (s, 3H) were assigned to H3-H6, H2 and  $\text{NHCOCH}_3$ , respectively. The appearance of new proton positions after quaternization at 3.15 (s, 3H), 2.90 (s, 3H), 2.64 (m, 9H), 2.45 (m, 6H) and 2.30 (m, 3H) were attributed to 6- $\text{OCH}_3$ , 3- $\text{OCH}_3$ ,  $\text{N}^+(\text{CH}_3)_3$ ,  $\text{N}(\text{CH}_3)_2$  and  $\text{NHCH}_3$ .

The spectrum of 4-CBS-TMC showed the proton of aromatic ring at 7.97 (d, 2H,  $J = 8.0$  Hz, Ph), 7.78 (d, 2H,  $J = 8.0$  Hz, Ph). The protons of H3-H6 (m, 5H), 6- $\text{OCH}_3$  (s, 3H), 3- $\text{OCH}_3$  (s, 3H), H2 (s, 1H),  $\text{N}^+(\text{CH}_3)_3$  (m, 9H),  $\text{N}(\text{CH}_3)_2$  (m, 6H),  $\text{NHCH}_3$  (m, 3H) and  $\text{NHCOCH}_3$  (s, 3H) were shifted to 4.10-3.38, 3.33, 3.10, 2.94, 2.82, 2.63, 2.43 and 1.84 ppm, respectively. The  $^1\text{H}$  NMR spectra were confirmed that TMC and 4-CBS-TMC were successfully prepared.

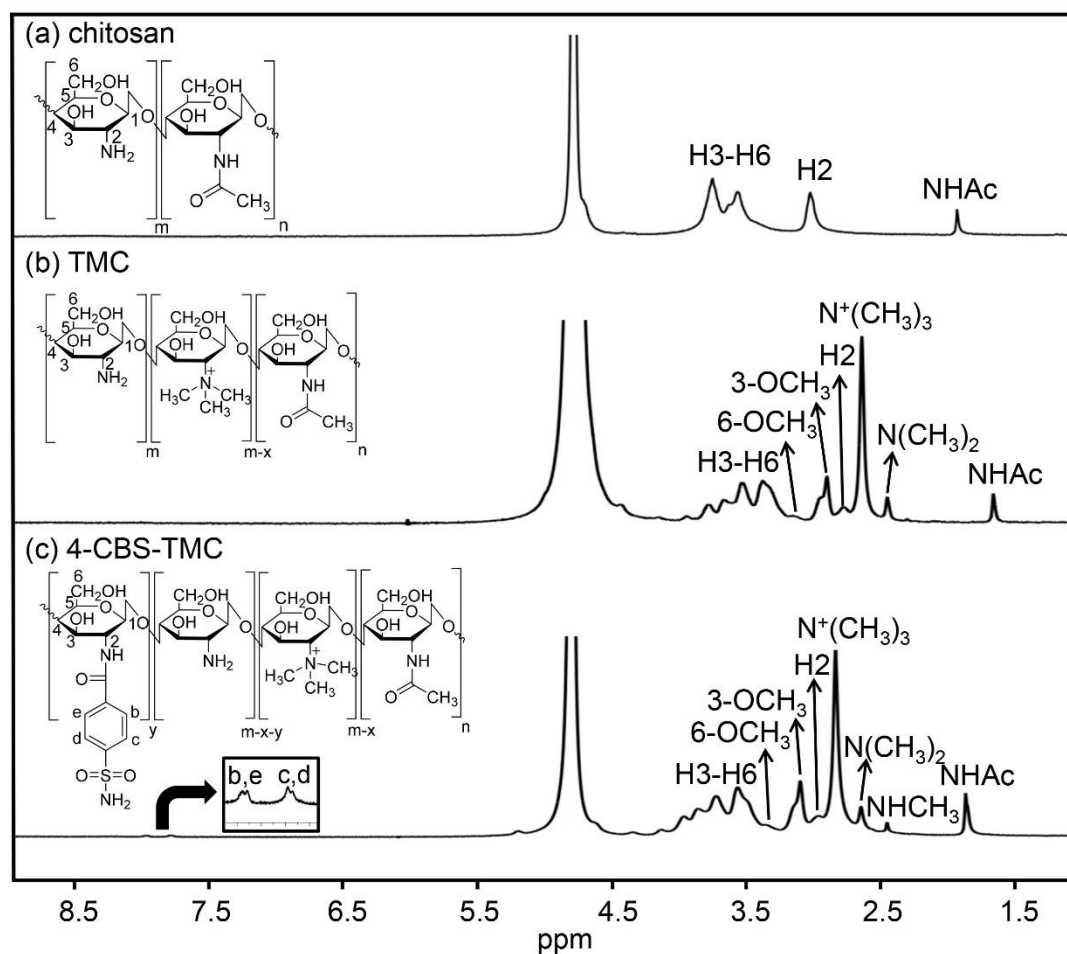
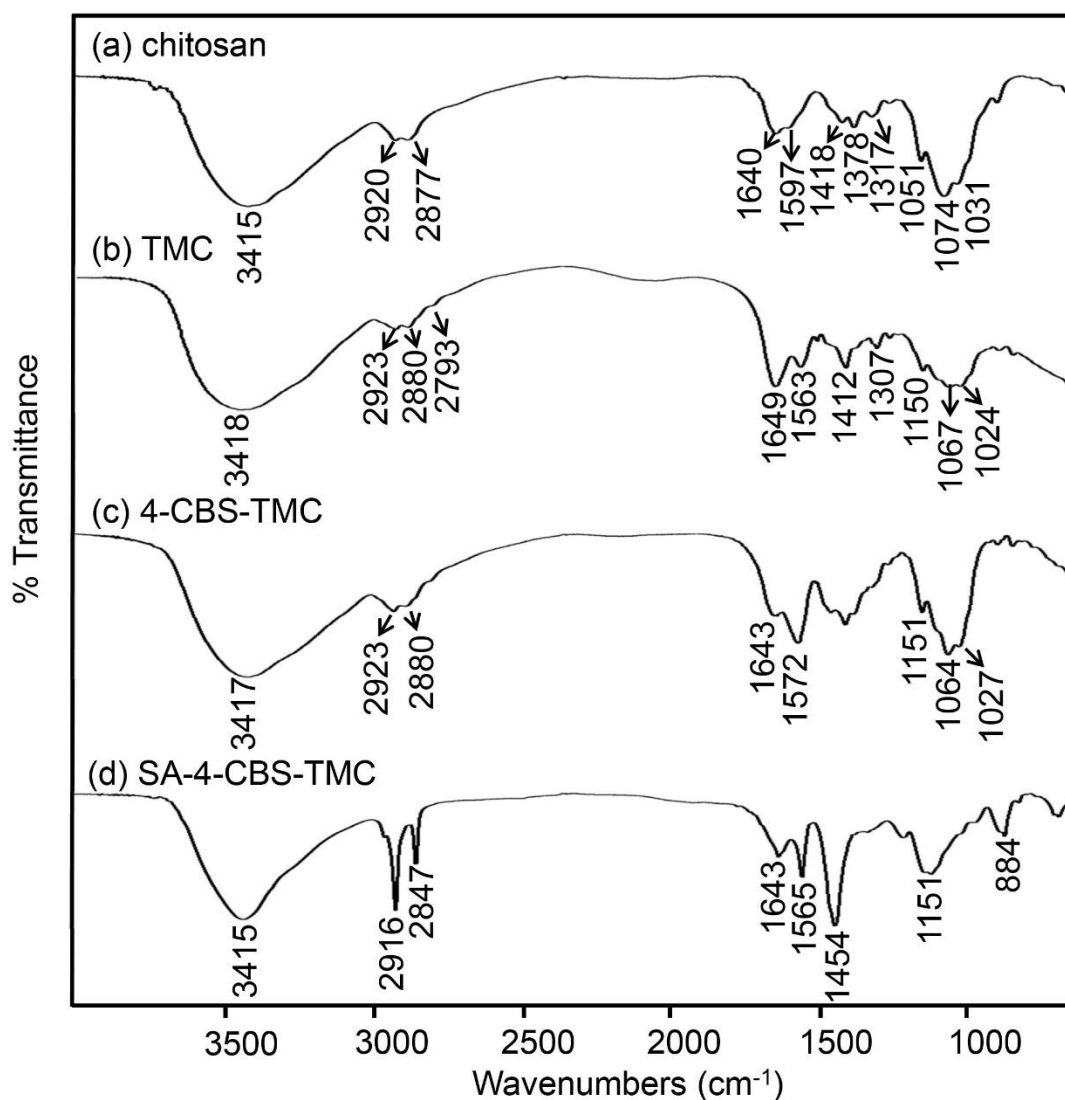


Figure 4.1  $^1\text{H}$  NMR spectra of the (a) chitosan, (b) TMC and (c) 4-CBS-TMC.

#### 4.3.2.2 Fourier Transformed Infrared spectroscopy (FT-IR)

FT-IR spectrum of SA-4-CBS-TMC (Figure 4.2) had the presence of amide band I and II at  $1643\text{ cm}^{-1}$  at  $1565\text{ cm}^{-1}$ , respectively, strong intensity peaks of C-H aliphatic stretching of SA substituent at  $2916\text{ cm}^{-1}$  and  $2874\text{ cm}^{-1}$ , and methyl group bending of long chain SA on TMC backbone. However, no absorption peak of carboxyl groups of SA ( $1703\text{ cm}^{-1}$ ) was found in SA-4-CBS-TMC spectrum, indicating that there was no unreacted SA in product.



**Figure 4.2** FT-IR spectra of the (a) chitosan, (b) TMC, (c) 4-CBS-TMC and (d) SA-4-CBS-TMC.

#### 4.3.2.3 X-ray diffraction (XRD)

The XRD diffractogram (Figure 4.3) revealed two primary diffraction regions, one at approximately 6°-10° (2 $\theta$ ) and another at approximately 19°-24° (2 $\theta$ ). The peak in the low angle region is relatively strong and sharp, indicating the highly substituted molecular order of SA on the TMC backbone. The second peak found at the higher angle was low and broad due to the steric effects of 4-CBS on the backbone.

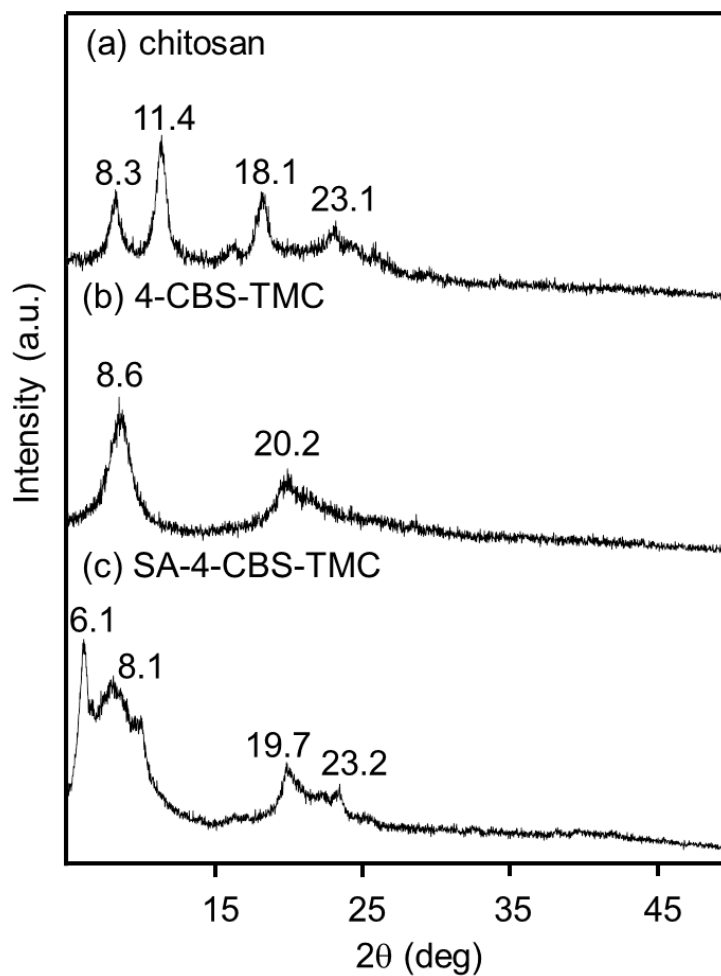
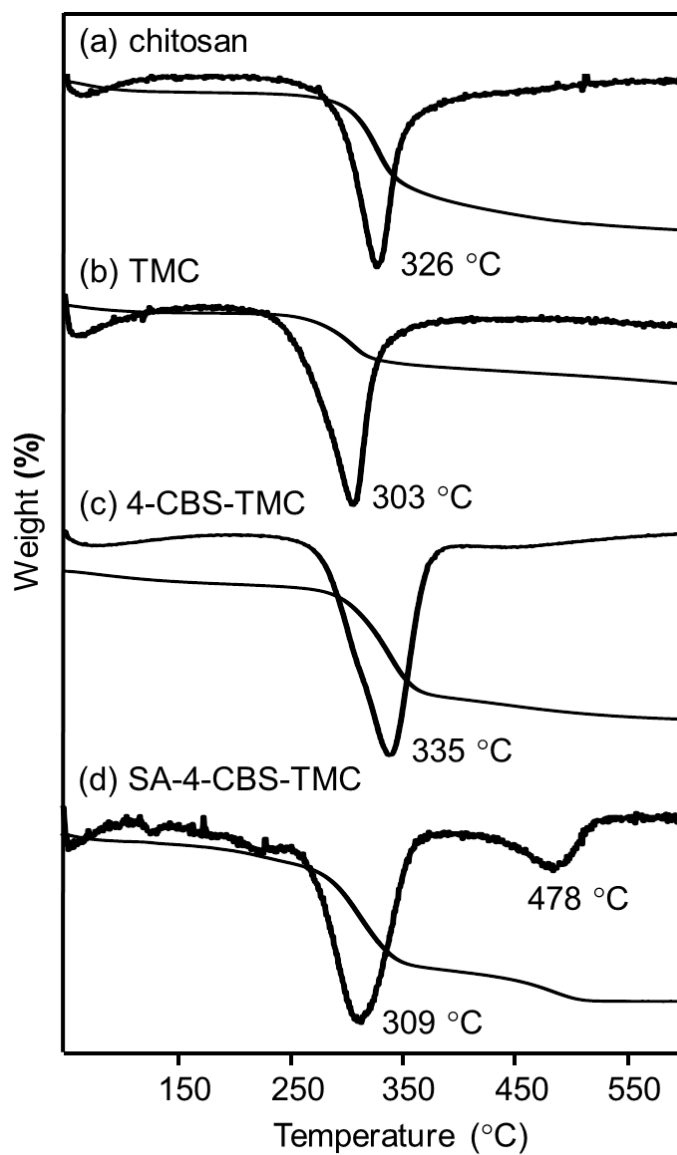


Figure 4.3 XRD patterns of (a) chitosan, (b) 4-CBS-TMC and (c) SA-4-CBS-TMC.

#### 4.3.2.4 Thermogravimetric analysis (TGA)

The thermal stability of SA-4-CBS-TMC was confirmed by TGA (Figure 4.4), which showed a weight loss of the backbone at higher temperatures (478 °C) compared to TMC (303 °C) and 4-CBS-TMC (335 °C). This result indicates that SA-4-CBS-TMC had a more crystalline XRD pattern, leading to high thermal stability and resistance to degradation.



**Figure 4.4** TGA thermogram of (a) chitosan, (b) TMC, (c) 4-CBS-TMC and (d) SA-4-CBS-TMC.

#### 4.3.3 The degree of quaternization and the degree of 4-CBS substitution

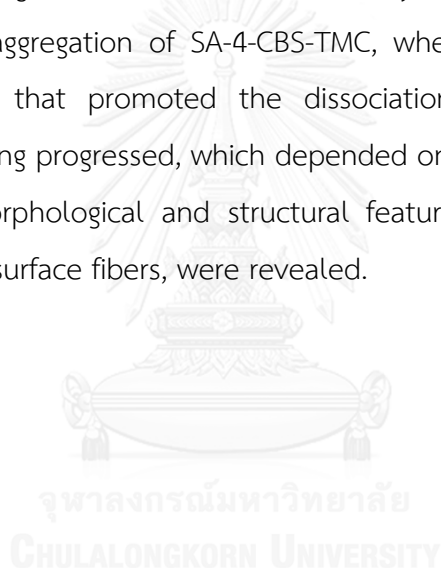
$^1\text{H}$  NMR analysis showed the degree of TMC quaternization at 26.84% and the degree of substitution of 4-CBS on TMC at 7.78%.

#### 4.3.4 Effect of the concentration on self-assembly of SA-4-CBS-TMC

To illustrate the self-assembly of the synthetic polymer, we aimed to reduce the complexity of the self-assembled PA, such as instability and denaturing under harsh conditions. The molecular design of the SA-4-CBS-TMC nanofibers is shown in Figure 4.5. The PAs were designed with long alkyl hydrophobic blocks on one end of hydrophilic peptide sequences, creating an amphiphilic hybrid molecule. The self-assembly of non-amphiphiles is difficult to induce because the property variation between the core and the end groups may not be large enough to induce a phase separation [109]. Figure 4.5 displays the chemical structure of one SA-4-CBS-TMC molecule, incorporating the four key structural features: the 4-CBS substituent,  $-N^+(CH_3)_3$  of the quaternized chitosan, SA hydrophobic tail and the chitosan backbone. The first key component, the aromatic 4-CBS substituent, induced  $\pi$ - $\pi$  aromatic stacking interactions between small aromatic rings and allowed the formation of well-ordered nanofibers. These interactions provided discrete nanostructures due to the extremely rigid characteristic of the nanofibers when re-dispersed in distilled water. The second key component, the quaternized chitosan  $-N^+(CH_3)_3$ , enhanced the nanofiber solubility in water without altering the pH. Normally, charges can be induced in PA amino acids by changing the pH and the concentration of electrolyte in the solution [110]. Therefore, pH is a critical factor for generating successful self-assembled nanofibers. The third key element was the inclusion of various hydrophobic tails with different alkyl lengths, such as palmitic acid [109], phospholipids [105] and SA [111], to assemble the nanofibers. SA served one of the most important roles for designing this molecular feature. SA contains hydrophobic regions to control the self-assembly of amphiphiles by shielding the amphiphiles from water to create 4-CBS and  $-N^+(CH_3)_3$  signals on the nanofiber periphery. The last key component, the chitosan backbone, formed intramolecular hydrogen bonds, which led to further enhanced horizontal molecular packing at both very low and high polymer dispersed concentrations. Therefore, intermolecular hydrogen bonding caused the connection of SA-4-CBS-TMC nanofibers, one factor for molecular packing. Utilizing these key factors, nanofibers were fabricated in water. The hydrophobic core of the SA substitution was buried



within the structure such that it did not contact water, whereas the hydrophilic segments, such as  $-N^+(CH_3)_3$  of the chitosan backbone and the 4-CBS substituent, surrounded the SA core and resided adjacent to the water phase. The driving forces of aromatic 4-CBS stacking, hydrogen bonding along the chitosan backbone, the hydrophobic interactions of the alkyl SA tails and the electrostatic repulsion of  $-N^+(CH_3)_3$  enhanced the helical structure formation and facilitated the self-assembly of SA-4-CBS-TMC nanofibers. Self-assembly of chitosan derivatives based amphiphile exhibited the helical structure such as octanoyl-chitosan-polyethylene glycol monomethyl ether (acylChitoMPEG) which was determined by SAXS [112]. The aromatic 4-CBS stacking, chitosan backbone and alkyl SA tails were attractive forces that promoted the aggregation of SA-4-CBS-TMC, whereas the  $-N^+(CH_3)_3$  was the charged component that promoted the dissociation of SA-4-CBS-TMC. As the molecular-level packing progressed, which depended on a delicate balance of energy contribution, the morphological and structural features, including length, packing density and order of surface fibers, were revealed.



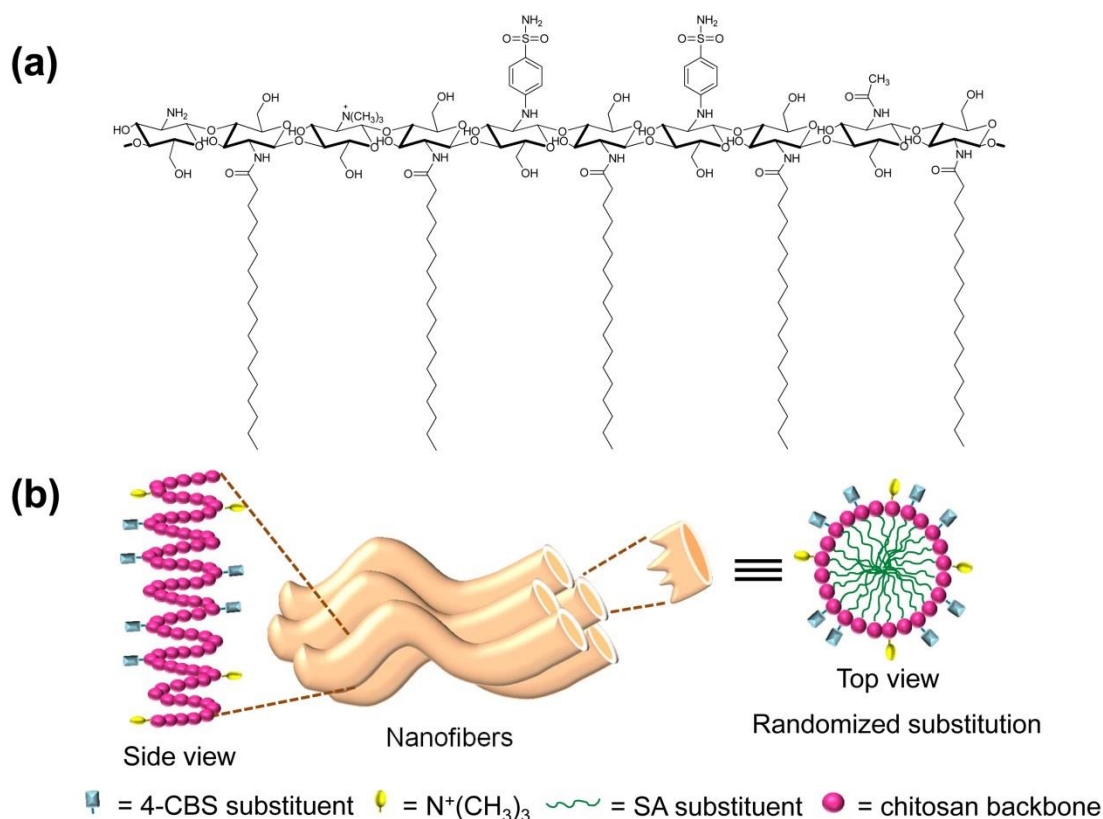


**Figure 4.5** (a) The molecular structure of SA-4-CBS-TMC and (b) The molecular design of SA-4-CBS-TMC nanofibers.

Factors that can control molecular structure assembly include pH, solvents, co-assembly molecules, temperature and re-dispersed concentration. Self-assembly induced through pH change is unstable at physiological pH unless an internal cross-link with a co-assembly molecule forms an electrostatic stable molecule containing the opposite charge. A class of PA-assembled nanofibers has been prepared under physiological conditions in the presence of polyvalent metal ions, such as  $Mg^{2+}$ ,  $Ca^{2+}$ ,  $Ba^{2+}$ ,  $Cu^{2+}$ ,  $Zn^{2+}$  and  $Gd^{3+}$ . However, these various divalent metal ions were difficult to prepare [6]. Temperature is also an important factor that affects the tolerance of protein and peptides in self-assembling.

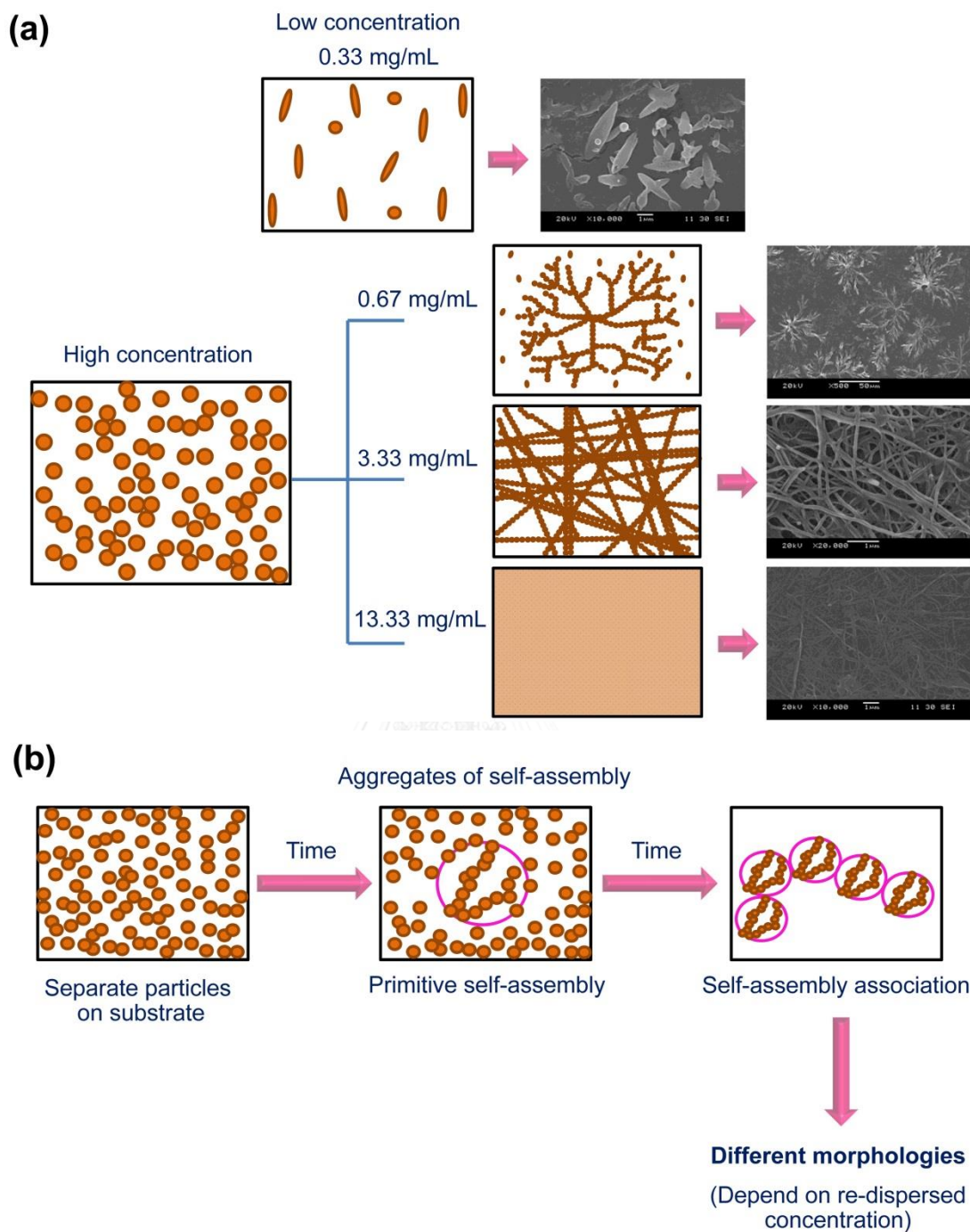


**Figure 4.6** (a) A schematic phase diagram of SA-4-CBS-TMC assemblies, which are dependent on concentration in distilled water, ranging from 0.33 to 13.33 mg/mL. (b) The formation stages of SA-4-CBS-TMC particles dependent on re-dispersion in distilled water.

In this study, for the self-assembly of SA-4-CBS-TMC molecules, re-dispersion concentrations ranging from 0.33 to 13.33 mg/mL in distilled water were first

considered to control the fabrication of nanofibers (Figure 4.6a). As shown in Figure 4.6b, in the early stages, while the SA-4-CBS-TMC particles were dispersed in distilled water, the peripheral chitosan backbone was separated. Next, the particles gradually swelled, resulting in aggregation due to the random walk process, and became primitively self-assembled. This process allowed an alteration in self-assembly structure in response to changing the concentration of SA-4-CBS-TMC in distilled water. The final nanofiber shape, size and self-assembled stability expressed an optimum thermodynamic state, which was characterized by a combination of factors, such as chain stretching, interfacial tension and intercoronal chain interaction. The excellent long term stability of various morphologies dispersed in distilled water could be determined by re-observation by SEM. Although the self-assembly of a spherical geometry was quite general, other morphologies, such as short fibrous bundles, nanofibers, hyperbranched structures and films, were observed at different re-dispersion concentrations. All of morphologies were not change in shape and size over time.

#### 4.3.4.1 Spherical shapes and short fibrous bundles

At a low concentration (0.33 mg/mL), the morphologies of SA-4-CBS-TMC structures included spherical shapes and short fibrous bundles (Figure 4.7). The relative stability of the various possible packing self-assemblies was believed to be primarily controlled by the balance of three energies: chain stretching, interfacial tension and intercoronal chain interactions. When the concentration was low, the amount of SA-4-CBS-TMC was too low to provide the high intercoronal chain repulsion of  $-N^+(CH_3)_3$  on the surface. The SA-4-CBS-TMC structure was determined by a delicate balance of forces operating at the interfacial region of the 4-CBS and  $-N^+(CH_3)_3$  groups and within the hydrophobic core of aggregated SA, inducing a spherical shape (Figure 4.7a). The spherical shape resulted in the minimum total free energy and therefore was the first morphology that was assumed by the structure. However, the formation of SA-4-CBS-TMC into spheres could not continue indefinitely because the stretching energy due to the entropy of SA became limited as the radius of the sphere increased during core formation. Consequently, the high stretching energy would begin to induce short

fibrous bundles instead of spheres to reduce the thermodynamic penalty of chain stretching (Figure 4.7b).

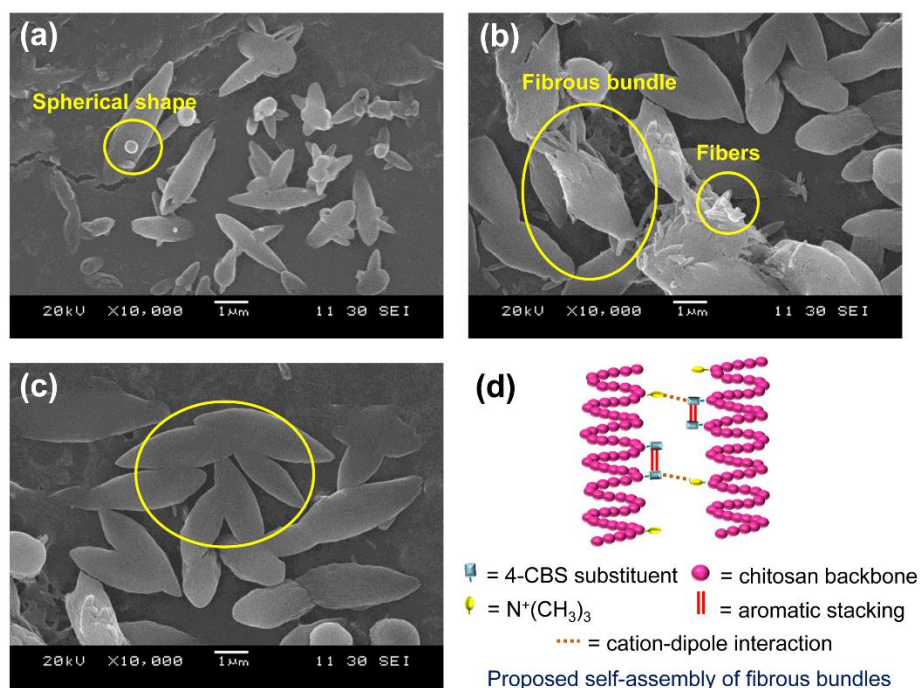


**Figure 4.7** The morphologies of SA-4-CBS-TMC at low concentration (0.33 mg/mL): (a) spherical shapes, (b) fibrous bundles, (c) fibrous bundle merge and (d) the proposed self-assembly of fibrous bundles.

Several short fibrous chains linked themselves along the horizontal axis to create a fibrous bundle (Figure 4.7b). The proposed self-assembly process of the fibrous bundle structures is shown in Figure 4.7d. The quaternary amino group of the chitosan backbone and the sulfonamide group of 4-CBS provided cation-dipole interaction. Moreover, the stacking force of 4-CBS prolonged the length of the bundles. Nevertheless, only short fibrous bundles occurred due to the minimal amount of SA-4-CBS-TMC. The SEM image (Figure 4.7c) shows the merging of the fibrous bundles, which was dependent on the interfacial tension force. The bundles merged to reduce the interfacial tension, creating a stable SA-4-CBS-TMC molecule.

#### 4.3.4.2 Tree-like morphology or hyperbranched structure

The tree-like morphology, or the hyperbranched structure shown in Figure 4.8, was able to be formed at a concentration of 0.67 mg/mL. The formation of the structure began as the aggregation of many nuclei (Figure 4.8a), a state of lower free energy [112]. The concept of diffusion-limited aggregation (DLA), or the irreversible aggregation of small particles into clusters, has been previously developed [113]. The DLA concept received significant attention because it was a fundamental model for pattern growth and provided a basic understanding of complex aggregate formation of different shapes [114]. The model assumed that particles originate far from a developing immobile structure and undergo a random walk in their surrounding space. The particles stick to an existing structure when encountered. Therefore, the aggregated nuclei of SA-4-CBS-TMC became part of the primitive self-assembly that led to the formation of extremely complicated multi-branches (Figure 4.8b). These branches grew from the central nucleus and were composed of short helical SA-4-CBS-TMC nanofibers with a width on the order of ~100 nm (Figure 4.8c). Moreover, these branches repelled each other due to the repulsive positive charge of the  $-N^+(CH_3)_3$  group. Generally, a hyperbranched structure formed and grew rapidly at the ends of the self-assembly rather than from other perimeter sites because the perimeter sites near the center were occluded [115].



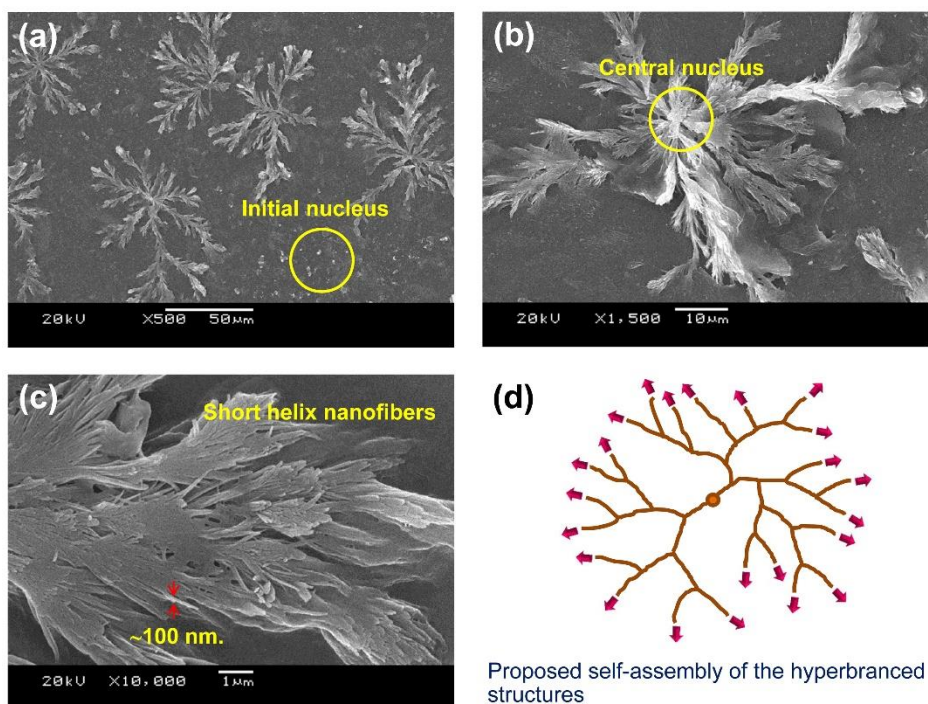


**Figure 4.8** The morphologies of SA-4-CBS-TMC at high concentration (0.67 mg/mL): the (a) initial nucleus, (b) central nucleus, (c) short helical nanofibers of ~100 nm and (d) proposed self-assembly of hyperbranched structures.

The proposed hyperbranched self-assembly feature with a tip-splitting head is shown in Figure 4.8d, which illustrates the formation of distinct borders. The angles between the main and side branches, considered from the center outward, do not have fixed values. The widths of the branches were much narrower compared to the total length of each branch. Moreover, the branches were formed with a uniform width. When a branch reached a certain width, it split to generate new branches, and both the parent branch and the new branches continued to proliferate. This pattern generated an approximately geometrical ellipse, with a largest diameter of approximately 60  $\mu\text{m}$ . Thus hyperbranched self-assembly of SA-4-CBS-TMC at a high concentration was successfully prepared.

#### 4.3.4.3 Nanofiber formations

At a concentration of 3.33 mg/mL, nanofiber formations were observed (Figure 4.9). The SEM micrograph of SA-4-CBS-TMC (Figure 4.9b) revealed a nanofiber cross-

section with a convex spherical surface due to helical molecular packing. The aromatic 4-CBS substituents, creating  $\pi$ - $\pi$  aromatic stacking, and the amino groups of the chitosan backbone, governing hydrogen bonding, exposed active functional groups on the surface of the fibers. As the SA aliphatic tails were aggregated, they repelled the distilled water and induced formation of the helix. Methylation of  $-N^+(CH_3)_3$ , which formed an intercoronal interaction, induced elongation of the nanofiber axis. Moreover, the SEM micrographs depicted connected horizontal SA-4-CBS-TMC nanofibers (Figure 4.9c), which was partly due to hydrogen bonding of the amino groups of the chitosan backbone and the sulfonamide groups of the 4-CBS substituent.

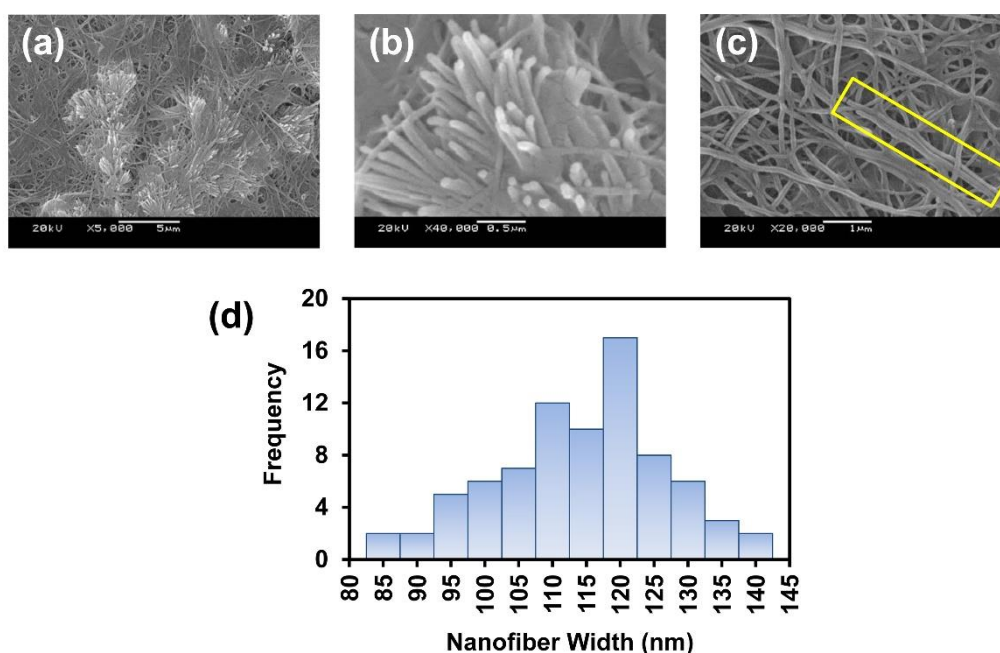


**Figure 4.9** Morphologies of SA-4-CBS-TMC at high concentration (3.33 mg/mL). (a) Elongated nanofibers, (b) a cross-section of nanofibers (c) connected horizontal nanofibers are depicted, and (d) the histogram of SA-4-CBS-TMC nanofiber widths measured from SEM images.

The orientation of hydrogen bonding was important in the formation of nanofibers. A minimum number of hydrogen bonds was necessary for the formation of the SA-4-CBS-TMC nanofibers. Due to the low number of hydrogen bonds, the energy of the remaining hydrogen bonds was not enough to induce nanofiber



aggregation. This phenomenon was only able to form self-assembled spheres. Therefore, the disruption of the hydrogen bonds of the amino groups on the chitosan backbone by  $-N^+(CH_3)_3$  substituents was able to prevent SA-4-CBS-TMC from donating hydrogen bonds. Considering the 4-CBS substituent as a short aromatic chain, 4-CBS was further from the SA nanofiber core compared to the amino groups of the chitosan backbone. 4-CBS was also less tightly governed by hydrogen bonding. Another class of peptide nanostructures has been previously reported involving the use of short aromatic peptides to form well-ordered nanostructures. Previous studies reported that the formation of closed-caged nanospheres was most likely due to geometrically restricted interactions between aromatic moieties, such as diphenylglycine polypeptide. A simpler analogue, the Alzheimer's  $\beta$ -amyloid diphenylalanine structural motif, is a flexible and less restricted peptide that forms discrete nanotubes due to the stacking of aromatic residues [116]. Therefore, the partial elimination of the amino group of the chitosan backbone and a less restricted aromatic interaction were critical for the formation of elongated nanofibers (Figure 4.9a). The peak of the histogram of SA-4-CBS-TMC nanofiber widths (Figure 4.9d) at these concentrations, derived from SEM images, was determined to be  $112.23 \pm 11.96$  nm with a narrow width distribution. Haider et al. attempt to fabricate electrospun chitosan nanofibers with their highly aligned narrow diameter  $\sim 130$  nm; however, the chemical neutralization of ammonium into amine was needed for the preparation to increase stability in aqueous medium [117]. Although Stendahl et al. fabricated self-assembly of PA ( $C_{16}A_4G_3S(P)KGE-COOH$ ) into gel-forming networks of cylindrical aggregates with approximate diameter narrower than SA-4-CBS-TMC nanofibers  $\sim 15$  fold, lengths that frequently exceed one micrometer and the concentration, electronic structure, and hydration of counterions significantly influence self-assembly and mechanical properties [118]. Therefore, these re-dispersion concentrations are an easy and stable technique to create the appropriate ratio to form well-defined, self-assembled nanofibers with stable structure for nanotechnology applications.

#### 4.3.4.4 Thin films

At very high concentration (13.33 mg/mL), the space between polymeric units was very limited (Figure 4.10). The concentration promoted growth onto functionalized interfaces. The nanofibers did not have enough space to permit facile growth. Therefore, the high polymer content induced aggregation into thin films.

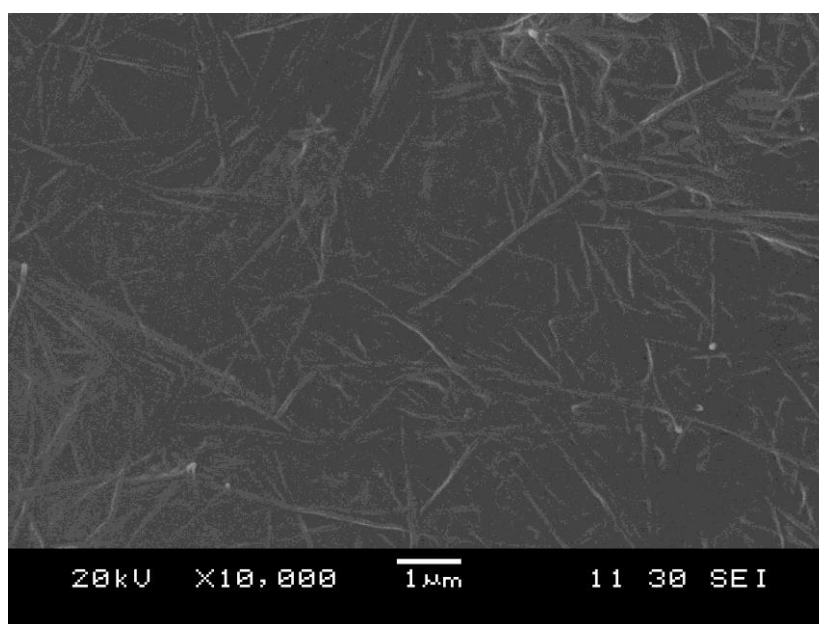


**Figure 4.10** The morphology of SA-4-CBS-TMC at the high concentration (13.33 mg/mL).

#### 4.3.5 Swelling behaviour

The swelling behavior indicates the relative ease and speed of liquid penetration into a polymer matrix, which is an essential step and important influence on the kinetics of the drug release process. In addition, the swelling behavior of mucoadhesive polymers has a strong influence on their adhesive properties, water-uptake and stability. A rapid swelling behavior may improve the inter-diffusion process between the polymer and the mucus layer, providing a strong adhesion and then leading to an enhanced drug delivery rate [119]. The swelling behavior of chitosan, TMC and 4-CBS-TMC films was observed in pH 1.2, pH 4, pH 5.5, pH 6.4, pH 7.4 and distilled water (Figure 4.11).

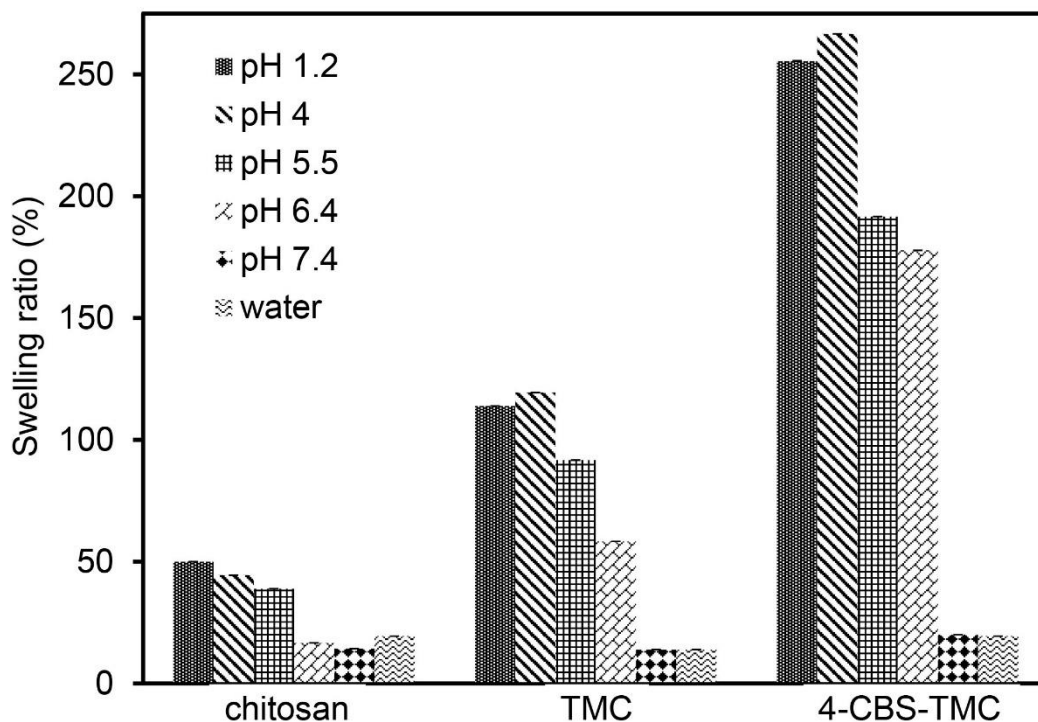


**Figure 4.11** Swelling behaviors of the chitosan, TMC and 4-CBS-TMC in simulated gastric fluid (SGF, pH 1.2), 0.1 N simulated duodenum buffer (SDF, pH 4.0), 0.1 N phosphate buffer (PB, pH 5.5), simulated jejunum fluid (SJF, pH 6.4), simulated ileum fluid (SIF, pH 7.4) and water.

In the acidic medium (SGF, SDF, PB and SJF) within 6 h of immersion, the TMC and 4-CBS-TMC swelled about 2.28, 2.69, 2.36 and 3.50-folds and 5.11, 6.00, 4.93 and 10.66-folds of the chitosan. The degree of swelling of all samples were significantly higher in acidic medium than in pH 7.4 and water, due to the  $-NH_2$  groups being protonated ( $-NH_3^+$ ) at  $pH < 6.5-6.7$  [120]. After that the hydrogen bonds were dissociated and induced the network to become loose leading to an increased degree of swelling [121]. TMC provided larger swelling ratio than chitosan owing to the repulsive force among the positive charge of quarternized chitosan backbone. In case of 4-CBS-TMC, excluding the repulsive force of positive charge, 4-CBS substituents prevented the intermolecular interactions between the  $-NH_2$  groups of chitosan which affected higher swelling ratio than that of chitosan and TMC.

The swelling behavior of all samples in SIF and water was not clearly difference, but lower than that seen in acidic media. They revealed only about 15%- 20% swelling ratio. In case of SJF and SIF could be explained by the deprotonation of amino group in chitosan backbone. The  $\text{-NH}_3^+$  groups of chitosan were uncharged leading to a re-association of the hydrogen bonds and, consequently, weaker interactions between the polymer chains and reduced degree of swelling. In water, it mainly depended on the difference in the osmotic pressure inside and outside of the chitosan specimen [122]. Therefore, more water could penetrate into the polymeric networks to increase the degree of swelling.

#### 4.3.6 Mucoadhesive properties

Chitosan, TMC, 4-CBS-TMC and SA-4-CBS-TMC were investigated and received considerable attention as mucoadhesive polymer based on the viscometric changes of porcine gastric mucin and polymers in both SGF and PB buffer. Because of at a pH of above 6, chitosan becomes deprotonated and losses its charge and so becomes insoluble [123]. Mucoadhesion governed the increased localization and residence time at the site of drug absorption. Moreover, it provided an intensified contact with the mucosa and, subsequently, increased the drug concentration gradient at the required site [1].

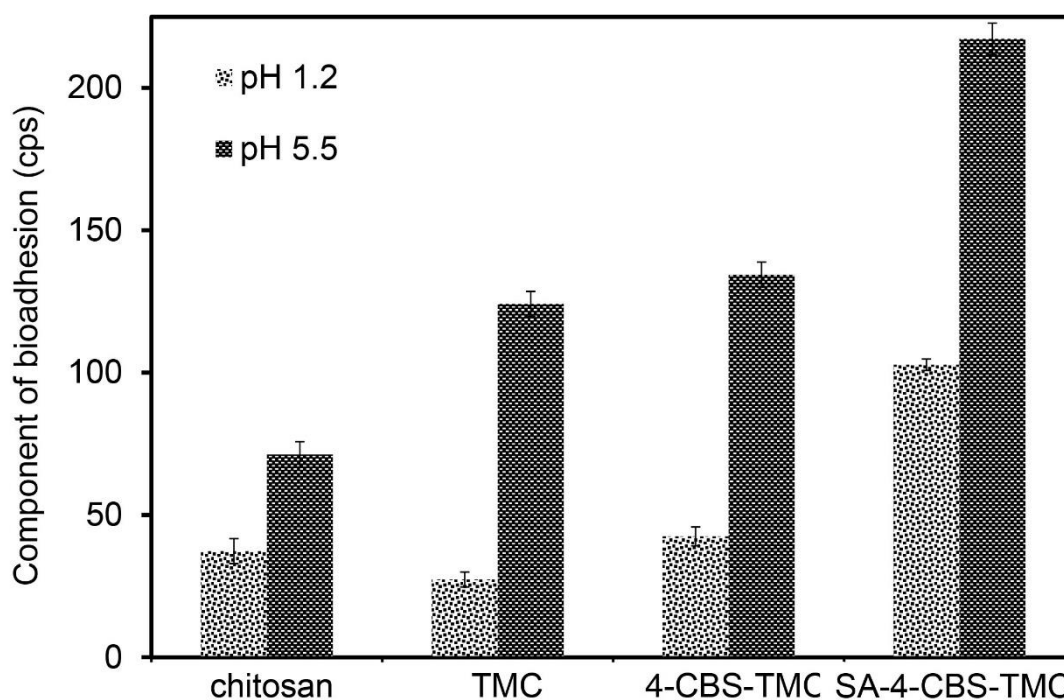


**Figure 4.12** The component of mucoadhesion (cps) of chitosan, TMC, 4-CBS-TMC and SA-4-CBS-TMC in SGF, pH 1.2 and PB, pH 5.5. Data are shown as the mean  $\pm$  1 SD and are derived from three independent repeats.

The mucoadhesion of chitosan, TMC 4-CBS-TMC and SA-4-CBS-TMC in SGF and PB were summarized in Figure 4.12. In SGF, chitosan showed a component of mucoadhesion of 37.3 cps, while the TMC showed lower component of mucoadhesion (27.4 cps), than that for chitosan. In SGF, the amine ( $-\text{NH}_2$ ) groups of chitosan were partially protonated to the ammonium cation ( $-\text{NH}_3^+$ ) because  $\text{pK}_a$  of chitosan was 5.6. It was not completely interact with negative charge of native mucin ( $\text{pK}_a = 2.6$ ). However, it displayed higher the component of mucoadhesion than TMC. The high degree of quaternization may be decreased the mucoadhesive properties. It was explained by changes in the conformation of the respective TMC polymer due to interactions between the fixed positive charges on C-2 position [1]. In case of 4-CBS-TMC, it showed only slightly higher mucoadhesive component at 42.5 cps than chitosan. The mucoadhesive forces were likely to be dominated by electronic

interactions and hydrophobic effects of the  $-CH_3$  and aromatic part of 4-CBS groups on the polymer backbone that interact with the  $-CH_3$  groups on the mucin side chains.

In PB, the 4-CBS-TMC and TMC revealed significantly higher components of mucoadhesiveness than chitosan for 1.74 folds and 1.89 folds, respectively. The mucoadhesive property of all polymers in PB at pH 5.5 was higher than that in SGF at pH 1.2. Because the amino group of all polymers performed the good dissociation in pH 5.5, the ionic interaction with the anionic form of the sialic acid of mucin was preferred. Moreover, the hydrophobic effect caused the higher mucoadhesive force of 4-CBS-TMC than TMC.

On the other hand, the mucoadhesion of SA-4-CBS-TMC after re-dispersed in SGF and PB exhibited significantly higher mucoadhesive properties than that of the native chitosan. As very high content of SA substituent increased the hydrophobic part, the mucoadhesive properties and viscosity of the mixture increase. Therefore, the mucoadhesion is typically related to the mucoadhesive force between the interacting polymer and the mucin.

#### 4.4 Conclusions

In summary, SA-4-CBS-TMC nanofibers were easily synthesized by re-dispersion in distilled water while controlling the chemical functionality of 4-CBS and the amino groups of the chitosan backbone on the fiber surfaces. This polymer exhibited suitable swelling and favourable mucoadhesion with the mucus membrane. Therefore, this polymer could be useful in nanotechnology applications, such as drug delivery.

## CHAPTER V

### CONCLUSION AND SUGGESTION

#### 5.1 Conclusion

In the present study, the mucoadhesive SM-chitosan hydrogel and self-assembled SA-4-CBS-TMC nanofiber were synthesized for using as drug delivery carrier. The SM-chitosan hydrogel can be successfully synthesized via methyl acrylate as an intermedia to overcome the problem of slippery mucilage. The obtained hydrogel provided higher mucoadhesion than native chitosan 2.61-folds with 6.21% of degree of sulfanilamide substitution. Furthermore, SM-chitosan hydrogel provided acid resistance in simulated gastric acid (SGF, pH 1.2).

Self-assembled SA-4-CBS-TMC nanofiber was successfully fabricated by only re-dispersing the compound in distilled water at a concentration  $3.33 \text{ mg mL}^{-1}$  which was easy and stable one step procedure. The nanofiber assembly relied on a balance between the hydrophobic effect of SA, the aromatic stacking of 4-CBS, the electrostatic interactions of  $-\text{N}^+(\text{CH}_3)_3$  and the hydrogen bonding of chitosan backbone. The well-organized nanofiber exhibited the good thermal stability at high temperature ( $478 \text{ }^\circ\text{C}$ ) Moreover, it exhibited the highest mucoadhesion in phosphate buffer (PB, pH 5.5) compared to native chitosan due to high content of SA substituent to provide hydrobolic interaction with mucus membrane. Therefore, the mucoadhesive SM-chitosan and SA-4-CBS-TMC were a suitable polymer for applying as a drug carrier in acidic condition.

#### 5.2 Suggestions for the future work

- Enhance the eradication of hydrogel in acidic condition and control gelation to prolong mucoadesion for drug delivery system.
- Develop the mucoadhesive self-assembled drug carrier for hydrophobic drug delivery in gastrointestinal tract in order to provide high content of drug encapsulation and prolong the residence time of intended drug at the site of absorption.

## REFERENCES

1. Snyman, D., Hamman, J.H., and Kotze, A.F., *Evaluation of the mucoadhesive properties of N-trimethyl chitosan chloride*. Drug Development and Industrial Pharmacy, 2003. **29**(1): p. 61-69.
2. He, P., Davis, S.S., and Illum, L., *In vitro evaluation of the mucoadhesive properties of chitosan microspheres*. International Journal of Pharmaceutics, 1998. **166**(1): p. 75-88.
3. Smart, J.D., Kellaway, I.W., and Worthington, H.E.C., *An in-vitro investigation of mucosa-adhesive materials for use in controlled drug delivery*. Journal of Pharmacy and Pharmacology, 1984. **36**(5): p. 295-299.
4. Dhawan, S., Singla, A.K., and Sinha, V.R., *Evaluation of mucoadhesive properties of chitosan microspheres prepared by different methods*. AAPS PharmSciTech, 2004. **5**(4): p. 122-128.
5. Nagarwal, R.C., Singh, P.N., Kant, S., Maiti, P., and Pandit, J.K., *Chitosan nanoparticles of 5-fluorouracil for ophthalmic delivery: characterization, in-vitro and in-vivo study*. Chemical and Pharmaceutical Bulletin, 2011. **59**(2): p. 272-278.
6. Sogias, I.A., Williams, A.C., and Khutoryanskiy, V.V., *Why is chitosan mucoadhesive?* Biomacromolecules, 2008. **9**(7): p. 1837-1842.
7. Bernkop-Schnurch, A., Schwarz, V., and Steininger, S., *Polymers with thiol groups: a new generation of mucoadhesive polymers?* Pharmaceutical Research, 1999. **16**(6): p. 876-881.
8. Kast, C.E. and Bernkop-Schnurch, A., *Thiolated polymers--thiomers: development and in vitro evaluation of chitosan-thioglycolic acid conjugates*. Biomaterials, 2001. **22**(17): p. 2345-2352.
9. Langoth, N., Kahlbacher, H., Schoffmann, G., Schmerold, I., Schuh, M., Franz, S., Kurka, P., and Bernkop-Schnurch, A., *Thiolated chitosans: design and in vivo evaluation of a mucoadhesive buccal peptide drug delivery system*. Pharmaceutical Research, 2006. **23**(3): p. 573-579.



10. Atyabi, F., Moghaddam, F.A., Dinarvand, R., Zohuriaan-Mehr, M.J., and Ponchel, G., *Thiolated chitosan coated poly hydroxyethyl methacrylate nanoparticles: Synthesis and characterization*. Carbohydrate Polymers, 2008. **74**(1): p. 59-67.
11. Kafedjiiski, K., Hoffer, M., Werle, M., and Bernkop-Schnurch, A., *Improved synthesis and in vitro characterization of chitosan-thioethylamidine conjugate*. Biomaterials, 2006. **27**(1): p. 127-135.
12. Bernkop-Schnürch, A., Scholler, S., and Biebel, R.G., *Development of controlled drug release systems based on thiolated polymers*. Journal of Controlled Release, 2000. **66**(1): p. 39-48.
13. Bernkop-Schnurch, A., Krauland, A.H., Leitner, V.M., and Palmberger, T., *Thiomers: potential excipients for non-invasive peptide delivery systems*. European Journal of Pharmaceutics and Biopharmaceutics, 2004. **58**(2): p. 253-263.
14. Suvannasara, P., Juntapram, K., Praphairaksit, N., Siralermukul, K., and Muangsin, N., *Mucoadhesive 4-carboxybenzenesulfonamide-chitosan with antibacterial properties*. Carbohydrate Polymers, 2013. **94**(1): p. 244-252.
15. Suvannasara, P., Siralermukul, K., and Muangsin, N., *Electrosprayed 4-carboxybenzenesulfonamide-chitosan microspheres for acetazolamide delivery*. International Journal of Biological Macromolecules, 2014. **64**: p. 240-246.
16. Van Vlierberghe, S., Samal, S.K., and Dubruel, P., *Development of mechanically tailored gelatin-chondroitin sulphate hydrogel films*. Macromolecular Symposia, 2011. **309-310**(1): p. 173-181.
17. Piyakulawat, P., Praphairaksit, N., Chantarasiri, N., and Muangsin, N., *Preparation and evaluation of chitosan/carrageenan beads for controlled release of sodium diclofenac*. AAPS PharmSciTech, 2007. **8**(4): p. 120-130.
18. Berger, J., Reist, M., Mayer, J.M., Felt, O., and Gurny, R., *Structure and interactions in chitosan hydrogels formed by complexation or aggregation for biomedical applications*. European Journal of Pharmaceutics and Biopharmaceutics, 2004. **57**(1): p. 35-52.

19. Giri, T.K., Thakur, A., Alexander, A., Ajazuddin, Badwaik, H., and Tripathi, D.K., *Modified chitosan hydrogels as drug delivery and tissue engineering systems: present status and applications*. Acta Pharmaceutica Sinica B, 2012. **2**(5): p. 439-449.
20. Moura, M.J., Faneca, H., Lima, M.P., Gil, M.H., and Figueiredo, M.M., *In situ forming chitosan hydrogels prepared via ionic/covalent co-cross-linking*. Biomacromolecules, 2011. **12**(9): p. 3275-3284.
21. Elizalde-Peña, E.A., Flores-Ramirez, N., Luna-Barcenas, G., Vásquez-García, S.R., Arámbula-Villa, G., García-Gaitán, B., Rutiaga-Quiñones, J.G., and González-Hernández, J., *Synthesis and characterization of chitosan-g-glycidyl methacrylate with methyl methacrylate*. European Polymer Journal, 2007. **43**(9): p. 3963-3969.
22. Sajeesh, S. and Sharma, C.P., *Mucoadhesive hydrogel microparticles based on poly (methacrylic acid-vinyl pyrrolidone)-chitosan for oral drug delivery*. Drug Delivery, 2011. **18**(4): p. 227-235.
23. Li, N. and Bai, R., *Copper adsorption on chitosan-cellulose hydrogel beads: behaviors and mechanisms*. Separation and Purification Technology, 2005. **42**(3): p. 237-247.
24. Mourya, V.K. and Inamdar, N.N., *Chitosan-modifications and applications: Opportunities galore*. Reactive and Functional Polymers, 2008. **68**(6): p. 1013-1051.
25. Sieval, A.B., Thanou, M., Kotze, A.F., Verhoef, J.C., Brussee, J., and Junginger, H.E., *Preparation and NMR characterization of highly substituted N-trimethyl chitosan chloride*. Carbohydrate Polymers, 1998. **36**(2-3): p. 157-165.
26. Thanou, M.M., Kotze, A.F., Scharringhausen, T., Luessen, H.L., de Boer, A.G., Verhoef, J.C., and Junginger, H.E., *Effect of degree of quaternization of N-trimethyl chitosan chloride for enhanced transport of hydrophilic compounds across intestinal caco-2 cell monolayers*. Journal of Controlled Release, 2000. **64**(1-3): p. 15-25.

27. Lazzari, M., Rodriguez-Abreu, C., Rivas, J., and Lopez-Quintela, M.A., *Self-assembly: a minimalist route to the fabrication of nanomaterials*. Journal of Nanoscience and Nanotechnology, 2006. **6**(4): p. 892-905.
28. Rösler, A., Vandermeulen, G.W.M., and Klok, H.-A., *Advanced drug delivery devices via self-assembly of amphiphilic block copolymers*. Advanced Drug Delivery Reviews, 2001. **53**(1): p. 95-108.
29. Hu, F.Q., Zhao, M.D., Yuan, H., You, J., Du, Y.Z., and Zeng, S., *A novel chitosan oligosaccharide-stearic acid micelles for gene delivery: properties and in vitro transfection studies*. International Journal of Pharmaceutics, 2006. **315**(1-2): p. 158-166.
30. Taubert, A., Napoli, A., and Meier, W., *Self-assembly of reactive amphiphilic block copolymers as mimetics for biological membranes*. Current Opinion in Chemical Biology, 2004. **8**(6): p. 598-603.
31. Palmer, L.C. and Stupp, S.I., *Molecular self-assembly into one-dimensional nanostructures*. Accounts of Chemical Research, 2008. **41**(12): p. 1674-1684.
32. Van Tomme, S.R., Mens, A., van Nostrum, C.F., and Hennink, W.E., *Macroscopic Hydrogels by Self-Assembly of Oligolactate-Grafted Dextran Microspheres*. Biomacromolecules, 2007. **9**(1): p. 158-165.
33. Hartgerink, J.D., Beniash, E., and Stupp, S.I., *Self-assembly and mineralization of peptide-amphiphile nanofibers*. Science, 2001. **294**(5547): p. 1684-1688.
34. Elisseeff, J., *Hydrogels: Structure starts to gel*. nature materials, 2008. **7**(4): p. 271-273.
35. Gu, J.M., Robinson, J.R., and Leung, S.H., *Binding of acrylic polymers to mucin/epithelial surfaces: structure-property relationships*. Critical Reviews in Therapeutic Drug Carrier Systems, 1988. **5**(1): p. 21-67.
36. Good, W.R., *Transderm-nitro controlled delivery of nitroglycerin in the transdermal route*. Drug Development and Industrial Pharmacy, 1983. **9**(4): p. 647-670.
37. Thornton, D.J. and Sheehan, J.K., *From mucins to mucus: toward a more coherent understanding of this essential barrier*. Proceedings of the American Thoracic Society, 2004. **1**(1): p. 54-61.

38. Carlstedt, I. and Sheehan, J.K., *Structure and macromolecular properties of cervical mucus glycoproteins*. Symposia of the Society for Experimental Biology, 1989. **43**: p. 289-316.
39. Allen, A., Cunliffe, W.J., Pearson, J.P., and Venables, C.W., *The adherent gastric mucus gel barrier in man and changes in peptic ulceration*. Journal of Internal Medicine, 1990. **732**: p. 83-90.
40. Kerss, S., Allen, A., and Garner, A., *A simple method for measuring thickness of the mucus gel layer adherent to rat, frog and human gastric mucosa: influence of feeding, prostaglandin, N-acetylcysteine and other agents*. Clinical Science, 1982. **63**(2): p. 187-195.
41. Sonju, T., Christensen, T.B., Kornstad, L., and Rolla, G., *Electron microscopy, carbohydrate analyses and biological activities of the proteins adsorbed in two hours to tooth surfaces in vivo*. Caries Research, 1974. **8**(2): p. 113-122.
42. Smart, J.D., *The basics and underlying mechanisms of mucoadhesion*. Advanced Drug Delivery Reviews, 2005. **57**(11): p. 1556-1568.
43. Peppas, N.A. and Sahlin, J.J., *Hydrogels as mucoadhesive and bioadhesive materials: a review*. Biomaterials, 1996. **17**(16): p. 1553-1561.
44. Ponchel, G., Touchard, F., Duchêne, D., and Peppas, N.A., *Bioadhesive analysis of controlled-release systems. I. Fracture and interpenetration analysis in poly(acrylic acid)-containing systems*. Journal of Controlled Release, 1987. **5**(2): p. 129-141.
45. Kinloch, A.J., *The science of adhesion*. Journal of Materials Science, 1980. **15**(9): p. 2141-2166.
46. Jiménez-castellanos, M.R., Zia, H., and Rhodes, C.T., *Mucoadhesive drug delivery systems*. Drug Development and Industrial Pharmacy, 1993. **19**(1-2): p. 143-194.
47. Peppas, N.A. and Sahlin, J.J., *Hydrogels as mucoadhesive and bioadhesive materials: a review*. Biomaterials, 1996. **17**(16): p. 1553-61.
48. Ahuja, A., Khar, R.K., and Ali, J., *Mucoadhesive drug delivery systems*. Drug Development and Industrial Pharmacy, 1997. **23**(5): p. 489-515.

49. Dubolazov, A.V., Nurkeeva, Z.S., Mun, G.A., and Khutoryanskiy, V.V., *Design of mucoadhesive polymeric films based on blends of poly(acrylic acid) and (hydroxypropyl)cellulose*. *Biomacromolecules*, 2006. **7**(5): p. 1637-1643.
50. Kim, T.H., Ahn, J.S., Choi, H.K., Choi, Y.J., and Cho, C.S., *A novel mucoadhesive polymer film composed of carbopol, poloxamer and hydroxypropylmethylcellulose*. *Archives of Pharmacal Research*, 2007. **30**(3): p. 381-386.
51. Keely, S., Rullay, A., Wilson, C., Carmichael, A., Carrington, S., Corfield, A., Haddleton, D.M., and Brayden, D.J., *In vitro and ex vivo intestinal tissue models to measure mucoadhesion of poly (methacrylate) and N-trimethylated chitosan polymers*. *Pharmaceutical Research*, 2005. **22**(1): p. 38-49.
52. Lim, S.T., Martin, G.P., Berry, D.J., and Brown, M.B., *Preparation and evaluation of the in vitro drug release properties and mucoadhesion of novel microspheres of hyaluronic acid and chitosan*. *Journal of Controlled Release*, 2000. **66**(2-3): p. 281-292.
53. Lehr, C.-M., Bouwstra, J.A., Schacht, E.H., and Junginger, H.E., *In vitro evaluation of mucoadhesive properties of chitosan and some other natural polymers*. *International Journal of Pharmaceutics*, 1992. **78**(1-3): p. 43-48.
54. Pires, C.T.G.V.M.T., Vilela, J.A.P., and Airoidi, C., *The Effect of chitin alkaline deacetylation at different condition on particle properties*. *Procedia Chemistry*, 2014. **9**(0): p. 220-225.
55. Chung, Y., Tsai, C., and Li, C., *Preparation and characterization of water-soluble chitosan produced by Maillard reaction*. *Fisheries Science*, 2006. **72**(5): p. 1096-1103.
56. Pacheco, N., Garnica-Gonzalez, M.n., Gimeno, M., Bárzana, E., Trombotto, S.p., David, L., and Shirai, K., *Structural characterization of chitin and chitosan obtained by biological and chemical methods*. *Biomacromolecules*, 2011. **12**(9): p. 3285-3290.
57. Chopra, S., Mahdi, S., Kaur, J., Iqbal, Z., Talegaonkar, S., and Ahmad, F.J., *Advances and potential applications of chitosan derivatives as mucoadhesive*

- biomaterials in modern drug delivery*. Journal of Pharmacy and Pharmacology, 2006. **58**(8): p. 1021-1032.
58. Filee, P., Freichels, A., Jerome, C., Aqil, A., Colige, A., and Tchemtchoua, T.V., *Chitosan biomimetic scaffolds and methods for preparing the same*. 2011, Google Patents.
  59. Borchard, G., Lueβen, H.L., de Boer, A.G., Verhoef, J.C., Lehr, C.-M., and Junginger, H.E., *The potential of mucoadhesive polymers in enhancing intestinal peptide drug absorption. III: Effects of chitosan-glutamate and carbomer on epithelial tight junctions in vitro*. Journal of Controlled Release, 1996. **39**(2-3): p. 131-138.
  60. Helander, I.M., Nurmiäho-Lassila, E.L., Ahvenainen, R., Rhoades, J., and Roller, S., *Chitosan disrupts the barrier properties of the outer membrane of Gram-negative bacteria*. International Journal of Food Microbiology, 2001. **71**(2-3): p. 235-244.
  61. Rabea, E.I., Badawy, M.E., Stevens, C.V., Smagghe, G., and Steurbaut, W., *Chitosan as antimicrobial agent: applications and mode of action*. Biomacromolecules, 2003. **4**(6): p. 1457-1465.
  62. Singla, A.K. and Chawla, M., *Chitosan: some pharmaceutical and biological aspects - an update*. Journal of Pharmacy and Pharmacology, 2001. **53**(8): p. 1047-1067.
  63. Ilium, L., *Chitosan and its use as a pharmaceutical excipient*. Pharmaceutical Research, 1998. **15**(9): p. 1326-1331.
  64. Jeon, C. and Ha Park, K., *Adsorption and desorption characteristics of mercury(II) ions using aminated chitosan bead*. Water Research, 2005. **39**(16): p. 3938-3944.
  65. Yuan, Y., Chesnutt, B.M., Utturkar, G., Haggard, W.O., Yang, Y., Ong, J.L., and Bumgardner, J.D., *The effect of cross-linking of chitosan microspheres with genipin on protein release*. Carbohydrate Polymers, 2007. **68**(3): p. 561-567.
  66. El-Gibaly, I., *Development and in vitro evaluation of novel floating chitosan microcapsules for oral use: comparison with non-floating chitosan microspheres*. International Journal of Pharmaceutics, 2002. **249**(1-2): p. 7-21.

67. Sogias, I.A., Williams, A.C., and Khutoryanskiy, V.V., *Chitosan-based mucoadhesive tablets for oral delivery of ibuprofen*. International Journal of Pharmaceutics, 2012. **436**(1-2): p. 602-610.
68. Chandy, T. and Sharma, C.P., *Chitosan matrix for oral sustained delivery of ampicillin*. Biomaterials, 1993. **14**(12): p. 939-944.
69. Krajewska, B., *Diffusion of metal ions through gel chitosan membranes*. Reactive and Functional Polymers, 2001. **47**(1): p. 37-47.
70. Mi, F.-L., Shyu, S.-S., Wu, Y.-B., Lee, S.-T., Shyong, J.-Y., and Huang, R.-N., *Fabrication and characterization of a sponge-like asymmetric chitosan membrane as a wound dressing*. Biomaterials, 2001. **22**(2): p. 165-173.
71. Lee, Y.-M., Park, Y.-J., Lee, S.-J., Ku, Y., Han, S.-B., Klokkevold, P.R., and Chung, C.-P., *The bone regenerative effect of platelet-derived growth factor-BB delivered with a chitosan/tricalcium phosphate sponge carrier*. Journal of Periodontology, 2000. **71**(3): p. 418-424.
72. Huang, M., Khor, E., and Lim, L.-Y., *Uptake and cytotoxicity of chitosan molecules and nanoparticles: effects of molecular weight and degree of deacetylation*. Pharmaceutical Research, 2004. **21**(2): p. 344-353.
73. Chen, L., Zhu, J., Li, Y., Lu, J., Gao, L., Xu, H., Fan, M., and Yang, X., *Enhanced nasal mucosal delivery and immunogenicity of anti-caries DNA vaccine through incorporation of anionic liposomes in chitosan/DNA complexes*. PLOS ONE, 2013. **8**(8): p. e71953.
74. Muzzarelli, R.A.A., Boudrant, J., Meyer, D., Manno, N., DeMarchis, M., and Paoletti, M.G., *Current views on fungal chitin/chitosan, human chitinases, food preservation, glucans, pectins and inulin: A tribute to Henri Braconnot, precursor of the carbohydrate polymers science, on the chitin bicentennial*. Carbohydrate Polymers, 2012. **87**(2): p. 995-1012.
75. Nishimura, K., Nishimura, S., Nishi, N., Numata, F., Tone, Y., Tokura, S., and Azuma, I., *Adjuvant activity of chitin derivatives in mice and guinea-pigs*. Vaccine, 1985. **3**(5): p. 379-384.
76. Okamoto, Y., Minami, S., Matsushashi, A., Sashiwa, H., Saimoto, H., Shigemasa, Y., Tanigawa, T., Tanaka, Y., and Tokura, S., *Polymeric N-acetyl-D-glucosamine*

- (chitin) induces histionic activation in dogs. *Journal of Veterinary Medical Science*, 1993. **55**(5): p. 739-742.
77. Shu, X.Z. and Zhu, K.J., *Controlled drug release properties of ionically cross-linked chitosan beads: the influence of anion structure*. *International Journal of Pharmaceutics*, 2002. **233**(1-2): p. 217-225.
78. Shen, E.C., Wang, C., Fu, E., Chiang, C.Y., Chen, T.T., and Nieh, S., *Tetracycline release from tripolyphosphate-chitosan cross-linked sponge: a preliminary in vitro study*. *Journal of Periodontal Research*, 2008. **43**(6): p. 642-648.
79. Brack, H.P., Tirmizi, S.A., and Risen Jr, W.M., *A spectroscopic and viscometric study of the metal ion-induced gelation of the biopolymer chitosan*. *Polymer*, 1997. **38**(10): p. 2351-2362.
80. Dambies, L., Vincent, T., Domard, A., and Guibal, E., *Preparation of chitosan gel beads by ionotropic molybdate gelation*. *Biomacromolecules*, 2001. **2**(4): p. 1198-1205.
81. Bhattarai, N., Gunn, J., and Zhang, M., *Chitosan-based hydrogels for controlled, localized drug delivery*. *Advanced Drug Delivery Reviews*, 2010. **62**(1): p. 83-99.
82. Anitha, A., Deepa, N., Chennazhi, K.P., Nair, S.V., Tamura, H., and Jayakumar, R., *Development of mucoadhesive thiolated chitosan nanoparticles for biomedical applications*. *Carbohydrate Polymers*, 2011. **83**(1): p. 66-73.
83. Bernkop-Schnürch, A., *Thiomers: A new generation of mucoadhesive polymers*. *Advanced Drug Delivery Reviews*, 2005. **57**(11): p. 1569-1582.
84. Hamman, J.H. and Kotze, A.F., *Effect of the type of base and number of reaction steps on the degree of quaternization and molecular weight of N-trimethyl chitosan chloride*. *Drug Development and Industrial Pharmacy*, 2001. **27**(5): p. 373-380.
85. Pawlak, A. and Mucha, M., *Thermogravimetric and FTIR studies of chitosan blends*. *Thermochimica Acta*, 2003. **396**(1-2): p. 153-166.
86. Lewandowska, K., *Miscibility and thermal stability of poly(vinyl alcohol)/chitosan mixtures*. *Thermochimica Acta*, 2009. **493**(1-2): p. 42-48.



87. Taboada, E., Cabrera, G., and Cardenas, G., *Synthesis and characterization of new arylamine chitosan derivatives*. Journal of Applied Polymer Science, 2004. **91**(2): p. 807-812.
88. Lavertu, M., Xia, Z., Serreqi, A.N., Berrada, M., Rodrigues, A., Wang, D., Buschmann, M.D., and Gupta, A., *A validated <sup>1</sup>H NMR method for the determination of the degree of deacetylation of chitosan*. Journal of Pharmaceutical and Biomedical Analysis, 2003. **32**(6): p. 1149-1158.
89. Sashiwa, H., Kawasaki, N., Nakayama, A., Muraki, E., Yajima, H., Yamamori, N., Ichinose, Y., Sunamoto, J., and Aiba, S.-i., *Chemical modification of chitosan. Part 15: Synthesis of novel chitosan derivatives by substitution of hydrophilic amine using N-carboxyethylchitosan ethyl ester as an intermediate*. Carbohydrate Research, 2003. **338**(6): p. 557-561.
90. Patel, V., Prajapati, B., and Patel, M., *Design and characterization of chitosan-containing mucoadhesive buccal patches of propranolol hydrochloride*, in *Acta Pharmaceutica*. 2007. p. 61-72.
91. Johnson, P. and Rainsford, K.D., *The physical properties of mucus: Preliminary observations on the sedimentation behaviour of porcine gastric mucus*. Biochimica et Biophysica Acta (BBA) - General Subjects, 1972. **286**(1): p. 72-78.
92. Roy, S., Pal, K., Anis, A., Pramanik, K., and Prabhakar, B., *Polymers in mucoadhesive drug-delivery systems: a brief note*. Designed Monomers and Polymers, 2009. **12**(6): p. 483-495.
93. Feng, L., Li, S., Li, H., Zhai, J., Song, Y., Jiang, L., and Zhu, D., *Super-hydrophobic surface of aligned polyacrylonitrile nanofibers*. Angewandte Chemie International Edition, 2002. **41**(7): p. 1221-1223.
94. Martin, C.R., *Membrane-based synthesis of nanomaterials*. Chemistry of Materials, 1996. **8**(8): p. 1739-1746.
95. Ma, P.X. and Zhang, R., *Synthetic nano-scale fibrous extracellular matrix*. Journal of Biomedical Materials Research, 1999. **46**(1): p. 60-72.
96. Deitzel, J.M., Kleinmeyer, J.D., Hirvonen, J.K., and Beck Tan, N.C., *Controlled deposition of electrospun poly(ethylene oxide) fibers*. Polymer, 2001. **42**(19): p. 8163-8170.

97. Liu, G., Ding, J., Qiao, L., Guo, A., Dymov, B.P., Gleeson, J.T., Hashimoto, T., and Saijo, K., *Polystyrene-block-poly(2-cinnamoyl ethyl methacrylate) nanofibers-preparation, characterization, and liquid crystalline properties*. Chemistry-A European Journal, 1999. **5**(9): p. 2740-2749.
98. Whitesides, G.M. and Grzybowski, B., *Self-assembly at all scales*. Science, 2002. **295**(5564): p. 2418-2421.
99. Huang, Z.-M., Zhang, Y.Z., Kotaki, M., and Ramakrishna, S., *A review on polymer nanofibers by electrospinning and their applications in nanocomposites*. Composites Science and Technology, 2003. **63**(15): p. 2223-2253.
100. Homayoni, H., Ravandi, S.A.H., and Valizadeh, M., *Electrospinning of chitosan nanofibers: Processing optimization*. Carbohydrate Polymers, 2009. **77**(3): p. 656-661.
101. Duan, B., Dong, C., Yuan, X., and Yao, K., *Electrospinning of chitosan solutions in acetic acid with poly(ethylene oxide)*. Journal of Biomaterials Science Polymer Edition, 2004. **15**(6): p. 797-811.
102. Bhattarai, N., Edmondson, D., Veisoh, O., Matsen, F.A., and Zhang, M., *Electrospun chitosan-based nanofibers and their cellular compatibility*. Biomaterials, 2005. **26**(31): p. 6176-6184.
103. Geng, X., Kwon, O.H., and Jang, J., *Electrospinning of chitosan dissolved in concentrated acetic acid solution*. Biomaterials, 2005. **26**(27): p. 5427-5432.
104. Gan, H., Li, Y., Liu, H., Wang, S., Li, C., Yuan, M., Liu, X., Wang, C., Jiang, L., and Zhu, D., *Self-assembly of conjugated polymers and ds-oligonucleotides directed fractal-like aggregates*. Biomacromolecules, 2007. **8**(5): p. 1723-1729.
105. Niece, K.L., Hartgerink, J.D., Donners, J.J., and Stupp, S.I., *Self-assembly combining two bioactive peptide-amphiphile molecules into nanofibers by electrostatic attraction*. Journal of the American Chemical Society, 2003. **125**(24): p. 7146-7147.
106. Paramonov, S.E., Jun, H.-W., and Hartgerink, J.D., *Self-assembly of peptide-amphiphile nanofibers: the roles of hydrogen bonding and amphiphilic packing*. Journal of the American Chemical Society, 2006. **128**(22): p. 7291-7298.

107. Beniash, E., Hartgerink, J.D., Storrie, H., Stendahl, J.C., and Stupp, S.I., *Self-assembling peptide amphiphile nanofiber matrices for cell entrapment*. Acta Biomaterialia, 2005. **1**(4): p. 387-397.
108. Juntapram, K., Praphairaksit, N., Siraleartmukul, K., and Muangsinn, N., *Synthesis and characterization of chitosan-homocysteine thiolactone as a mucoadhesive polymer*. Carbohydrate Polymers, 2012. **87**(4): p. 2399-2408.
109. Zhang, D., Li, J., Chen, S., Li, T., Zhou, J., Cheng, X., and Zhang, A., *Hybrid Self-Assembly, Crystal, and Fractal Behavior of a Carboxy-Ended Hyperbranched Polyester/Copper Complex*. Macromolecular Chemistry and Physics, 2013. **214**(3): p. 370-377.
110. Cui, H., Webber, M.J., and Stupp, S.I., *Self-assembly of peptide amphiphiles: from molecules to nanostructures to biomaterials*. Biopolymers, 2010. **94**(1): p. 1-18.
111. Kokkoli, E., Mardilovich, A., Wedekind, A., Rexeis, E.L., Garg, A., and Craig, J.A., *Self-assembly and applications of biomimetic and bioactive peptide-amphiphiles*. Soft Matter, 2006. **2**(12): p. 1015-1024.
112. Huang, Y., Yu, H., Guo, L., and Huang, Q., *Structure and self-assembly properties of a new chitosan-based amphiphile*. Journal of Physical Chemistry B, 2010. **114**(23): p. 7719-7726.
113. Witten, T.A. and Sander, L.M., *Diffusion-limited aggregation*. Physical Review B, 1983. **27**(9): p. 5686-5697.
114. Ma, Z., Zhang, G., Zhai, X., Jin, L., Tang, X., Yang, M., Zheng, P., and Wang, W., *Fractal crystal growth of poly(ethylene oxide) crystals from its amorphous monolayers*. Polymer, 2008. **49**(6): p. 1629-1634.
115. Reches, M. and Gazit, E., *Formation of closed-cage nanostructures by self-assembly of aromatic dipeptides*. Nano Letters, 2004. **4**(4): p. 581-585.
116. Hornof, M., Weyenberg, W., Ludwig, A., and Bernkop-Schnurch, A., *Mucoadhesive ocular insert based on thiolated poly(acrylic acid): development and in vivo evaluation in humans*. Journal of Controlled Release, 2003. **89**(3): p. 419-428.







APPENDIX A

Standard curve of mucin (type II) and free and adsorbed mucin  
on polymers (Chapter III)

### Standard curve of mucin glycoprotein (type II)

The concentration versus absorbance of mucin glycoprotein (type II) was determined by UV-Vis spectrophotometer as the same conditions described in chapter III and was presented in Table A1. The plot of calibration curve of mucin glycoprotein (type II) was illustrated in Figure A1.

**Table A1** Absorbance of various concentrations of mucin glycoprotein (type II) in SGF (pH 1.2), SDF (pH 4.0), PB (pH 5.5) and SIF (pH 6.4) which was determined by UV-Vis spectrophotometer.

Concentration (mg/2mL)	Absorbance (A)			
	SGF (pH 1.2)	SDF (pH 4.0)	PB (pH 5.5)	SIF (pH 6.4)
0.05	0.024	0.151	0.352	0.003
0.10	0.057	0.179	0.386	0.068
0.20	0.107	0.279	0.525	0.142
0.30	0.159	0.388	0.668	0.238
0.40	0.223	0.522	0.855	0.312
0.50	0.296	0.598	1.007	0.398
0.60	0.369	0.677	1.148	0.502
1.00	0.679	0.938	-	0.876

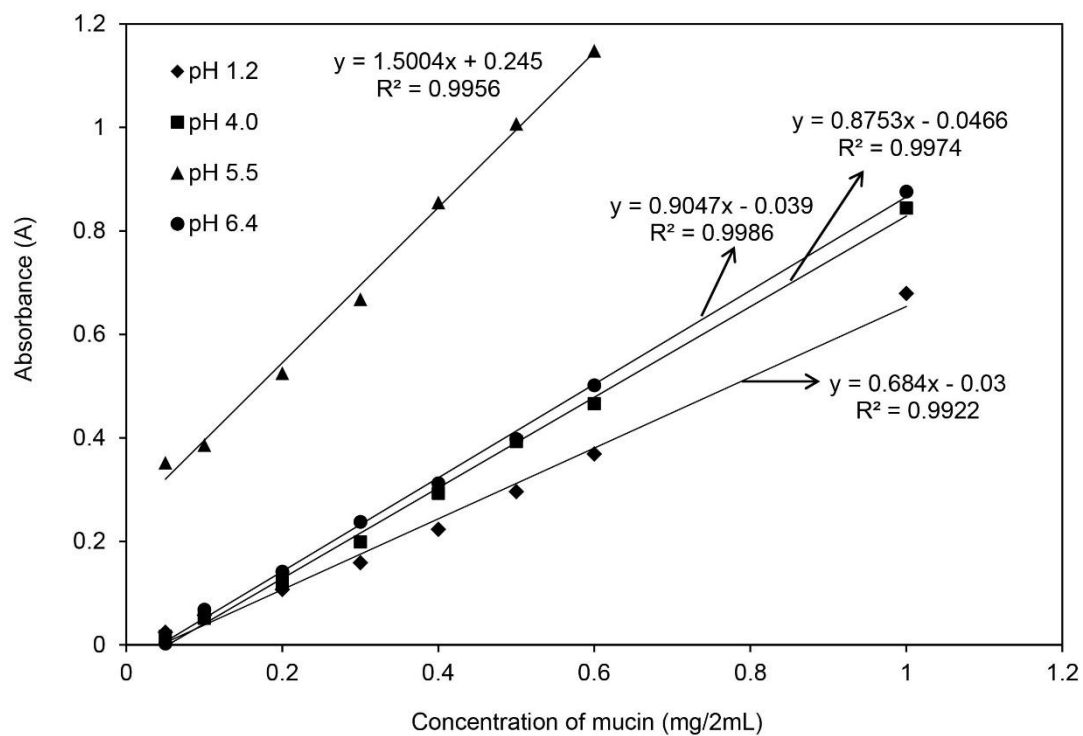


**Figure A1** Standard curve of mucin glycoprotein (type II) in SGF (pH 1.2), SDF (pH 4.0), PB (pH 5.5) and SIF (pH 6.4).



### Free and adsorbed mucin glycoprotein (type II) on polymers

Free and adsorbed mucin glycoprotein (type II) on chitosan, *N*-carboxymethyl ester and SM-chitosan in SGF (pH 1.2), SDF (pH 4.0), PB (pH 5.5) and SIF (pH 6.4) were calculated from the equations of standard curve in Figure A1 and were shown in Table A2, Table A3, Table A4 and Table A5.

**Table A2** Absorption of free and adsorbed mucin glycoprotein (type II) on chitosan, *N*-carboxymethyl ester and SM-chitosan in SGF (pH 1.2) determined by UV-Vis spectrophotometer.

Polymers	Absorbance (A) of mucin at the concentration of 2 mg/mL	Free mucin (mg/mL)	Absorbed mucin (mg/mL)
chitosan	0.169 ± 0.008	0.145 ± 0.006	0.854 ± 0.006
<i>N</i> -carboxymethyl chitosan	0.137 ± 0.003	0.122 ± 0.002	0.878 ± 0.002
SM-chitosan	0.125 ± 0.008	0.113 ± 0.006	0.887 ± 0.006

**Table A3** Absorption of free and adsorbed mucin glycoprotein (type II) on chitosan, *N*-carboxymethyl ester and SM-chitosan in SDF (pH 4.0) determined by UV-Vis spectrophotometer.

Polymers	Absorbance (A) of mucin at the concentration of 2 mg/mL	Free mucin (mg/mL)	Absorbed mucin (mg/mL)
chitosan	0.967 ± 0.032	0.487 ± 0.018	0.506 ± 0.009
<i>N</i> -carboxymethyl chitosan	0.427 ± 0.038	0.174 ± 0.022	0.811 ± 0.010
SM-chitosan	0.460 ± 0.056	0.193 ± 0.033	0.815 ± 0.023

**Table A4** Absorption of free and adsorbed mucin glycoprotein (type II) on chitosan, *N*-carboxymethyl ester and SM-chitosan in PB (pH 5.5) determined by UV-Vis spectrophotometer.

Polymers	Absorbance (A) of mucin at the concentration of 2 mg/mL	Free mucin (mg/mL)	Absorbed mucin (mg/mL)
chitosan	0.907 ± 0.045	0.221 ± 0.015	0.770 ± 0.001
<i>N</i> -carboxymethyl chitosan	0.436 ± 0.050	0.064 ± 0.016	0.934 ± 0.013
SM-chitosan	0.391 ± 0.027	0.849 ± 0.009	0.957 ± 0.008

**Table A5** Absorption of free and adsorbed mucin glycoprotein (type II) on chitosan, *N*-carboxymethyl ester and SM-chitosan in SIF (pH 6.4) determined by UV-Vis spectrophotometer.

Polymers	Absorbance (A) of mucin at the concentration of 2 mg/mL	Free mucin (mg/mL)	Absorbed mucin (mg/mL)
chitosan	$1.637 \pm 0.091$	$1.361 \pm 0.544$	$0.074 \pm 0.050$
<i>N</i> -carboxymethyl chitosan	$0.771 \pm 0.108$	$0.656 \pm 0.255$	$0.553 \pm 0.059$
SM-chitosan	$0.909 \pm 0.105$	$0.768 \pm 0.300$	$0.476 \pm 0.058$

APPENDIX B  
Swelling behavior  
(Chapter IV)

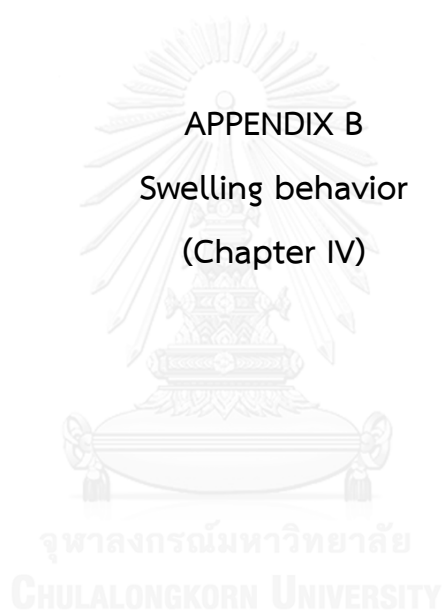


**Table B1** Swelling behaviors of chitosan, TMC and 4-CBS-TMC in SGF (pH 1.2).

Time (h)	Swelling ratio (%)		
	Chitosan	TMC	4-CBS-TMC
0	0.000 ± 0.000	0.000 ± 0.000	0.000 ± 0.000
0.05	19.444 ± 0.028	30.556 ± 0.024	66.667 ± 0.100
0.10	30.556 ± 0.028	100.000 ± 0.000	138.889 ± 0.208
0.15	38.889 ± 0.028	108.333 ± 0.000	166.667 ± 0.100
0.30	38.889 ± 0.028	111.111 ± 0.024	272.222 ± 0.153
0.45	38.889 ± 0.028	113.889 ± 0.024	255.556 ± 0.115
1	41.667 ± 0.00	113.889 ± 0.024	255.556 ± 0.115
2	41.667 ± 0.00	113.889 ± 0.024	255.556 ± 0.115
3	47.222 ± 0.028	113.889 ± 0.024	255.556 ± 0.115
4	47.222 ± 0.028	113.889 ± 0.024	255.556 ± 0.115
5	47.222 ± 0.028	113.889 ± 0.024	255.556 ± 0.115
6	50.000 ± 0.050	113.889 ± 0.024	255.556 ± 0.115

**Table B2** Swelling behaviors of chitosan, TMC and 4-CBS-TMC in SDF (pH 4.0).

Time (h)	Swelling ratio (%)		
	Chitosan	TMC	4-CBS-TMC
0	0.000 ± 0.000	0.000 ± 0.000	0.000 ± 0.000
0.05	19.444 ± 0.029	100.000 ± 0.000	111.111 ± 0.058
0.10	19.444 ± 0.029	111.111 ± 0.028	150.000 ± 0.000
0.15	19.444 ± 0.029	108.333 ± 0.050	183.333 ± 0.000
0.30	30.555 ± 0.029	113.889 ± 0.028	183.333 ± 0.000
0.45	33.333 ± 0.000	113.889 ± 0.028	244.444 ± 0.058
1	33.333 ± 0.000	116.667 ± 0.000	261.111 ± 0.058
2	36.111 ± 0.029	116.667 ± 0.000	261.111 ± 0.058
3	36.111 ± 0.029	116.667 ± 0.000	261.111 ± 0.058
4	38.889 ± 0.029	119.444 ± 0.028	261.111 ± 0.058
5	38.889 ± 0.029	119.444 ± 0.028	266.667 ± 0.000
6	44.444 ± 0.029	119.444 ± 0.028	255.667 ± 0.000

**Table B3** Swelling behaviors of chitosan, TMC and 4-CBS-TMC in PB (pH 5.5).

Time (h)	Swelling ratio (%)		
	chitosan	TMC	4-CBS-TMC
0	0.000 ± 0.000	0.000 ± 0.000	0.000 ± 0.000
0.05	19.444 ± 0.029	66.667 ± 0.000	25.000 ± 0.029
0.10	27.778 ± 0.029	77.778 ± 0.06	33.333 ± 0.029
0.15	27.778 ± 0.029	80.556 ± 0.029	33.333 ± 0.029
0.30	30.556 ± 0.029	80.556 ± 0.029	100.000 ± 0.000
0.45	33.333 ± 0.000	80.556 ± 0.029	183.333 ± 0.000
1	33.333 ± 0.000	80.556 ± 0.029	183.333 ± 0.000
2	36.111 ± 0.029	83.333 ± 0.000	183.333 ± 0.029
3	38.889 ± 0.029	83.333 ± 0.000	183.333 ± 0.050
4	38.889 ± 0.029	83.333 ± 0.000	183.333 ± 0.050
5	38.889 ± 0.029	83.333 ± 0.000	183.333 ± 0.050
6	38.889 ± 0.029	91.667 ± 0.050	191.667 ± 0.050

**Table B4** Swelling behaviors of chitosan, TMC and 4-CBS-TMC in SGF (pH 6.4).

Time (h)	Swelling ratio (%)		
	chitosan	TMC	4-CBS-TMC
0	0.000 ± 0.000	0.000 ± 0.000	0.000 ± 0.000
0.05	16.667 ± 0.000	16.667 ± 0.000	36.111 ± 0.076
0.10	16.667 ± 0.000	16.667 ± 0.000	72.222 ± 0.058
0.15	16.667 ± 0.000	25.000 ± 0.050	105.556 ± 0.208
0.30	16.667 ± 0.000	44.444 ± 0.058	122.222 ± 0.115
0.45	16.667 ± 0.000	47.222 ± 0.029	138.889 ± 0.058
1	16.667 ± 0.000	52.778 ± 0.029	150.000 ± 0.000
2	16.667 ± 0.000	58.333 ± 0.050	150.000 ± 0.000
3	16.667 ± 0.000	58.333 ± 0.050	161.111 ± 0.058
4	16.667 ± 0.000	58.333 ± 0.050	172.222 ± 0.058
5	16.667 ± 0.00	58.333 ± 0.000	177.778 ± 0.058
6	16.667 ± 0.00	58.333 ± 0.000	177.778 ± 0.058



**Table B5** Swelling behaviors of chitosan, TMC and 4-CBS-TMC in SJF (pH 7.4).

Time (h)	Swelling ratio (%)		
	chitosan	TMC	4-CBS-TMC
0	0.000 ± 0.000	0.000 ± 0.000	0.000 ± 0.000
0.05	14.286 ± 0.000	5.556 ± 0.029	10.000 ± 0.000
0.10	14.286 ± 0.000	5.556 ± 0.029	10.000 ± 0.000
0.15	14.286 ± 0.000	5.556 ± 0.029	11.667 ± 0.029
0.30	14.286 ± 0.000	5.556 ± 0.029	20.000 ± 0.000
0.45	14.286 ± 0.000	5.556 ± 0.029	20.000 ± 0.000
1	14.286 ± 0.000	13.889 ± 0.029	20.000 ± 0.000
2	14.286 ± 0.000	13.889 ± 0.029	20.000 ± 0.000
3	14.286 ± 0.000	13.889 ± 0.029	20.000 ± 0.000
4	14.286 ± 0.000	13.889 ± 0.029	20.000 ± 0.000
5	14.286 ± 0.000	13.889 ± 0.029	20.000 ± 0.000
6	14.286 ± 0.000	13.889 ± 0.029	20.000 ± 0.000

**Table B6** Swelling behaviors of chitosan, TMC and 4-CBS-TMC in water.

Time (h)	Swelling ratio (%)		
	Chitosan	TMC	4-CBS-TMC
0	0.000 ± 0.000	0.000 ± 0.000	0.000 ± 0.000
0.05	16.667 ± 0.000	13.889 ± 0.029	16.667 ± 0.000
0.10	16.667 ± 0.000	13.889 ± 0.029	16.667 ± 0.000
0.15	16.667 ± 0.000	13.889 ± 0.029	19.444 ± 0.029
0.30	16.667 ± 0.000	13.889 ± 0.029	19.444 ± 0.029
0.45	19.444 ± 0.000	13.889 ± 0.029	19.444 ± 0.029
1	19.444 ± 0.029	13.889 ± 0.029	19.444 ± 0.029
2	19.444 ± 0.029	13.889 ± 0.029	19.444 ± 0.029
3	19.444 ± 0.029	13.889 ± 0.029	19.444 ± 0.029
4	19.444 ± 0.029	13.889 ± 0.029	19.444 ± 0.029
5	19.444 ± 0.029	13.889 ± 0.029	19.444 ± 0.029
6	19.444 ± 0.029	13.889 ± 0.029	19.444 ± 0.029

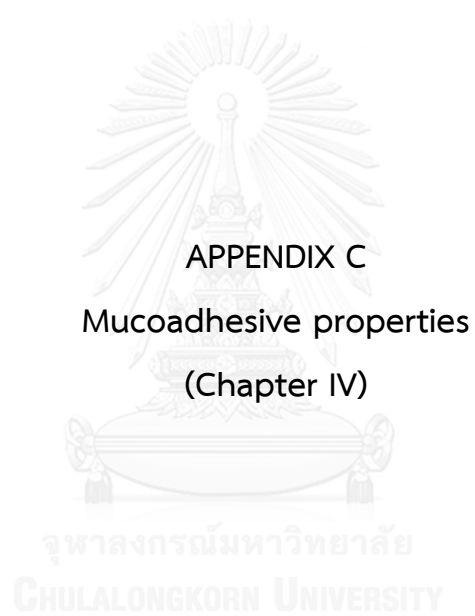


**Table C1** The component of bioadhesion in SGF (pH 1.2) and PB (pH 5.5).

Polymer	Component of bioadhesion (cps)	
	SGF (pH 1.2)	PB (pH 5.5)
Chitosan	37.300 ± 4.40	71.267 ± 4.46
TMC	27.347 ± 2.62	124.180 ± 4.36
4-CBS-TMC	42.483 ± 3.36	134.423 ± 4.41
SA-4-CBS-TMC	102.783 ± 2.02	217.243 ± 5.53



APPENDIX D  
Preparation of stock solution



## Reagents

- 1.) 1 N Hydrochloric Acid: Exactly measured 8.3 ml of 12.1 N HCl was added to 50 ml distilled water in 100 ml volumetric flask and the volume was adjusted with distilled water.
- 2.) 1 N Sodium Hydroxide: Four grams of NaOH were placed in a 100 ml volumetric flask and diluted with distilled water to volume and the solution was mixed.
- 3.) Simulated Gastric Fluid (SGF, pH 1.2): 6 g of sodium chloride were placed in a 3000 ml round bottom flask, and 2500 ml of distilled water and 21 ml of 1 N HCl were added. The volume was adjusted and the solution pH was adjusted to 1.5 with either 1 N HCl or 0.2 N NaOH. No enzymes were added to the fluid.
- 4.) 0.1 N Simulated duodenum buffer (SDF, pH 4.0): Prepare a 0.2 M sodium acetate solution. Weigh 27.2 g of sodium acetate trihydrate into a one liter volumetric flask. Add 800 ml of deionized water, mix and dissolve. Bring the pH down to 4.0 with glacial acetic acid. Finally adjust the volume to one liter with deionized water.
- 5.) 0.1 N phosphate buffer (PB, pH 5.5): Dissolve 272 g of sodium acetate in 500 ml of water and add slowly 50 ml of glacial acetic acid and sufficient water to produce 1000 ml. Adjust pH, if necessary.
- 6.) Simulated jejunum fluid (SJF, pH 6.4): Dissolve 2.5 g of disodium hydrogen phosphate, 2.5 of sodium dihydrogen phosphate and 8.2 g of sodium chloride in 950 ml of water. Adjust the pH of the solution to 6.4 with 1 M sodium hydroxide or 1 M hydrochloric acid, if necessary. Dilute to 1000.0 ml with water.
- 7.) Simulated ileum fluid (SIF, pH 7.4): 20.4 g of potassium monobasic phosphate were placed in a 3000 ml round bottom volumetric flask, and 570 ml of 0.2 NaOH were added. The volume was adjusted with distilled water. The solution pH was adjusted to 7.4 with either 1 N HCl or 0.2 N NaOH. No enzymes were added to the fluid.

## VITA

Name: Phruetchika Suvannasara Gender: Female

Date of Birth: 18 October 1985 Nationality: Thai Religion: Buddhism

Address: 205/27, Ngamwongwan Rd., Thung Song Hong, Laksi, Bangkok,  
10210 Thailand

Ph.D. in Materials Science, School of Materials Science, Japan Advanced  
Institute of Science and Technology, Nomi, Ishikawa, Japan

Ph.D. in Petrochemistry, Program in Petrochemistry, Chulalongkorn  
University, Bangkok, Thailand

M.Sc. in Petrochemistry and Polymer Science, Program in Petrochemistry  
and Polymer Science, Chulalongkorn University, Bangkok, Thailand

B.Sc. in Chemistry, Department of Chemistry, Thammasat University,  
Bangkok, Thailand

### PUBLICATIONS

1.) Suvannasara, P., Praphairaksit, N. & Muangsin, N. (2014). RSC Advances,  
4, 58664-58673.

2.) Suvannasara, P., Tateyama, S., Miyazato, A., Matsumura, K., Shimoda, T.,  
Ito, Takashi, Yamagata, Y., Fujita, T., Takaya, N. & Kaneko, T. (2014). Macromolecules,  
47, 1586-1593.

3.) Suvannasara, P., Praphairaksit, N., Siralertmukul, K. & Muangsin, N. (2014).  
International Journal of Biological Macromolecule, 64, 240-246.

4.) Songsurang, K., Suvannasara, P., Phurat, C., Puthong, S., Siralertmukul, K.  
& Muangsin, N. (2013). Carbohydrate Polymers, 98, 1335-1342.

5.) Suvannasara, P., Juntapram, K., Praphairaksit, N., Siralertmukul, K. &  
Muangsin, N. (2013). Carbohydrate Polymers, 94, 244-252.